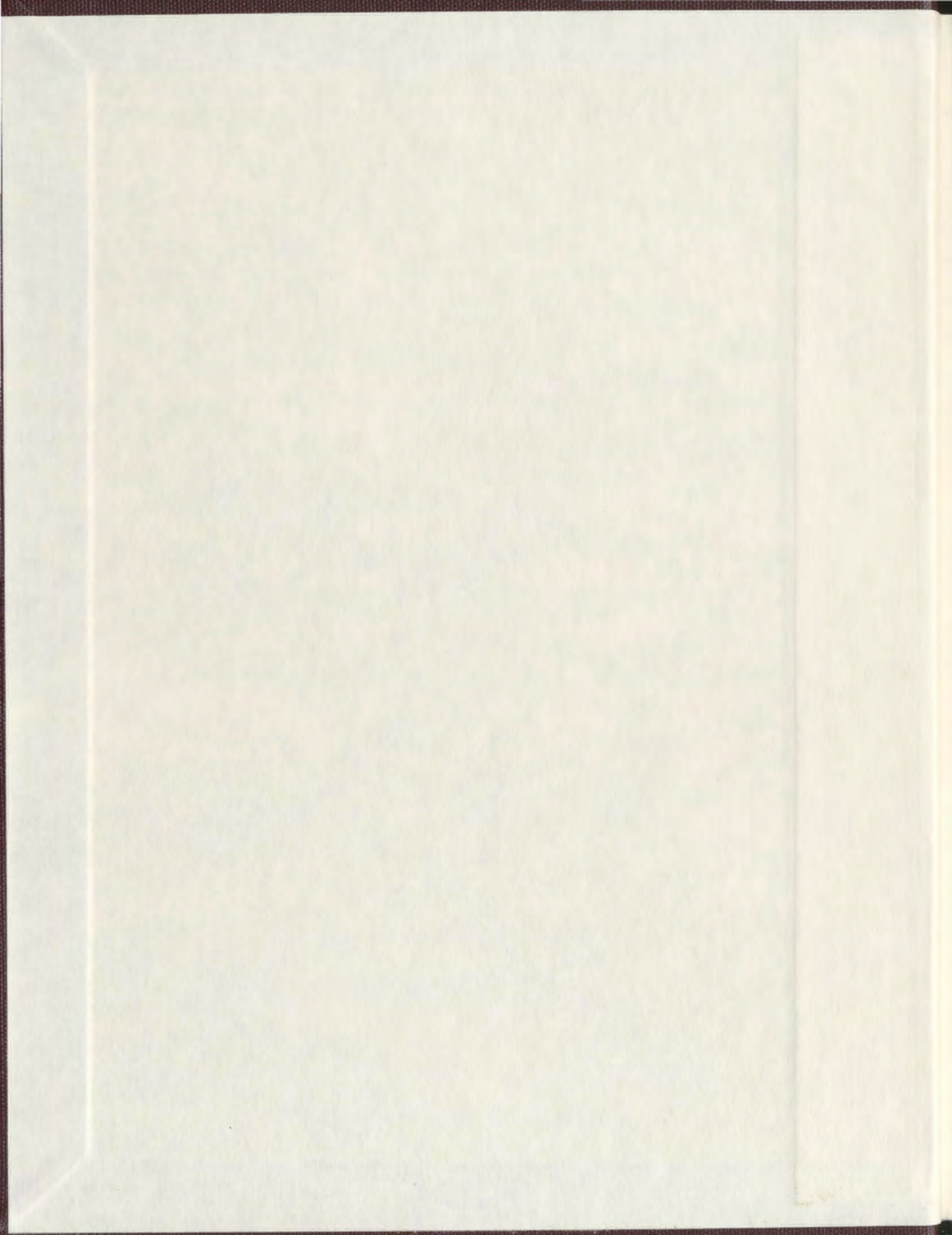


DIAGENESIS AND POROSITY DEVELOPMENT OF  
PALEOZOIC CARBONATE AND EARLY TO MID  
CRETACEOUS SILICICLASTIC RESERVOIR  
INTERVALS, HOPEDALE BASIN, LABRADOR SHELF

STEPHEN SAMUEL SCHWARTZ



**DIAGENESIS AND POROSITY DEVELOPMENT OF PALEOZOIC  
CARBONATE AND EARLY TO MID CRETACEOUS SILICICLASTIC  
RESERVOIR INTERVALS, HOPEDALE BASIN, LABRADOR SHELF**

© Stephen Samuel Schwartz, B.Sc. (Honours)

A thesis submitted to the School of Graduate Studies  
in partial fulfillment of the requirements  
for the degree of  
Master of Science

Department of Earth Sciences  
Memorial University of Newfoundland  
June 2008



## ABSTRACT

Paleozoic carbonates and siliciclastic basins Early to Mid Cretaceous sandstones are observed in the Hopedale and Saglek and represent prerift and synrift sedimentation prior and during the development of the Labrador Shelf, respectively. Both of these sediments have been (and are) of hydrocarbon importance, particularly acting as regional reservoirs, with exploration drilling commencing in the 1970's and ending in the early to mid 1980's. The result was 27 exploration wells and more than 100 000 line km of seismic data acquired from the Canadian side of the Labrador Sea. Hydrocarbons, existing mainly as gas and gas condensates, have been discovered in 5 wells in the Hopedale Basin: Snorri J-90, Hopedale E-33, North Bjarni F-06, Bjarni O-82, and Gudrid H-55. Reserves are estimated at 4.2 Tcf of natural gas and 123 million barrels of NGL. Play types include both siliciclastic (e.g. North Bjarni) and carbonate reservoirs (e.g. Gudrid H-55). North Bjarni has reserves at 2.2 Tcf of gas and 82 million barrels of NGL.

The Hopedale Basin carbonates are represented by dolomites and limestones, and were investigated in cores from three exploration wells: Indian Harbour M-52, Gudrid H-55, and Roberval K-92. Core samples from Roberval K-92 (3578 – 3582 m and 3870 – 3873.5 m), Gudrid H-55 (2676 – 2680 m), and Indian Harbour M-52 (3952 – 3958 m) were collected for petrographic investigations and geochemical analyses. Two main types of carbonates are recognized; a wackstone with limited dolomitization (Indian Harbour M-52) and dolostone (Roberval K-92 & Gudrid H-55). Three dolomite phases (D1, D2 and D3) have been petrographically and geochemically identified and correlated between wells, indicating diagenesis as a result of progressive burial. Trace element and stable isotope geochemistry, along with fluid inclusion data, support petrographic data and aid

in the understanding the origin and nature of the dolomitizing fluids. All porosity is recognized as secondary and is a result of several stages of dissolution and dolomitization. However, precipitation of calcite cements has occluded porosity, creating reservoir heterogeneity.  $^{87}\text{Sr}/^{86}\text{Sr}$  values, sampled from micritic calcite and dolomites, suggest that deposition likely started in the Early to Mid-Ordovician with early dolomitization occurring no later than this time.

The Bjarni Formation represents the main siliciclastic reservoir on the Labrador Shelf and is composed mainly of fluvial to alluvial sandstones, with interbedded to interlaminated lacustrine shales. Six exploration wells from different stratigraphic depths and locations within the Hopedale Basin, containing approximately 31 m of Bjarni Formation sandstone, were logged, sampled, and petrographically analyzed from intervals that include Bjarni H-81 (2157 – 2164 m), Ogmund E-72 (2234 – 2240 m), North Bjarni F-06 (2452 – 2458 m), Herjolf M-92 (2632 – 2640 m), Roberval K-92 (3095 – 3112.5 m), and North Leif I-05 (3110 – 3113.5 m). Petrographic and core analysis have identified compositionally and texturally varied sandstones, ranging from  $\text{Q}_{90.5}\text{F}_{2.0}\text{L}_{7.7}$  to  $\text{Q}_{38.5}\text{F}_{39.0}\text{L}_{22.5}$ , that contain diagenetic minerals such as iron oxides (e.g. hematite), chlorite, ferroan and non-ferroan calcite cements, kaolinite, and quartz overgrowths/cements. Both intergranular (initial) and intragranular (secondary) porosities are recognized and are a result of sediment maturity and diagenesis, respectively. Diagenetic minerals are observed occluding mainly intergranular porosity reducing the total porosity, while the intragranular porosity, present in all studied intervals, supplements the total porosity, improving the reservoir quality.

## ACKNOWLEDGEMENTS

The author wishes to thank, first and foremost, Michael Enachescu for the initiation of this project and his abundant help during the entire process. Thank-you to Karem Azmy and Rudi Meyer for their help, guidance, and insight, particularly with their respective supervised thesis chapters. Thanks to many other people who were or are still at Memorial University of Newfoundland: Ian Atkinson, Michelle Miskell, John Hanchar, Diane Guzzwell, Alison Pye, Pam King, Wilfredo Diegor, Duncan McIlroy, Mark Wilson, Vanessa Bennett, Chris Buchanan, Phil Baluk, Darren Thomeier, Allison Cocker, Erin Gillis, Angie Dearin, Leon Normore, Nikki Tonkin, Christopher Phillips, Michelle Martin, Jordan Stead, Mike Greene, and James Conliffe. Additional thanks to Dr. Dieter Buhl at Ruhr University, Bochum, Germany, Nigel Blamey at National University of Ireland, Galway, Ireland, Denis Lavoie at the Geological Survey of Canada (Quebec), Matthew Harvey (ConocoPhillips), Simon Haynes (Shell), and Jason Pemberton (Shell). Dave Mills and Jason Newell at CNLOPB provided core viewing and sampling. Seismic images are courtesy of GSI. The author would like to give an extended thank-you to PPSC, NSERC, PRAC, and CSPG for funding this project.

מסור אל אוי סבא רבא – שמואל

## LIST OF FIGURES

<u>FIGURE NUMBER</u>	<u>PAGE NUMBER</u>
<b>Fig. 1.1:</b> <i>A.</i> Map of Canada highlighting Newfoundland and Labrador (dark grey) and the offshore sedimentary basins (yellow). <i>B.</i> Mesozoic sedimentary rift basins (all the way to 300 m water depth; yellow) of Newfoundland and Labrador (after Enachescu, 1992).	2
<b>Fig. 1.2:</b> Exploration wells on the Labrador Shelf numbered from the Saglek Basin (north) to the Hopedale Basin (south). Modified after Atkinson & Fagan, 2001.	3
<b>Fig. 1.3:</b> Five exploration wells with hydrocarbons on the Labrador Shelf. Modified after CNLOPB.	5
<b>Fig. 1.4:</b> Diagram indicating processes involved with diagenesis and diagenetic products (i.e. The Diagenetic Cycle). Also shown is the affect of diagenesis on porosity with burial. Modified after Morrow and McIlreath, 1990.	8
<b>Fig. 1.5:</b> Schematic illustration of the diagenetic burial environments (red). Modified after Choquette and James, 1990.	10
<b>Fig. 1.6:</b> Two-way time cross-section through the North Bjarni F-06 Field indicating the main nearshore structural elements of the Hopedale Basin, Labrador Shelf. <i>A.</i> Seaward-dipping, orthogonally trending master fault; <i>B.</i> Horst-Graben and; <i>C.</i> Seaward-dipping Cretaceous and Tertiary sediements onlapping with pre-rift basement. Modified from GSC, 1987; Atkinson and Fagan, 2001; Martin, 2007; Enachescu et al., 2007.	16
<b>Fig. 1.7:</b> Litho-Tectono Stratigraphy of the Labrador Shelf. Modified after Enachescu, 2006; Martin, 2007; McWhae et al., 1980.	18
<b>Fig. 1.8:</b> <i>A.</i> Generalized geological province map of the Archean-Proterozoic craton in Labrador (modified after the Government of Newfoundland and Labrador, 2008). <i>B.</i> Approximate locations of Paleozoic basins (yellow) extending from the Labrador Shelf to Texas (modified from Atkinson & Fagan, 2001).	20
<b>Fig. 2.1:</b> Locations of all exploration wells (and core) studied in the Hopedale Basin (red dots) along with sample listings (boxes) and their distribution. Samples were named based on the well name, core/box number, and number per interval studied. Modified after Atkinson and Fagan (2001).	27
<b>Fig. 2.2:</b> Lower ( <b>A.</b> ) and upper ( <b>B.</b> ) half width graphs indicating the 95% Confidence bounds from observed percentages. ( <b>A.</b> ), $50 - 7.0 = 43\%$ and ( <b>B.</b> ) $50 + 7.0 = 57\%$ . Graphs modified from Howarth, 1998.	31

**Fig 3.1:** *A.* Map of Canada highlighting Newfoundland and Labrador (dark grey) and the offshore sedimentary basins (yellow). *B.* Mesozoic sedimentary rift basins (all the way to 300 m water depth; yellow) of Newfoundland and Labrador (after Enachescu, 1992). 38

**Fig. 3.2:** Stratigraphy and tectonic evolution of the Labrador Shelf, including major unconformities (Modified after Enachescu, 2006). 40

**Fig. 3.3:** *A.* Partial image of the original dip seismic line crossing Gudrid H-55 discovery well. *B.* Generalized interpreted schematic cross-section through Gudrid H-55 well exemplifying Paleozoic carbonates resting on top of a Pre-Cambrian horst block. Seismic courtesy of GSI. 41

**Fig. 3.4:** Exploration wells in the Hopedale and Saglek Basins, Labrador Shelf. Larger red dots indicate carbonate wells studied. Modified after Atkinson & Fagan, 2001. 43

**Fig. 3.5:** Sample locations, numbers, and depths of studied core from Gudrid H-55, Roberval K-92, and Indian Harbour M-52. Note that between Roberval K-92 core 6 and 7 there is a break of approximately 312.5 m. 44

**Fig. 3.6:** Dolomite generations (D1, D2, & D3) in each well plotted against crystal size. 47

**Fig. 3.7:** Paragenetic sequence of Labrador Shelf carbonates of studied wells. Events based on petrography and geochemical evidence. Asterisk indicate cements that were unable to be sampled for geochemistry. 55

**Fig. 3.8:** *A.* Fe vs. Mn and *B.* Mn vs. Sr scatter plots of dolomite and calcite cements from Roberval K-92 (black filling), Gudrid H-55 (grey filling), and Indian Harbour M-52 (white fill). 59

**Fig. 3.9:** *A.* Fe vs. Sr and *B.*  $\delta^{18}\text{O}$  vs.  $\delta^{13}\text{C}$  scatter plots of dolomite and calcite cements from Roberval K-92 (black filling), Gudrid H-55 (grey filling), and Indian Harbour M-52 (white fill). 60

**Fig. 3.10:** Temperature vs.  $\delta^{18}\text{O}_{\text{diagenetic fluid}}$  for various  $\delta^{18}\text{O}_{\text{dolomite}}$  values that were reconstructed from the equation  $10^3 \ln \alpha = 3.2 \times 10^2 T^{-2} - 3.3$  (Land, 1983). The vertical bars indicate the ranges for  $\delta^{18}\text{O}_{\text{fluid}}$  based on the most enriched and depleted sample for the given dolomite generation, while shaded areas mark the preferred temperature ranges. 63

**Fig. 3.11:** Schematic diagram of the diagenetic burial environments in a generalized platform carbonate setting. Dolomite, calcite, and porosity phase ("PP") are placed in their interpreted burial realms based on petrography and geochemistry (see text for abbreviations). 65

- Fig. 3.12:** Average  $^{87}\text{Sr}/^{86}\text{Sr}$  and  $\delta^{13}\text{C}$  values from calcite and dolomite cements compiled with Veizer et al. (1999) reference  $^{87}\text{Sr}/^{86}\text{Sr}$  and  $\delta^{13}\text{C}$  curves. **68**
- Fig. 4.1:** Map of Eastern Canada highlighting the offshore Mesozoic sedimentary basins (yellow) and Grand Banks (grey). Modified after Enachescu, 1992. **75**
- Fig. 4.2:** A map showing the locations of the exploration wells in the Hopedale (dark grey) and Saglek (light grey) basins, Labrador Shelf. Included are Enachescu (2006) subbasins (between dashed red lines). Larger red dots indicate wells studied. Modified after Atkinson and Fagan, 2001). **76**
- Fig. 4.3:** Stratigraphy and tectonic evolution of the Labrador Shelf, including major unconformities (Modified after Enachescu, 2006). **78**
- Fig. 4.4:** Bjarni Formation core logged from well Ogmund E-72. **83**
- Fig. 4.5:** Bjarni Formation core logged from well Herjolf M-92. **86**
- Fig. 4.6:** *A.* Bjarni Formation core logged from well Bjarni H-81 and *B.* Bjarni Formation core logged from well North Bjarni F-06. **87**
- Fig. 4.7:** Bjarni Formation core logged from well Roberval K-92. **90**
- Fig. 4.8:** Bjarni Formation core logged from well North Leif I-05. **91**
- Fig. 4.9:** Ternary diagrams plotted with individual samples from studied wells containing the Bjarni Formation sandstone. *A.* QFL plot (modified from Pettijohn, 1975; Nichols, 1999); *B.* Tectonic setting QFL ternary plot (modified from Dickinson et al., 1983). **93**
- Fig. 4.10:** Samples plotted on ternary diagrams indicating compositional changes within wells. See Figure 4.9 for QFL compositional names. **94**
- Fig. 4.11:** Total well authigenic minerals and intragranular porosity point count (Point Cts.) histograms of the sandstone from the studied Bjarni Formation core intervals; oxides (ox), calcite cement (cal), kaolinite (kaol), pyrite (py), quartz overgrowths (og), and intragranular porosity (IGP). Well numbers are located in the upper right corner of histograms. Modified after Atkinson & Fagan, 2001. **100**
- Fig. 4.12:** Porosity point count histograms of the sandstone from the studied Bjarni Formation core intervals; total porosity (TP), intergranular porosity (IP), and intragranular porosity (IGP). Well numbers are located in the upper right corner of histograms. Modified after Atkinson & Fagan, 2001. **106**

**Fig. 4.13:** Paragenetic sequence of diagenetic events based on petrography, stratigraphic well depth, and order of occurrence. Dashed lines are assumed events and line thickness indicates relative frequency of authigenic phase. 109

## LIST OF PLATES

### PLATE NUMBER

### PAGE NUMBER

**Plate 3.1:** Core images from, *A.* Gudrid H-55 (~2679.0 m), *B.* Roberval K-92 (~3871.5 m), and *C.* Indian Harbour M-52 (3954.6 m - 3955.2 m). Photo's courtesy of Matthew Harvey. 44

**Plate 3.2:** Plain-polarized light and cathodoluminescence photomicrographs of dolomites from Roberval K-92. *A-C*, Calcite filling intra-crystalline, vuggy, and micro-fracture porosity, respectively, *D*, D1 with interstitial and vuggy porosities, *E - H*, counter-part plain-polarized light and cathodoluminescence (showing zoning and smoothed edges from late dissolution). 49

**Plate 3.3:** Plain-polarized light and cathodoluminescence photomicrographs of dolomite and calcite from Gudrid H-55. *A-C*, calcite filling interstitial and vuggy porosity, *D*, oxides in a vug, *E-H*, PL and counterpart CL images showing calcite invading porosities. 50

**Plate 3.4:** Plain-polarized light and cathodoluminescence photomicrographs of dolomites and calcites from Indian Harbour M-52. *A & B*, micritic and fibrous cements, *C*, dolomite 1, *D*, algal aggregates and micritic cement, *E & F*, calcite 3 invading micritic cements, *G & H*, PPL and CL images of dolomite 1. 56

**Plate 3.5:** Photomicrographs showing different phases of porosity development. *A-D*, inter-crystalline and vuggy porosity in Roberval K-92, *E*, vuggy porosity in Gudrid H-55 and *F*, vuggy porosity from PD3. All images taken in plain-polarized light, except *A*, taken in cross-polarized light. 58

**Plate 4.1:** Images of Bjarni Formation core taken from the six wells studied. *A.* Ogmund E-72, core 2 (~2240 m - 2237 m) with possible random igneous boulder (arrow) amongst flaser to wavy laminations; *B.* North Bjarni F-06, core 1 (~2451.5 m) with dashed line indicating a calcite cemented horizon and arrow pointing to pyrite; *C.* Bjarni H-81, core 1 (~2156 m) indicating small scale faulting of wavy laminations (arrow); *D.* Herjolf M-92, core 1 (~2632 m - 2633 m) with dashed lines indicating cemented horizons and an arrow indicating pyrite; *E.* Roberval K-92, core 2 (~3097 m - 3100 m) with conglomeratic sandstone and inclined lenticular to wavy laminations; and *F.* North Leif I-05, core 1 (~3110.5 m) with arrows showing coal stringers and fragments. 84

**Plate 4.2:** Photomicrographs of quartz, lithic, accessory, and diagenetic minerals. *A.* (05-1-4), monocrystalline quartz (Qm); *B.* (81-1-1), monocrystalline quartz (Qm), oxides (ox), chlorite (chl), calcite cement (cal), and sillimanite (sil) ; *C, F (XPL).* (72-2-2), igneous grains (ig), monocrystalline quartz (Qm), biotite (bt), and clinoproxene (cpx); *D.* (72-2-1), igneous grains (ig), polycrystalline and monocrystalline quartz (Qp, Qm) and; *E.* (HJ-1-1), biotite (bt) and polycrystalline quartz (Qp). 95

**Plate 4.3:** Plain and cross-polarized light photomicrographs of potassium (kfld) and plagioclase (plg) feldspars. *A-A'* (72-2-1), cross-hatch twinning (*A'*) and (sericite) altered grains (dusty-brown; *A*); *B-B'* (81-1-3), cross-hatch twinning (microcline) and; *C-C'* (HJ- 3-1), perthite and simple twinning. 97

**Plate 4.4:** Photomicrographs of diagenetic minerals. *A. & B.* (92-C2-1a), inter- and intragranular-filling kaolinite (IP, IGP, kaol); *C.* (HJ-2-1), intergranular ferroan calcite cement (cal) and filling relict (intragranular porosity) feldspar grains ; *D.* (92-C2-1a), quartz overgrowths (Og); *E.* (HJ-5-3), pyrite (py) and intragranular porosity (IGP) in reflected light and; *F.* (HJ-5-3), pyrite (py), intragranular porosity (IGP), and calcite altered potassium feldspar (kfld-cal). 103

**Plate 4.5:** Photomicrographs of diagenetic minerals. *A (PL) & B (XPL)* (06-1-2), intergranular-filling non-ferroan (red-pink) calcite (IGP, cal); *C.* (72-2-2), intragranular-(IGP) filling calcite (cal); *D.* (HJ-2-1), intergranular-filling ferroan calcite (purple) and altered biotite (bt-ox); *E.* (XP; HJ-2-1), intergranular ferroan calcite and calcite altered potassium feldspar (kfld-cal) and; *F.* (HJ-1- 2), oxide-rimmed concavo-convex (cc) boundary between a larger igneous grain (ig) and smaller feldspar (fld) and monocrystalline quartz grains (Qm). 104

## LIST OF TABLES

<u>TABLE NUMBER</u>	<u>PAGE NUMBER</u>
<b>Table 2.1:</b> List of core and exploration wells studied. Also included are core depths and number of samples used for petrography, geochemistry, and fluid inclusions. Carbonate core is shaded blue while siliciclastic core is shaded yellow.	25
<b>Table 3.1:</b> Nomenclature used for naming dolomites (e.g., Azmy et al., 2001).	47
<b>Table 3.2:</b> Trace element, stable isotope, and strontium geochemical data from sampled dolomite and calcite generations from Roberval K-92, Gudrid H-55, and Indian Harbour M-52.	52
<b>Table 3.3:</b> Averages, ranges, and overall $^{87}\text{Sr}/^{86}\text{Sr}$ average for each cement sampled.	53
<b>Table 3.4:</b> Homogenization temperatures from D2 cements, taken from Roberval K-92 and Gudrid H-55.	53
<b>Table 4.1:</b> Core numbers, thicknesses, thin-sections, and well names used to study the Bjarni Formation sandstone.	81
<b>Table 4.2:</b> Well samples of QFL point count data from the Bjarni Formation sandstones normalized to 100%. Samples are arranged by stratigraphic depth. For subbasin locations, see <b>Figure 4.2</b> .	96
<b>Table 4.3:</b> Plagioclase and potassium feldspar point count ratios (P/K). Well averages are in bold text.	99
<b>Table 4.4:</b> Total and well-average (bold) diagenetic point counts. <b>OG</b> = quartz overgrowths; <b>IGP</b> = intragranular porosity.	101
<b>Table 4.5:</b> Point counts and averages (bold) for different porosity styles, arranged by stratigraphic depth. <b>IP</b> = intergranular porosity; <b>IGP</b> = intragranular porosity; <b>TP</b> = total porosity.	107
<b>Table 4.6:</b> Bjarni Formation sandstone sample temperatures. Calculated from 3.06°C per 100 m of stratigraphic depth (Issler, 1984).	114

## CHAPTER 1 INTRODUCTION

### 1.1 CONTEXT

Offshore Newfoundland & Labrador is located in northeastern Canada and contains several prolific hydrocarbon-producing basins with complex petroleum systems (**Fig. 1.1A**). One of these Mesozoic basins, the Jeanne d'Arc includes the producing Hibernia, Terra Nova, and White Rose fields, and a series of undeveloped smaller oil and gas fields. Other basins and subbasins of the Mesozoic rift trend need to be further explored and studied to evaluate their structural and tectonic setting, lithostratigraphy, distribution of reservoir and source rocks and petroleum potential (i.e. petroleum system). One such basin is the Hopedale Basin of the Labrador Sea, located just north of the Jeanne d'Arc and Orphan basins (**Fig. 1.1B**).

The Labrador Sea sedimentary area consists of a Mesozoic-age rift margin covering an area of approximately 175 000 km<sup>2</sup> with a maximum width of 320 km, extending from the northeast Newfoundland Shelf to the Hudson Strait (Keen & Piper, 1990; Enachescu, 2006). The Saglek and Hopedale basins constitute the entirety of the shelf, slope and deepwater and have been the site of past petroleum exploration in their shallower parts.

The two basins are separated by the Okak Arch (**Fig. 1.2**). The Hopedale Basin, the focus of this study, is the southerly basin, extending 500 km from the Okak Arch to the Cartwright Transfer Fault Zone to the south (Enachescu, 2006; Martin, 2007; Stead, 2008).

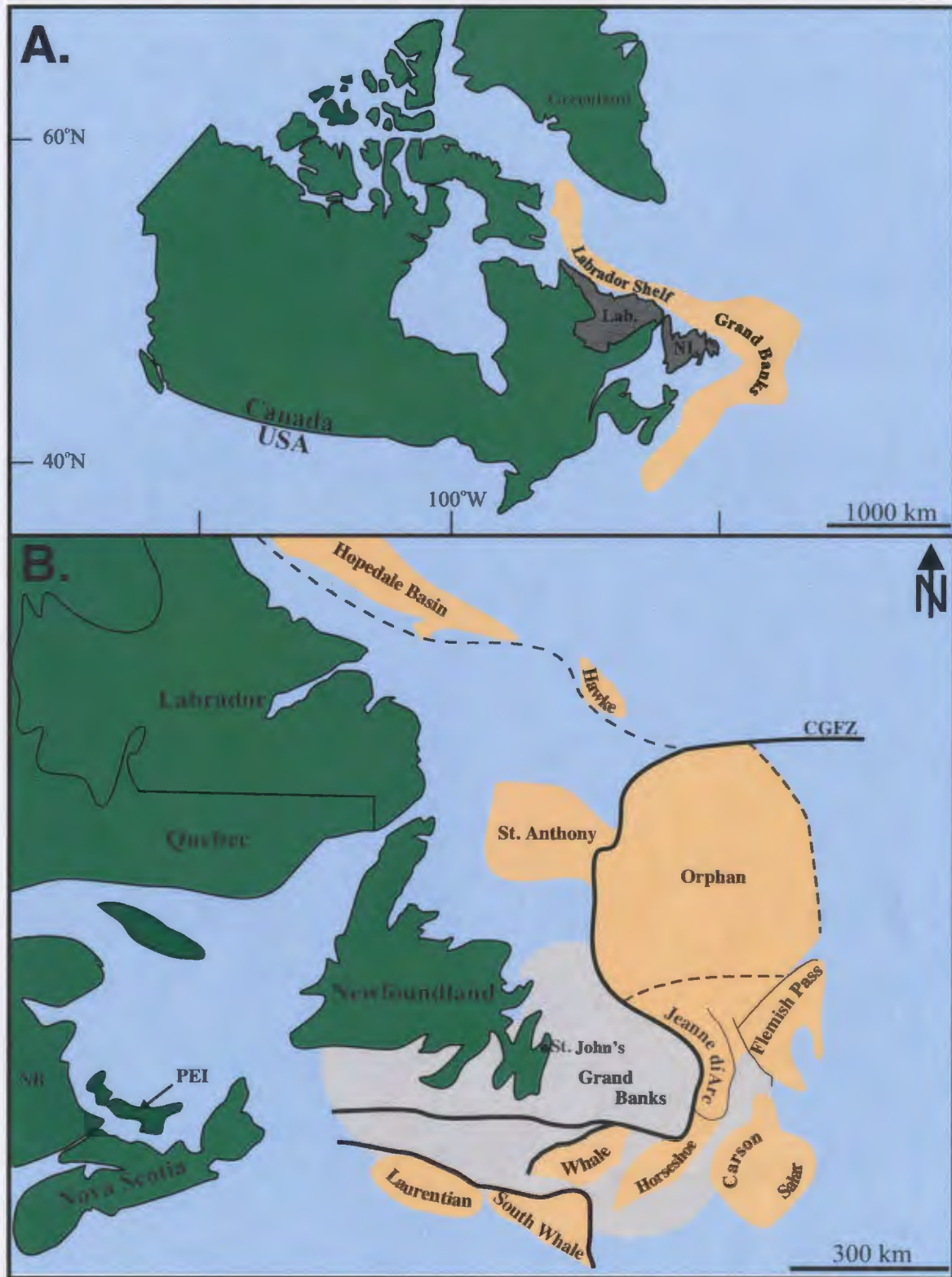


**Fig. 1.1.** *A.* Map of Canada highlighting Newfoundland and Labrador (dark grey) and the offshore sedimentary basins (yellow). *B.* Mesozoic sedimentary rift basins (all the way to 300 m water depth; yellow) of Newfoundland and Labrador (after Enachescu, 1992).

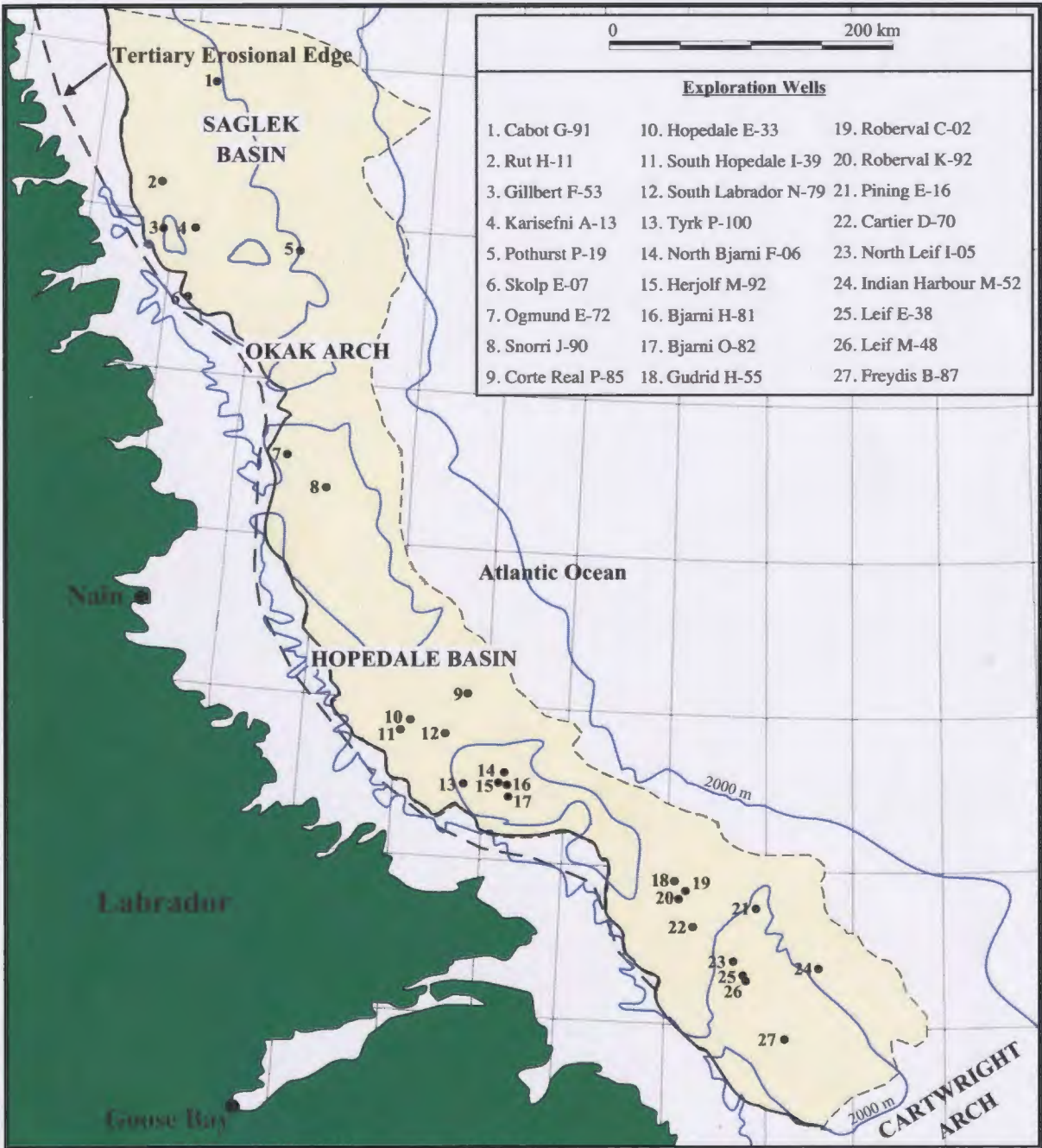
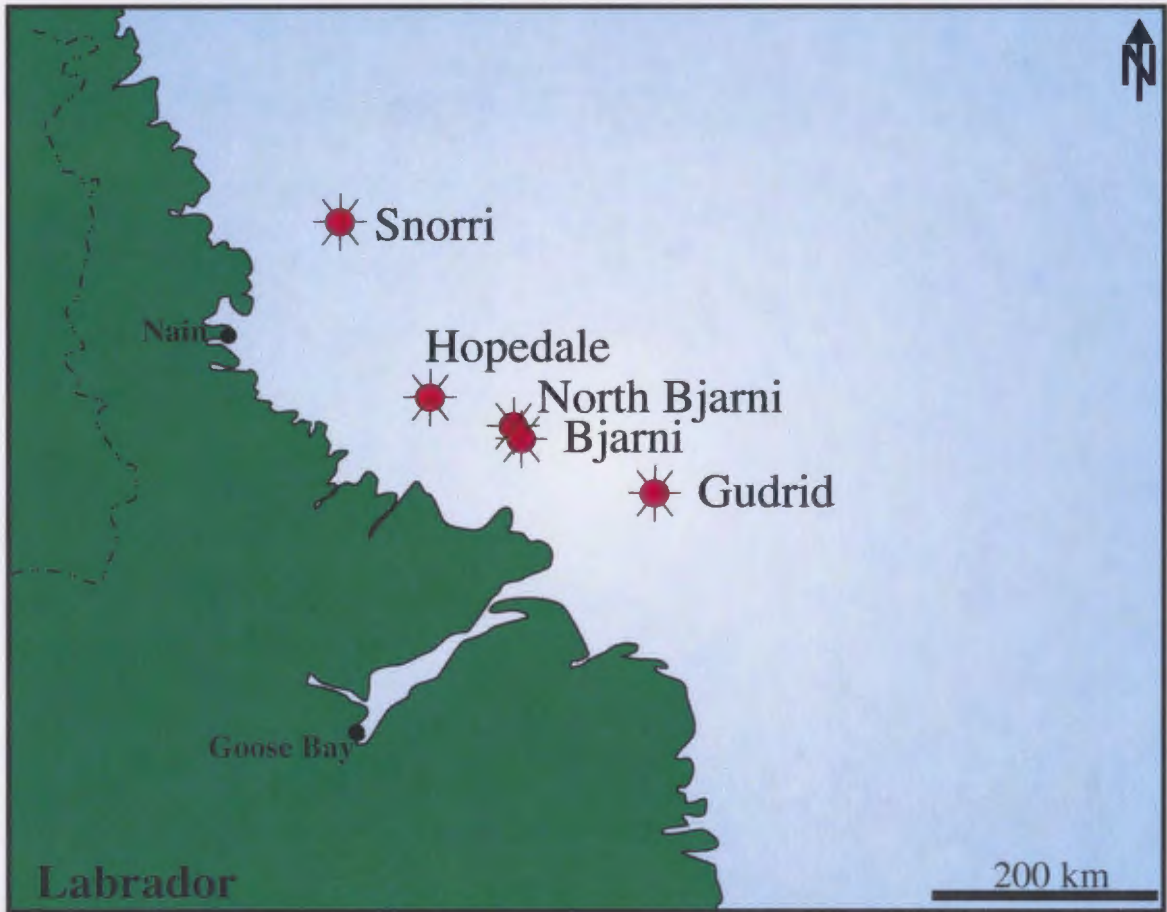


Fig. 1.2. Exploration wells on the Labrador Shelf numbered from the Saglek Basin (north) to the Hopedale Basin (south). Modified after Atkinson & Fagan, 2001.

The Labrador shelf has prominent characteristics consistent with that of Atlantic-type passive margins as described by Bally (1981): the continental shelf is flat compared with the steeply dipping continental slope and the area of the shelf is made up of a large sedimentary prism on top of extended cratonic crust, whereas the outer portion of the sedimentary prism lies on early Tertiary and Late Cretaceous peridotites and basalts (Balkwill et al., 1990; Enachescu, 2006; Martin, 2007).

Approximately 27 exploration wells were drilled and more than 100 000 line km of seismic data acquired from the Canadian side of the Labrador Sea. In the Hopedale Basin only 16 wells are significant from an exploration point of view (**Fig. 1.2**; Balkwill et al., 1990; Enachescu, 2006). Hydrocarbons, existing mainly as gas and gas condensates, have been discovered in 5 of these wells (**Fig. 1.3**): Snorri J-90, Hopedale E-33, North Bjarni F-06, Bjarni O-82, and Gudrid H-55. Reserves are estimated at 4.2 Tcf of natural gas and 123 million barrels of NGL (CNLOPB; Atkinson & Fagan, 2001). Play types include both siliciclastic (e.g. North Bjarni) and carbonate reservoirs (e.g. Gudrid H-55). North Bjarni has reserves at 2.2 Tcf of gas and 82 million barrels of NGL (CNLOPB; Atkinson & Fagan, 2001),

Currently there is only minor exploration interest in the Hopedale Basin due to its remote location and its vulnerability to natural hazards including high frequency of icebergs, long lasting pack ice and variable weather (Enachescu, 2006). These natural hazards have contributed to there being no exploration drilling or land sales in over 25 years. However, increasing demand for gas, high commodity prices and new drilling and production technologies will encourage companies to develop the existing discoveries



**Fig. 1.3.** Five exploration wells with hydrocarbons on the Labrador Shelf. Modified after CNLOPB

and explore for new ones (Martin, 2007). A Hopedale Basin landsale including 4 large exploration blocks is to be concluded during the summer of 2008 (Enachescu et al., 2008).

## **1.2 SCOPE & OBJECTIVES**

The principal aims of this thesis project are to study, in detail, both carbonate and siliciclastic reservoir intervals on the Labrador Shelf using petrographic and geochemical methods. An in-depth study of diagenesis and porosity evolution can provide both qualitative and quantitative insights into the geological evolution of these intervals and help to discuss reservoir characterization. By understanding reservoir quality, a potential petroleum system can be evaluated, and in this case, at the microscopic-scale. Within the constraints of the database, diagenesis, porosity and associated reservoir quality are evaluated in terms of their dependency on burial depth and stratigraphic/geographic location within the basin.

Systematic investigations into the details of diagenesis and associated porosity development have not been published to-date for the basin. Thus, a reservoir characterization study of the Labrador Shelf is of great relevance to provide further insight into this frontier exploration basin.

Specific thesis objectives include:

1. An understanding and reconstruction of diagenetic history in carbonate and siliciclastic reservoir intervals;
2. The nature and development of porosity types;

3. A comparison of diagenesis and porosity evolution at different stratigraphic levels across several well locations and;
4. The refinement, if possible of the unconfirmed broad age estimates of the drilled carbonate reservoir intervals.

This thesis is presented in a manuscript-style format, with the main body of the thesis (Chapters 3 and 4) containing separate papers (to be published at a later date) on the region's main reservoirs; Paleozoic carbonates and Early to Mid Cretaceous siliciclastic sediments (Bjarni Formation sandstone), respectively. They were separated into individual manuscripts because of the natural division and different methodologies used between the rock types; covering the same theme of diagenetic effects on porosity development and reservoir characterization. Chapters 1, 2, and 5 are meant to provide an introduction to the topics covered, general methodologies, and collective conclusions, respectively.

### 1.3 DIAGENESIS

Diagenesis can be described as the sum of all sediment changes from the moment of deposition, through lithification, and may lead to incipient metamorphism (**Fig. 1.4**). It includes chemical and biological reactions such as compaction, cementation, dissolution, recrystallization, and organic degradation (Larsen & Chilingar, 1979). Shallow burial diagenesis is often referred to as *eogenesis*, occurring within relatively short period after deposition. During this time, interstitial fluids are still in contact with the overlying water mass (Morrow & McIlreath, 1990). *Mesogenesis*, refers to intermediate burial where pore space has been occluded from overlying water mass, producing a closed system (Morrow

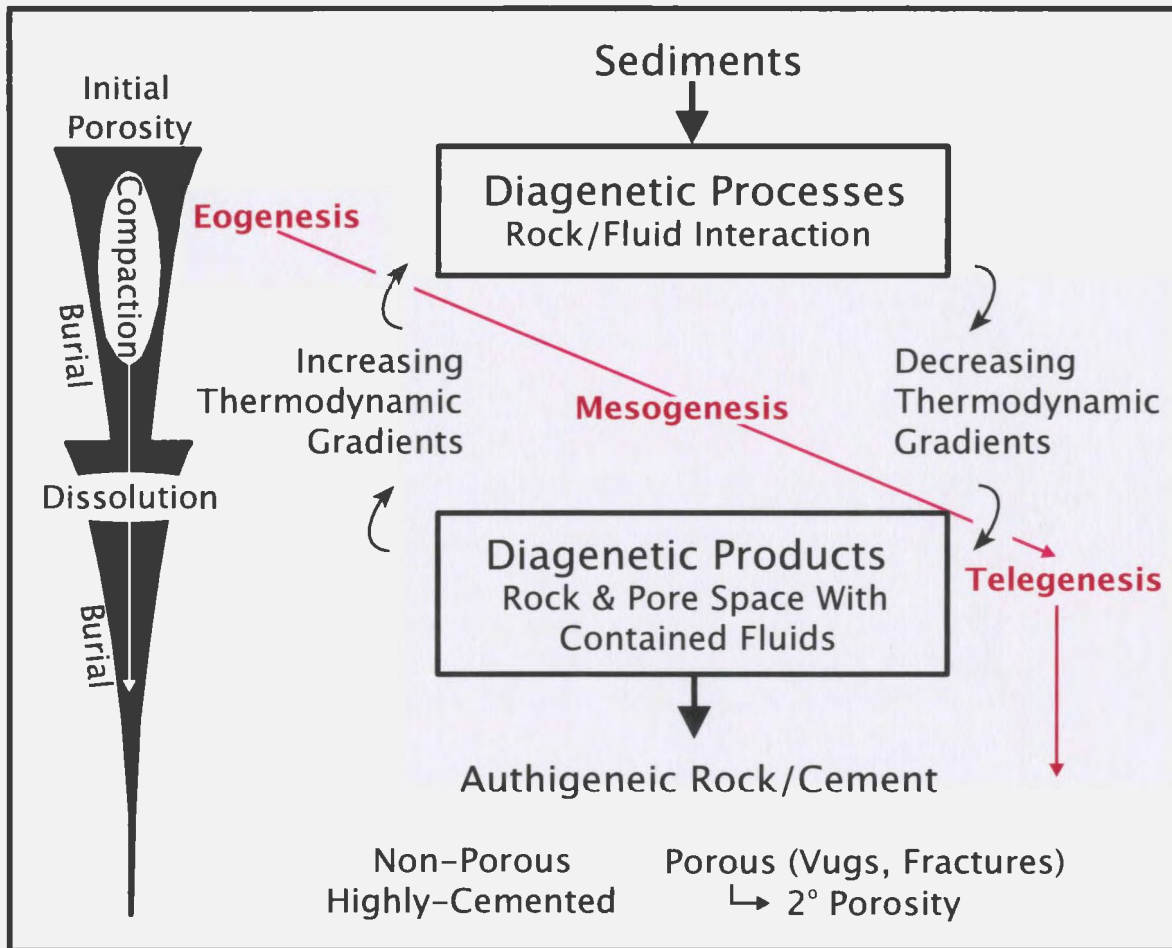


**Fig. 1.4.** Diagram indicating processes involved with diagenesis and diagenetic products (i.e. The Diagenetic Cycle). Also shown is the affect of diagenesis on porosity with burial. Modified after Morrow and McIlreath, 1990.

& McIlreath, 1990). When diagenesis is directly related to fluid movement from tectonic processes, such as uplift, it is called *telogenetic*, referring to the end or last diagenetic phase.

Ultimately, chemical composition of rocks is a reflection of the diagenetic history superimposed on their original composition (Azmy et al., 2001). In carbonate and siliciclastic successions, during the process of progressive burial, geochemical and mineralogical changes occur as fluid interaction with sediments modify trace elements (cf. Chapter 3), stable isotopes and mineral phases (cf. Brand & Veizer, 1980; Brand & Veizer, 1981).

The study of diagenesis within hydrocarbon-bearing reservoirs is important when classifying or determining their quality because diagenesis can enhance or reduce porosity (Fig. 1.4). For example, calcareous cements can act as barriers or baffles to fluid; clay mineralization can occupy pore throats reducing effective porosity. Arguably, porosity is one of the most important components in evaluating reservoir quality.

### **1.3.1 Carbonate Diagenesis**

Carbonate diagenesis is controlled by three general burial environments (Fig. 1.5). The first is marine diagenesis, occurring on the sea floor (i.e. sea floor diagenesis). Carbonates are initially deposited in this environment, forming hard and soft carbonate grains such as ooids and peloids, respectively. Micritic ( $\text{MgCO}_3$ ), fibrous ( $\text{MgCO}_3$ ), needle, and botryoidal cements are indicative of sea floor burial. Following sea floor diagenesis, the meteoric (or near surface) environment affects sediments due to freshwater from the vadose and phreatic zones (i.e. dissolution). In this environment

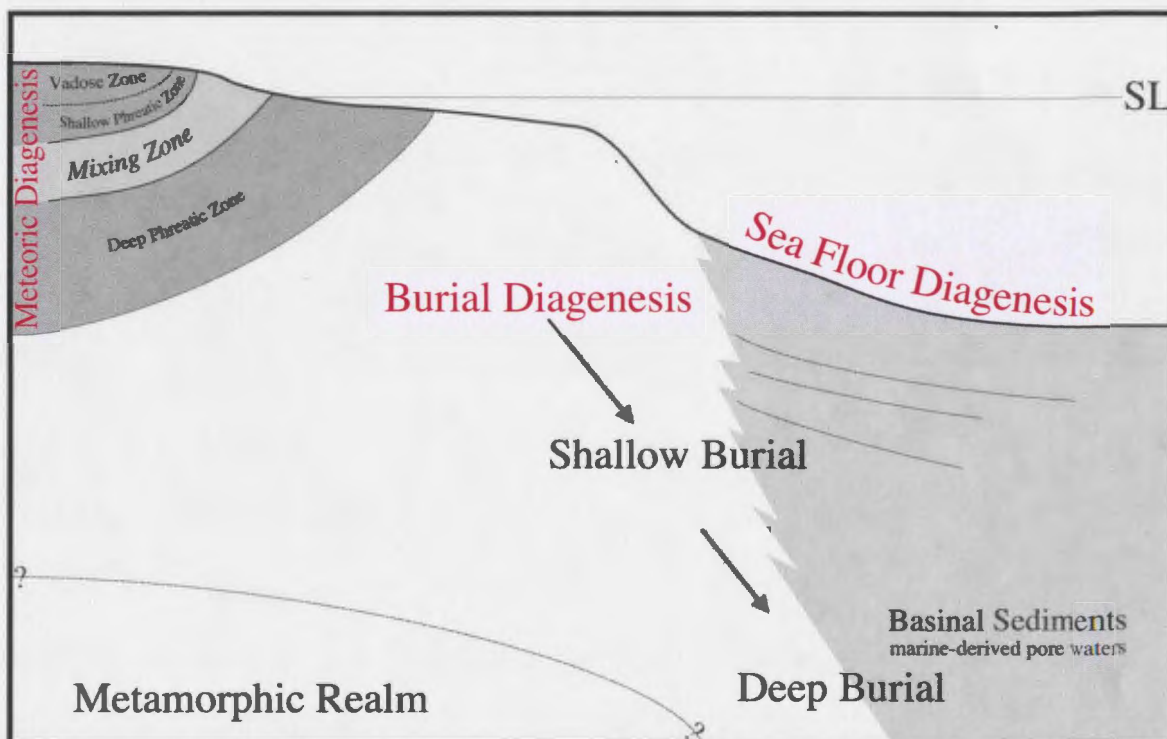


**Fig. 1.5.** Schematic illustration of the diagenetic burial environments (red). Modified after Choquette and James, 1990.

sediments get exposed to freshwater and additional circulating marine or saline enriched waters. Specifically, where the two waters meet, is called the mixing zone, where early dolomitization can occur (Morrow, 1978). Finally, in the burial diagenetic environment (isolated from the shallow phreatic), at a kilometer to several kilometers depth, sediments are in contact with pore waters of multiple potential origins. Cement types such as mosaic/drusy, poikilotopic calcite, and saddle dolomite (Choquette & James, 1990) are responsible for porosity reduction. Additionally, stylolitization and dissolution (i.e. solution porosity) are common in the shallow to deep burial realms (Choquette & James, 1990).

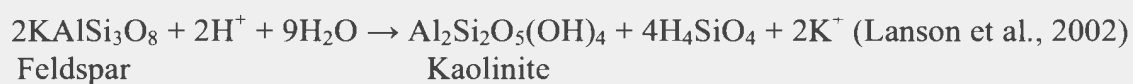
Progressive burial enriches some trace elements (e.g. Fe and Mn) in the successor phase (Veizer, 1983; Choquette & James, 1990; Brand & Veizer 1981) as a consequence of reducing conditions. For example, deep burial calcite cements are commonly ferroan (>500 ppm Fe<sup>2+</sup>) and enriched in Mn<sup>2+</sup> (>100 ppm) due to precipitation from at least moderately reducing pore water (Azmy, 1992)

Stable isotopes such as  $\delta^{18}\text{O}$ , are affected diagenetically with progressive burial and become depleted in the successor phase (Choquette & James, 1990), showing highly negative values. However,  $\delta^{13}\text{C}$  is considered to be less diagnostic of diagenetic alteration because of the relatively invariable content of dissolved CO<sub>2</sub> in a fluid with depth and temperature (cf. Brand and Veizer, 1981). The depletion of  $\delta^{18}\text{O}$  becomes occluded from successive mineral reactions and is used as a proxy for understanding diagenesis with progressive burial (cf. Brand and Veizer, 1981).

### 1.3.2 *Siliciclastic Diagenesis*

In siliciclastic-dominated reservoirs the most permeable units generally are sandstones, which become the conduit for the migrating fluids (Hutcheon, 1990). Siliciclastic diagenesis is controlled by numerous physical and chemical processes that include lithology, sediment texture and mineralogy, burial rate and depth, sedimentary and tectonic environments, climate, and organic activity (**Fig 1.5**).

Like carbonate diagenesis, authigenic cementation, secondary porosity, compaction, and hydrocarbon generation are some of the products during progressive burial. However, in siliciclastic depositional systems there are different authigenic minerals and mineral reactions. These minerals are authigenic quartz (overgrowths or cements), clay minerals (e.g. kaolinite, illite, smectite, chlorite group), calcite cements (e.g. siderite), oxides (e.g. iron oxide), and sericite. Authors have documented paragenetic sequences for the appearance and disappearance of these minerals, resulting in a genetic overlap (cf. Salem et al., 2005; Lima & De Ros, 2002; Khidir & Catuneanu, 2003). This is attributed to the multiple concurrent reactions that occur between the pore water and the allogenic minerals in the sandstone (Hutcheon, 1990). For example, during the process of feldspar dissolution, kaolinite can precipitate according to:



Similar reactions, from adding water or hydroxide to the system, will produce illite/muscovite and additional quartz, where illite can also react with water to produce a

hydrous kaolinite. Ultimately, there is no consensus on the factors governing clay mineral formation other than the mineral reactions themselves (Lanson et al., 2002).

Stable isotopes and trace elements are affected diagenetically and can be used in siliciclastic systems as proxies for burial depth, where the degree of diagenetic alteration and possible fluid source can be understood (cf. Brand and Veizer, 1981; Brand, 1986; Ayalon & Longstaffe, 1995; Khidir & Catuneanu, 2003; Normore, 2006).

#### **1.4 POROSITY**

Porosity is a measure of void spaces within a given volume of rock that can develop syngenetically (e.g. primary) or epigenetically (e.g. secondary) during burial. Porosity development is a complex process and is related to the depositional environment and, on a larger scale, to the tectonic setting.

The porosity development in carbonate rocks can be more complex because of their biologic origin and growth of framework of reefs, where porosity is created within grains, in addition to progressive burial (Choquette and Pray, 1970; Azmy, 1992). Porosity types can be described as a) fabric selective, including interparticle, intraparticle, intercrystalline, fenestral, moldic, shelter, and framework porosity, and b) non-fabric selective, which includes fracture, channel, vug, cavern, and stylitic (Choquette and Pray, 1970).

In siliciclastic rocks, the initial porosity is affected by the uniformity of grain size, shape of the grains, method of deposition and manner of packing, and compaction (Pettijohn, 1975). However, when considering diagenesis, initial porosity can often be

destroyed with further burial. For example, clay minerals, such as kaolinite, smectite, illite, and chlorite groups play an important role in fluid flow and reservoir quality. They can adhere to the surface of grains and destroy porosity (cf. Ramm & Bjørlykke, 1994; Brown & Ransom, 1996; Thyne et al., 2001). Also, quartz overgrowths or quartz cementation inhibit porosity in siliciclastic reservoirs (cf. Coalson et al., 1985; Kierkegaard, 1998). Other processes, such as calcite cementation or concretion growth, and compaction of sediments with increasing burial depth can also reduce porosity and diminish reservoir quality.

With continued basin evolution (i.e. sedimentation, burial, compaction, fluid movement), secondary porosity can be created. It is commonly an artifact, for example, of grain or carbonate shell dissolution, producing moldic or vuggy (intra- or intercrystalline) porosity (cf. Normore, 2006).

Effective porosity (cf. Koponen et al., 1997) is a critical component in hydrocarbon-bearing reservoirs. A fluid, such as hydrocarbons, needs to have the ability to flow freely between pores and pore throats (i.e. effective porosity). Therefore, if pores and pore networks are reduced as a result of diagenetic barriers, the overall reservoir quality is diminished (i.e. ineffective porosity).

## **1.5 TECTONIC EVOLUTION, STRUCTURAL ELEMENTS, AND STRATIGRAPHY**

### ***1.5.1 Tectonic Evolution***

The evolution of sedimentary basins is linked to Wilson Cycles - opening and closing of ocean basins - producing orogenies (e.g. Appalachian) and rift systems. The

latest Atlantic region cycle started in Late Triassic with intra-continental rifting. The development of the North Atlantic Margin (i.e. Nova Scotia-Newfoundland-Labrador) occurred as a consequence, during a series of zipper-like opening episodes, commencing no later than 160 Ma (Mid Jurassic) when North America separated from Africa, forming the present day Scotian Margin. Subsequently, the separation of North America and Iberia at, or before 125 Ma (Early-Mid Cretaceous), formed the Southern Newfoundland margin. Another stage of North America-Europe separation (120Ma) resulted in the creation of the present day Northern Newfoundland-Ireland conjugate margins. The latest stages of breakup took place when a) North America separated from Greenland at approximately 70 Ma (Late Cretaceous), resulting in the Labrador and Greenland Margins, which was followed by b) the Greenland and Europe separation no later than 55 Ma (Eocene; Loudon, 2002; Martin, 2006).

### ***1.5.2 Structural Elements***

The regional structural elements in the Labrador Margin include large northwest trending master faults, dipping both sea- and landward, linked to each other via smaller transfer faults, and rotated horst blocks and half grabens (**Fig. 1.6**; Balkwill & McMillian, 1990).

The Labrador Shelf differs from the Scotian and Newfoundland margins as it has not been affected by salt diapirism. As a result, its structural elements (extensional, inversion and compressional gravity sliding features) were created wholly as a result of rifting and ocean spreading during the margin's evolution (Enachescu, 2006).

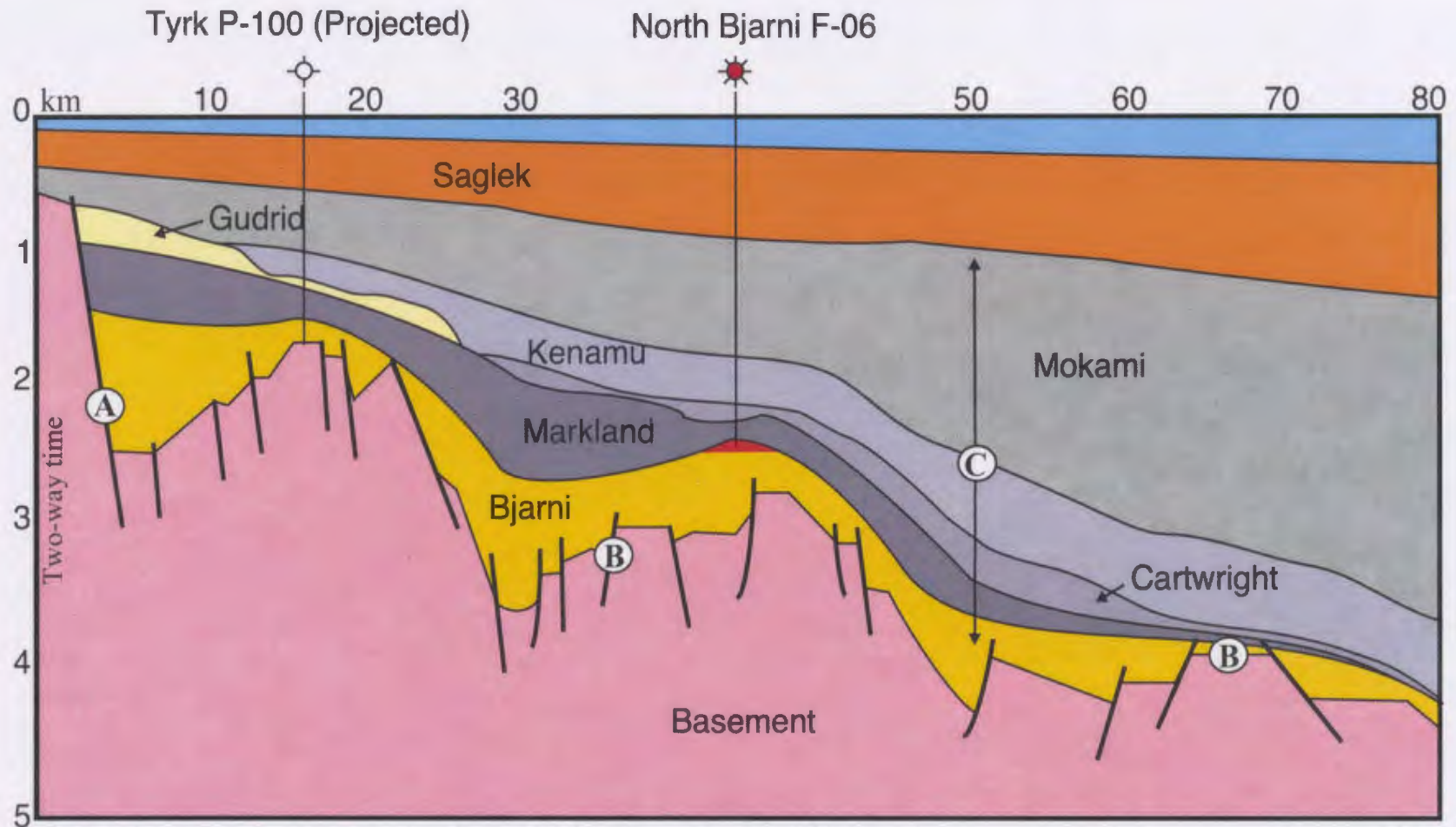


**Fig. 1.6.** Two-way time cross-section through the North Bjarni F-06 Field indicating the main nearshore structural elements of the Hopedale Basin, Labrador Shelf. **A.** Seaward-dipping, orthogonally trending master fault; **B.** Horst-Graben and; **C.** Seaward-dipping Cretaceous and Tertiary sediments onlapping with pre-rift basement. Modified from GSC, 1987; Atkinson and Fagan, 2001; Martin, 2007; Enachescu et al., 2007.

Three subdivisions of the Hopedale Basin, the Hamilton, Harrison, and Nain subbasins were proposed by Enachescu (2006). Subbasins contain parallel ridges as well as large fault blocks and rotated half grabens. These structural elements are separated along strike by transfer faults (with an offset of 10 - 15 km) and accommodation zones.

There are systematic changes in the landward rift system boundary along the Labrador margin. The rift system boundary changes from a hinge zone to a well-expressed basin-bounding fault along strike. Enachescu et al. (2006) also suggest that Mesozoic sedimentary infill onlap/terminate against this hinge zone/fault bound anywhere from 80 to 100 kilometres from the modern-day shoreline. Tertiary-age beds onlap the prerift basement around 40 to 75 kilometres from the present day shoreline on a lineament approximately parallel to the modern coastline (Enachescu et al., 2006; Martin, 2007).

### **1.5.3 Stratigraphy**

The Labrador Shelf stratigraphy is a reflection of the region's tectonic evolution, for simplicity were divided into three major evolutionary sequences: 1) Prerift-containing Precambrian and Paleozoic rocks; 2) Synrift-including Berriasian to Albian volcanics and clastic rocks and; 3) Postrift-consisting of thick clastic sedimentary rocks. All of three are separated by major unconformities (**Fig. 1.7** and Balkwill et al., 1990; Enachescu, 2006). Sediment lithologies are detailed by Umpleby (1979), McWhae et al. (1980), and Balkwill et al. (1990).

The prerift stage contains Paleozoic limestones, dolomites and clastics (**cf. Chapter 3**) overlaying Precambrian metamorphic basement rocks. This basement was

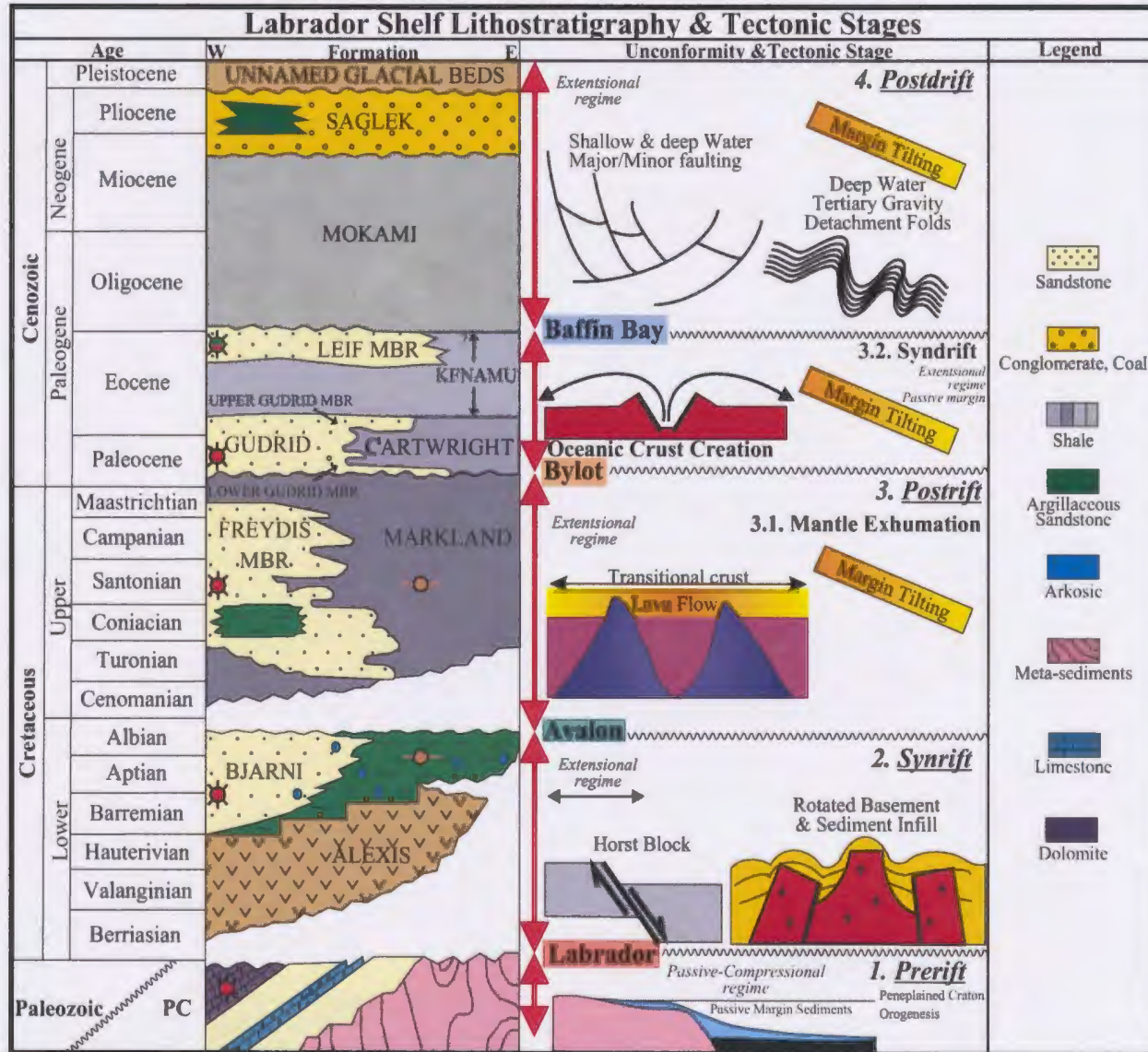


**Fig. 1.7.** Litho-Tectono Stratigraphy of the Labrador Shelf. Modified after Enachescu, 2006; Martin, 2007; McWhae et al., 1980.

partially peneplained before the Early Cretaceous Labrador phase rifting (i.e. Labrador Unconformity; **Fig. 1.7**; Enachescu et al., 2005; Enachescu, 2006; Martin and Enachescu, 2007).

Basement lithologies and ages are noted from exploration core and onshore craton exposures observed in Labrador (**Fig. 1.8A**) and southern Baffin Island. Lithologies are arranged in litho-tectonic domains ranging from the Grenville (southern Labrador) to the Makkovik (south-central coast), and Nain (central to northern coast) provinces. The Grenville Province contains metasedimentary and plutonic rocks with radiometric ages of approximately 1 Ga, the Nain Province contains granitic gneisses (2.5 Ga) that include older (3.6 Ga) Archean relicts (Balkwill and McMillan, 1990), and the Makkovik Province contains Archean craton rocks, some of which are Paleoproterozoic reworked, and calc-alkaline granitoid plutons (Wardle and Van Kranendonk, 1996; Ketchum et al., 2002).

The prerift Paleozoic carbonate sequence includes granitic intrusions, various volcanics, shelf clastics and evaporates. Paleozoic carbonates are described as a unmetamorphosed platform facies, distributed in the northern rim of the Canadian Maritime region, the St. Lawrence Platform (along the Gulf of St. Lawrence), extending to Michigan and as far south as Texas (**Fig. 1.8B**; Bell & Howie, 1990; Atkinson & Fagan, 2001). Between the Gaspé Peninsula and northwestern Newfoundland, the succession thickens southwards (Anticosti Basin). These rocks are exposed in southern Quebec, southeastern Labrador, on Anticosti Island, and in northwestern Newfoundland (Bell & Howie, 1990).

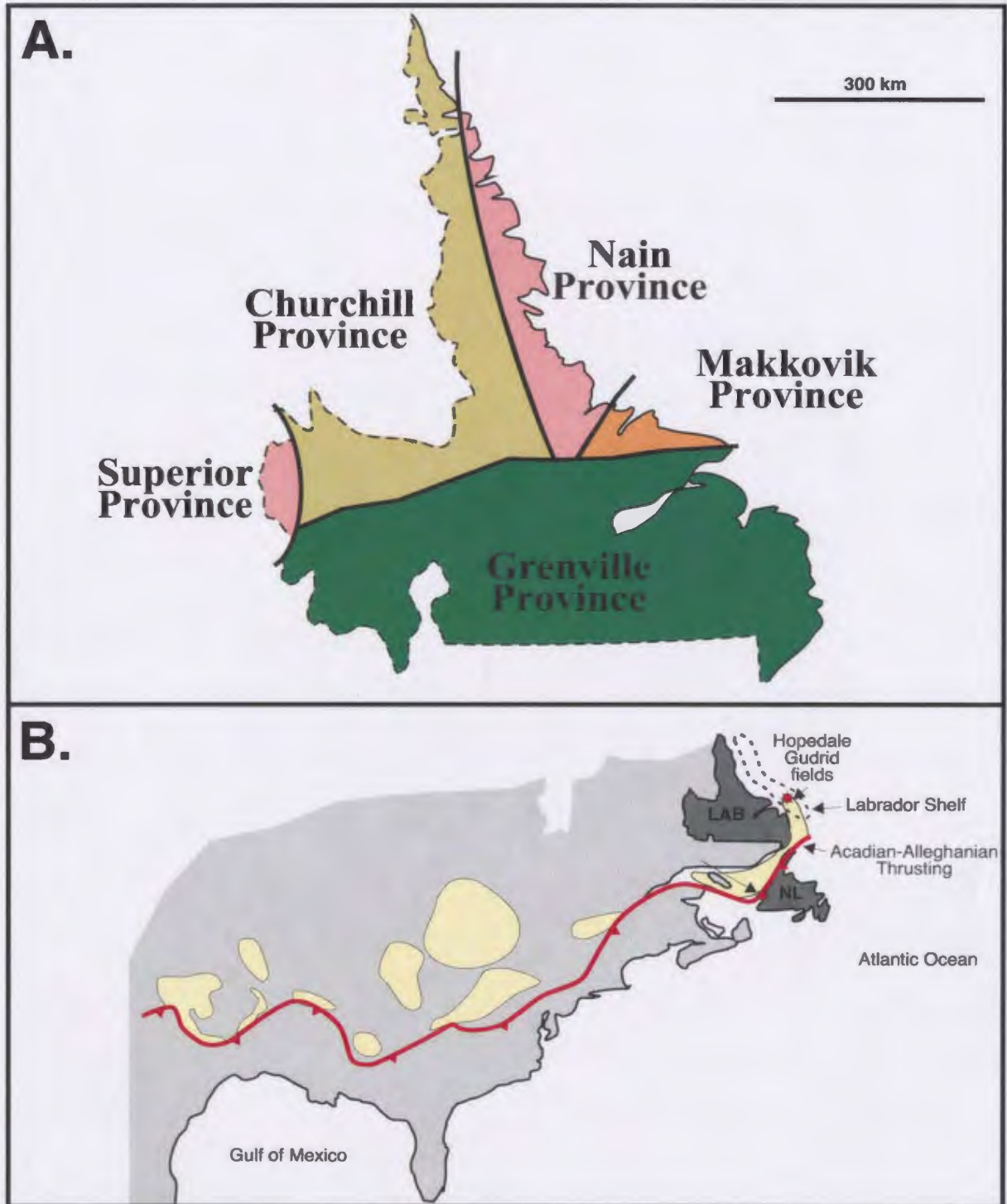


**Fig. 1.8.** *A.* Generalized geological province map of the Archean-Proterozoic craton in Labrador (modified after the Government of Newfoundland and Labrador, 2008). *B.* Approximate locations of Paleozoic basins (yellow) extending from the Labrador Shelf to Texas (modified from Atkinson & Fagan, 2001).

During the synrift stage, the Alexis and Bjarni formations filled the rift landscape containing grabens, horsts, rotated blocks and accommodation zones. The synrift sequences are contained between the Labrador and Avalon unconformities (**Fig. 1.7**). The Alexis Formation consists of volcanics (basalts and dykes) and epiclastic sediments, which may have been altered hydrothermally (McWhae et al., 1980). The Bjarni Formation (**cf. Chapter 4**) contains medium to coarse-grained sandstones, of alluvial to fluvial settings, with some finer-grained lacustrine sands and muds.

The postrift tectonic stage was divided by Enachescu (2006) into a mantle exhumation (predrift), drift, and postdrift substages. These were used by Martin (2007) and Stead (2008) for seismic stratigraphic studies and mapping of structural elements in the Hopedale Basin.

During the mantle exhumation substage, the Markland Formation was deposited above the Avalon Unconformity (**Fig. 1.7**). The Markland Formation represents a marine environment with shale being the dominant lithology. The Freydis Member of the Markland Formation represents a marginal marine, fine to coarse quartzose and arkosic sandstones (i.e. deltaic). The Markland Formation is situated below the Bylot Unconformity, which is beneath the next siliciclastic sequence.

Seaward progradation of sands and shales continued with syndrift deposition of the Gudrid, Cartwright and Kenamu formations, contained between the Bylot and Baffin Bay unconformities (**Fig. 1.7**; Balkwill and McMillian, 1990). Lithologies are described (McWhae et al., 1980) as distal (turbidite) quartzose to arkosic sandstones (Gudrid

Member), siltstones (Cartwright Formation), marine shales (Kenamu Formation), and fine-grained quartzose (possibly tidal) sandstones (Leif Member).

Postdrift sediments include the Mokami and Saglek formations and are followed by recent (Pleistocene) unnamed glacial deposits (**Fig. 1.7**). The Mokami Formation consists of neritic claystone and shale while the Saglek Formation consists of coarse clastic marginal marine rocks (McWhae et al., 1980).

The Labrador Shelf tectonic events and stratigraphic development is documented by Chalmers and Pulvertaft (2001); Enachescu (2006); Enachescu et al., 2007; Martin and Enachescu (2006 and 2007) and summarized by Martin (2007):

- “1. Pre- to early synrift deposition of the Alexis Formation and Lower Bjarni Member during late Berriasian, and Valanginian to Aptian time;
2. Synrift deposition of the Upper Bjarni Member onto the hanging walls of the fault blocks, which occurred between Aptian and Albian time;
3. Postrift deposition of the Markland Formation during the initiation of thermal subsidence and exhumation of continental mantle, which occurred between Cenomanian to mid- Campanian/Danian time;
4. Syndrift deposition of late Paleocene and Eocene-aged Cartwright and Kenamu formations and;
5. Postdrift sediments of the late Paleogene/Neogene-aged Mokami and Saglek formations.”

Enachescu (2006) proposed stratigraphy and tectonic stages for the Labrador Shelf based on a) correlation of seismic markers interpreted from modern seismic data with well

results and b) interpretation of the deep water features in conjunction with potential field data. This stratigraphic/tectonic scheme provides the large-scale framework of this thesis **(Fig. 1.7)**.

## CHAPTER 2 METHODS & DATA

### 2.1 INTRODUCTION

One of the objectives of this study is to investigate diagenesis and its effects on porosity, as related to reservoir quality, for the carbonate and siliciclastic cored-reservoir intervals from the Labrador Shelf. The carbonate portion of this study (cf. **Chapter 3**) made extensive use of trace elements and stable isotopes to discern diagenesis and the implications of dolomitization. In contrast, petrography (i.e. point counting) was the main technique used for the investigation of siliclastic rocks (cf. **Chapter 4**). Core from several exploration wells for both intervals provided the samples for analysis, including petrographic and geochemical analyses, data assimilation and preparation for documentation. Cored-wells, along with petrography, geochemistry, and microthermometry samples are shown in **Table 2.1**.

### 2.2 CORE ANALYSIS

Considering the large Labrador Sea area, which contains two basins with proven hydrocarbons, there is little exploratory well control and relatively few cores. Furthermore, core quantity and quality for some carbonate and siliciclastic recovered intervals were scant or in poor condition (e.g. Gudrid H-55 and North Bjarni F-06). As a result, some intervals were more complete with a larger core recovery percentage. The uneven core availability and quality resulted in some intervals having more samples than others.

Well	Formation	Core	Top (m)	Base (m)	Gross (m)	Rec. (m)	Rec. (%)	Petrog.	Geochem.	Fluid Incl.
Gudrid H-55	Paleozoic C.	1	2676	2680	4	3.9	97.5	7	15	2
Indian Harbour M-52	Paleozoic C.	1	3952	3958.1	6.1	4.8	78.7	4	9	
Roberval K-92	Paleozoic C.	6 7	3578 3870	3582.5 3874	4.5 4	4.05 3.48	90 87	3 5	3 10	2
Bjarni H-81	Bjarni	1	2157	2164	7	2.4	34.3	2		
N. Bjarni F-06	Bjarni	1	2452	2458	6	1.5	25	3		
Herjolf M-92	Bjarni	1	2632	2640	8	7.6	95	10		
North Leif I-05	Bjarni	1	3110	3113.5	3.5	3.45	98.6	4		
Ogmund E-72	Bjarni	2	2234	2240	6	5.3	88.3	3		
Roberval K-92	Bjarni	2	3095	3125	30	10.5	35	4		
<b>TOTAL</b>						<b>46.98</b>		<b>45</b>	<b>37</b>	<b>4</b>

**Table 2.1.** List of core and exploration wells studied. Also included are core depths and number of samples used for petrography, geochemistry, and fluid inclusions. Carbonate core is shaded blue while siliciclastic core is shaded yellow.

The first step of data acquisition was a full description of core, establishing a lithofacies framework for subsequent sampling. Logging forms for siliciclastic rocks included lithology, cement, grain sizes, and sedimentary structures. Analyses of the carbonate core intervals were heavily based on geochemistry and therefore, core details beyond rock-type were not necessary. Sandstone intervals were logged differently because the quantity and quality of the core was much better than for the carbonates. Moreover, the depositional environment(s) needed to be fully understood to provide a context for describing siliciclastic diagenesis.

A combined total of 46.98 m was studied for carbonate and siliciclastic core (**Table 2.1**).

### **2.3 DATA**

Cores from the Labrador Shelf were viewed and sampled at the CNLOPB core storage facility. A total of 45, 37, and 4 samples were produced for petrography, geochemistry (including microthermometry), respectively (**Table 2.1 and Fig. 2.1**). In addition, limited sets of thin-sections are available from CNLOPB. These were used as additional references, along with thin-sections specifically made for this thesis. CNLOPB offers a library and website ([www.cnlopb.nl.ca](http://www.cnlopb.nl.ca)) with limited company data and independent studies, such as drill stem tests or stratigraphic picks, from the Labrador Shelf. This information was accessed in addition to other sources of published literature.

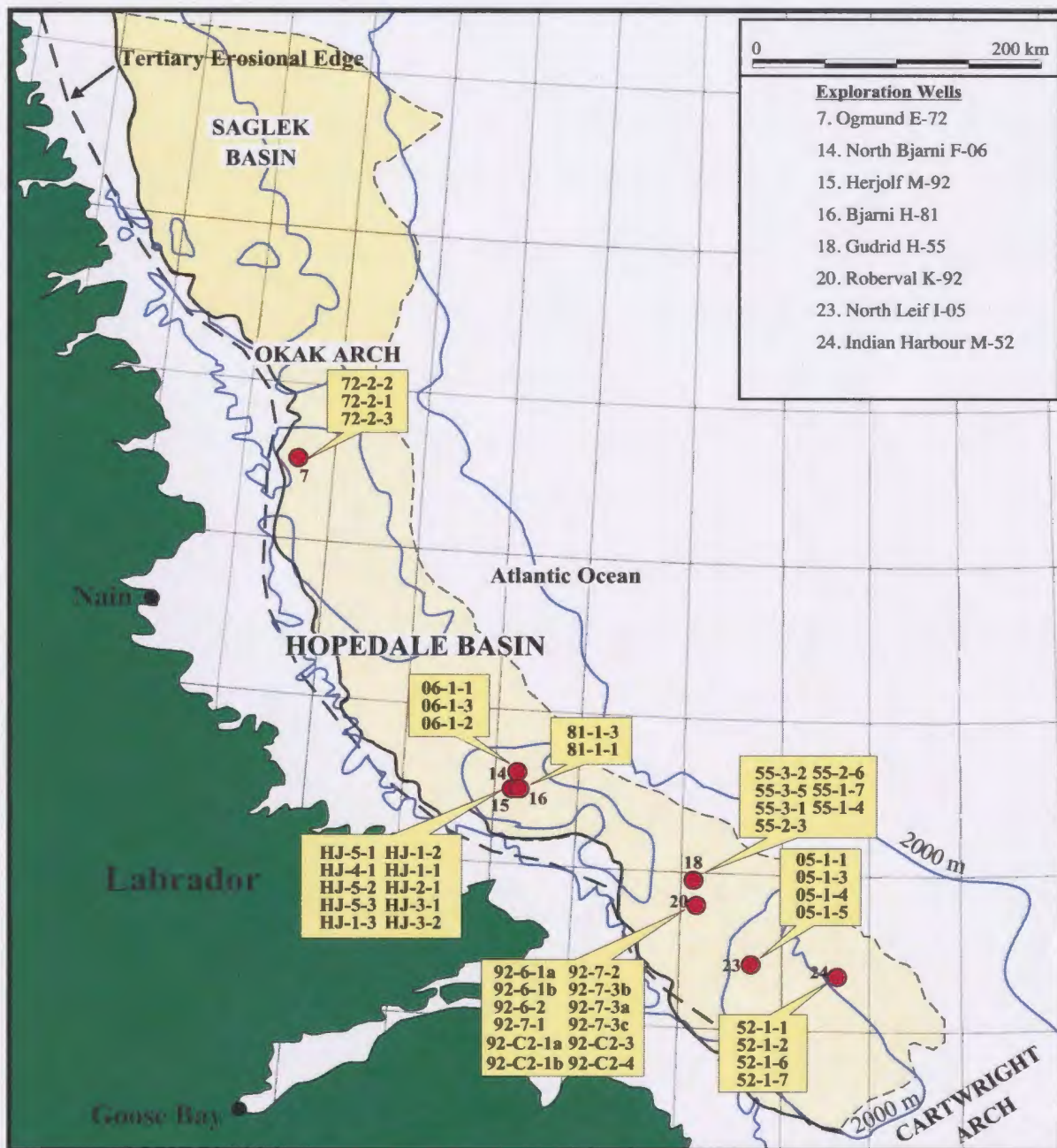


**Fig. 2.1.** Locations of all exploration wells (and core) studied in the Hopedale Basin (red dots) along with sample listings (boxes) and their distribution. Samples were named based on the well name, core/box number, and number per interval studied. Modified after Atkinson and Fagan (2001).

## 2.4 PETROGRAPHY

Petrography enabled thin-section identification of carbonate and siliciclastic rock components, types, and diagenetic features. This was done using plain polarized optical light (PL) and cathodoluminescence (CL) microscopy. Petrographic data was collected using thin section description forms, which include detrital framework grain parameters (mineral, size, sorting, roundness), matrix, diagenetic components (authigenic minerals and cements), and porosity (primary vs. secondary) analyses.

### 2.4.1 *Thin-section Preparation and PL microscopy*

Thin-sections were cut and polished to 30  $\mu\text{m}$ , then stained with a mixture of potassium ferricyanide and alizarin red and exposed to 55% hydrofluoric acid solution (cf. Dickson, 1966). The resultant staining was used for differentiation of carbonate cements and feldspar grains under plain polarized light during petrographic examination. Calcite and dolomite cements with varying amounts of  $\text{Fe}^{2+}$  (e.g.  $\text{Fe}^{2+}$ -free and  $\text{Fe}^{2+}$ -rich) will stain red to violet and clear to dark blue, respectively. Siliciclastic thin-sections were also impregnated in epoxy, filling porous areas blue-green. The result differentiates porosity from rock components or diagenetic features under plane polarized light (PL). Digital images (micrographs) for all thin-sections were taken using a *Nikon Eclipse E600W POL* polarizing microscope.

### 2.4.2 *Cathodoluminescence*

Cathodoluminescence (CL) of polished thin-sections is a useful tool for tracing variations in the elemental compositions of diagenetic fluids and identification of cement generations through progressive burial (cf. Boggs and Krinsley, 2006; Azmy et al., 2001). This is achieved when activators, cations such as  $\text{Mn}^{2+}$ ,  $\text{Sm}^{3+}$ ,  $\text{Eu}^{2+}$ , in the studied

medium (e.g. carbonate cements) become excited. The ratio of activator elements to quenchers ( $\text{Fe}^{2+}$ ,  $\text{Fe}^{3+}$ ,  $\text{Co}^{2+}$ , and  $\text{Ni}^{2+}$ ) in the mineral phase is the important influencing factor (Azmy, 1992; Machel et al., 1991). As a result, different cement generations emit a unique CL image that enables their differentiation.

Cathodoluminescence imaging was carried-out at Memorial University using a cold *ELM 3F* Cathodoluminoscope.

### ***2.4.3 Point Counting***

Upon deposition, minerals, some more than others (e.g. mica vs. quartz), become unstable and are susceptible to diagenetic change. It is therefore necessary to predefine a generalized mineral assemblage or rock type, providing a context, before diagenesis can be assessed. Therefore, a 200-point count-minimum of framework grains was completed for classification siliciclastic thin-sections (cf. Folk, 1968) using the Galehouse 'Line Method' (cf. Galehouse, 1969). This method uses equally spaced traverses along the thin-section where grains are counted at the intersection of cross-hairs, recording a number frequency for counted grains. In addition to framework grains, diagenetic grains were pointed counted (cf. **Chapter 4 methodology for further details**).

Sandstones were described and classified (Pettijohn, 1975; Folk, 1968) using QFL ternary diagrams to graphically represent compositions based on Quartz (Q), Feldspar (F), and Lithic (L) grain end members. Q is meant to represent the greatest stability and is the sum of monocrystalline quartz and chalcedony grains, and polycrystalline quartzite and chert. F represents the feldspar grains that are the most abundant of the unstable single-crystal grains. L is the sum of all the unstable grains (lithic or rock fragments),

which are aphanitic grains including chert and quartzite. Normalized QFL data was plotted using an Excel® application called *Ternplot*.

The uncertainty involved with point counting is documented by Howarth (1998) where half-width plots are presented to estimate upper and lower 95% confidence limits (**Fig. 2.2**) for sampling. To give an indication for the magnitude of the uncertainty for the point count results, for example, if  $n = 100$  (as a commonly counted number of quartz grains) and  $N = 200$  (the total number of grains counted), then the charts shown in Figure 2.2 can be used to estimate the uncertainty for a 95% confidence interval (CI). Entering the observed percentage, 50%, on the ordinate, and  $N = 200$  on the abscissa, the estimated width of the lower half of the CI is 7.0% (**Fig. 2.2a**), and that of the upper half is 7.0% (**Fig. 2.2b**). Therefore there is a 95% probability that the true value of the parameter is between 7.0 and 43%. Additional uncertainties associated with point counting are described in Chapter 4.

#### ***2.4.4 Fluid Inclusions and Microthermometry***

Fluid Inclusions have been used for many years to study magmatic-hydrothermal ore deposits (cf. Heinrich, 2007) and hydrocarbon-bearing systems (cf. Davies, 2006) to understand the genesis of the system and the origin of the fluids responsible for its economic importance. Furthermore, fluid inclusions, fluid-filled vacuoles trapped within minerals (Goldstein & Reynolds, 1994), have been applied to diagenetic studies involving carbonate and siliciclastic rocks (cf. Lavoie, 2005; Higgs et al., 2007), acting as ‘time capsules’ by recording past temperatures, pressures, and fluid composition (Goldstein & Reynolds, 1994) at time of formation.

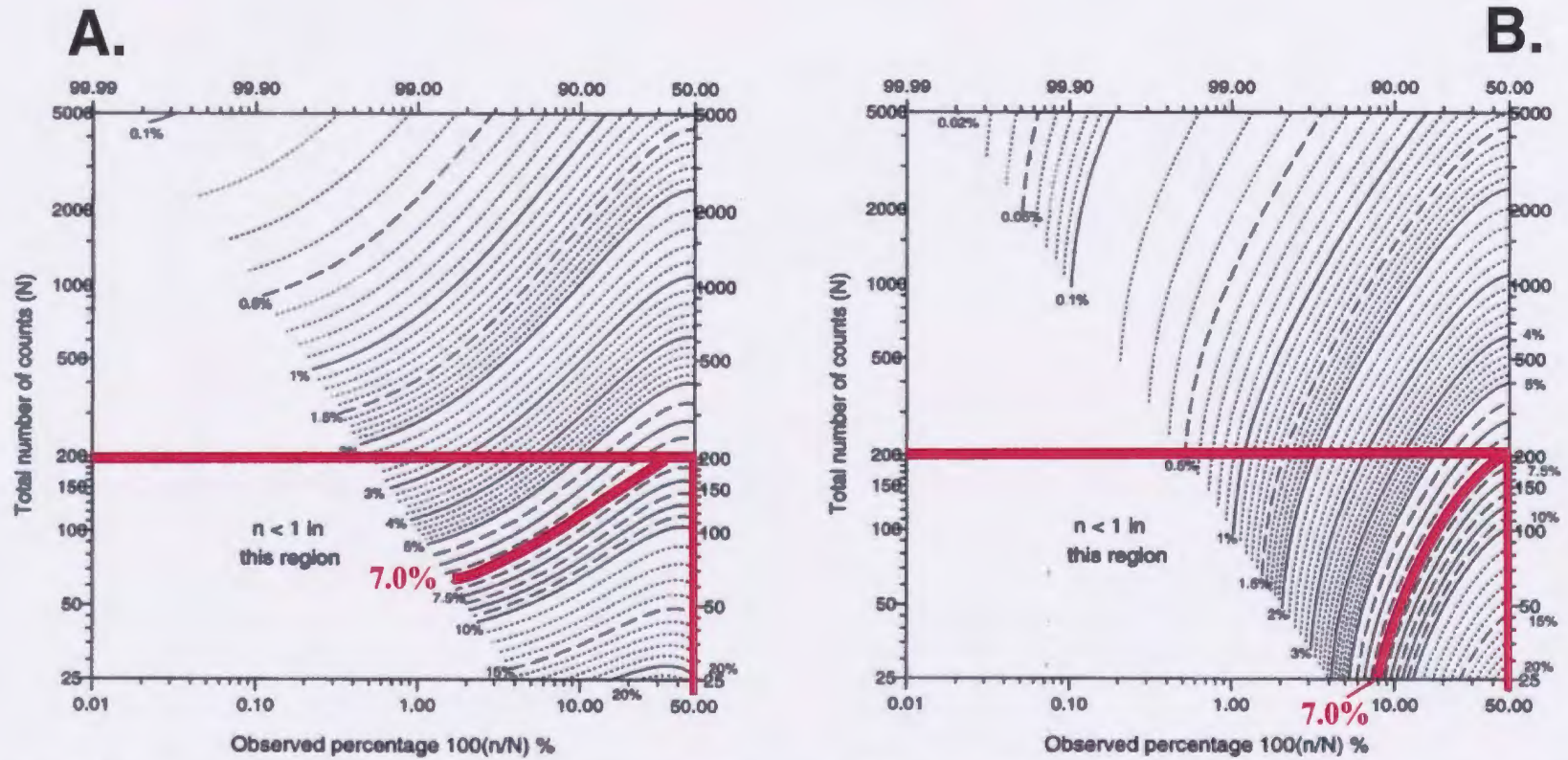


Fig. 2.2. Lower (A.) and upper (B.) half width graphs indicating the 95 % Confidence bounds from observed percentages. For (A.),  $50 - 7.0 = 43\%$  and (B.)  $50 + 7.0 = 57\%$ . Graphs modified from Howarth, 1998.

Primary, pseudoprimary, and secondary fluid inclusions were distinguished based on the criteria set by Goldstein & Reynolds (1994), using a Nikon microscope with a 40x Nikon objective lens. A *Linkam THMS-600* heating-freezing stage was used for microthermometry and the calibration was checked using  $T_m\text{CO}_2$ ,  $T_m\text{H}_2\text{O}$ , and  $T_h\text{H}_2\text{O}$  (-56.6, 0.0 and 374.1 °C). Accuracy in measurements around 0 and 100 °C is estimated between 0.1 and 0.2 °C respectively.

Only primary fluid inclusions were used for microthermometry and were recognized based on their relationship and distribution to the growth zonation within the dolomite crystal (cf. Goldstein and Reynolds, 1994).

## **2.5 GEOCHEMISTRY**

All samples analyzed geochemically were first polished, rinsed and cleaned with deionized water in an ultrasound bath, and dried at 50°C for 12 - 24 hours. A micro-drill was used to drill the area containing authigenic carbonate cement. Once the samples were drilled, this cement was collected and analyzed for geochemistry.

Stable isotopes,  $\delta^{18}\text{O}$ ,  $\delta^{13}\text{C}$ , &  $^{87/86}\text{Sr}$ , and trace elements, Fe, Mn, and Sr, were obtained from drilled sample-powder. Geochemical analyses of these can reveal cement generation-type and their diagenetic environment of precipitation through the burial history of sediments (i.e. diagenetic history), a significant issue in understanding the porosity development mechanism in the reservoir intervals. Stable isotopes and trace element data is important because they act as geochemical tracers, representing relict chemical compositions at time of deposition. For example, increasing  $\delta^{18}\text{O}$  values, along with increasing Mn and decreasing Sr, indicate progressive burial with depth (Azmy et

al., 2001). Primary Sr-isotopes, if preserved, can be used for refining the poorly dated reservoir carbonate intervals in Gudrid H-55, Indian Harbour M-52, and Roberval K-92 wells (e.g. Veizer et al., 1999).  $^{87/86}\text{Sr}$  analysis at times is not very successful, particularly if dolomitization was extensive and occurred under open system conditions. Therefore, the earliest cement generations, such as micritic lime-mud, or the earliest and finest grained-dolomite generation, must be used. If the original micritic fabric is preserved, sediment age and seawater compositions can be determined (cf. Veizer et al., 1999), resolving a depositional model for dolomitization and/or Paleozoic ages.

Specific geochemical analyses were performed following the analytical protocol outlined in Azmy et al. (1998; 2001; 2006). The C- and O- isotope measurements were run using a ThermoFinnigan Delta V PLUS IRMS connected to GasBench II. About 200  $\mu\text{g}$  of powder sample was reacted in inert atmosphere with ultrapure concentrated (100%) orthophosphoric acid at 70°C. The  $\text{CO}_2$  produced was automatically flushed through a chromatographic column and delivered to the source of the ThermoFinnigan DELTA V Plus isotope ratio mass spectrometer. The gas was ionized in a stream of helium and measured for isotope ratios. The analytical uncertainty was better than 0.1‰ ( $2\sigma$ ), determined by repeated measurements of NBS-19 ( $\delta^{18}\text{O} = -2.20$  ‰ and  $\delta^{13}\text{C} = +1.95$  ‰ V-PDB) and L-SVEC ( $\delta^{18}\text{O} = -26.64$  ‰ and  $\delta^{13}\text{C} = -46.6$  ‰ V-PDB) standards during each run of samples.

For trace element analyses, about 5 mg sample powder was digested in 5% (v/v) acetic acid for 70–80 min and the clear solution was decanted. The solution was evaporated and the precipitate was re-dissolved in nitric acid and run for measurements of Ca, Mg, Sr, Fe, and Mn concentrations (Coleman et al., 1989) using a HP 4500<sup>plus</sup>. The

concentrations of elements were recalculated based on 100% carbonates. The relative uncertainties of measurements were better than 5%.

For Sr isotope analyses, approximately 4 mg of sample powder was dissolved in 2.5N ultrapure HCl. After HCl evaporation, Sr was extracted with quartz glass ion exchange columns filled with Bio Rad AG50WX8 resin. Approximately 75–100 ng Sr was loaded on Re filaments using a Ta<sub>2</sub>O<sub>5</sub>–HNO<sub>3</sub>–HF–H<sub>3</sub>PO<sub>4</sub> solution. Measurements were performed with a Finnigan MAT 262 multi-collector mass spectrometer at the Institut für Geologie, Mineralogie und Geophysik, Ruhr Universität, Bochum, Germany (cf. Diener et al., 1996). Sr isotope ratio measurements were completed using two standard reference materials, NIST (NBS) 987 and USGS EN-1, which gave mean <sup>87</sup>Sr/<sup>86</sup>Sr values over the analyses interval of 0.710236 ± 0.000008 and 0.709151 ± 0.000008, respectively.

**CHAPTER 3  
(MANUSCRIPT 1)**

**DIAGENESIS OF PALEOZOIC PRERIFT CARBONATES OF THE  
HOPEDALE BASIN, LABRADOR SHELF: DOLOMITIZATION  
IMPLICATIONS AND AGE ASSESSMENT**

**SCHWARTZ, S.S.<sup>1</sup>, AZMY, K.<sup>1</sup>, BLAMEY, N.<sup>2</sup> AND ENACHESCU, M.E.<sup>1</sup>**

<sup>1</sup>Department of Earth Sciences, Memorial University of Newfoundland, St. John's, NL,  
Canada A1B 3X5

<sup>2</sup>Department of Earth & Ocean Sciences, National University of Ireland, Galway, United  
Kingdom

**ABSTRACT**

Paleozoic platform carbonates located in the Hopedale Basin of Labrador Shelf are drilled on the top of several basement highs but they may be present in a larger area including prerift basement lows. Paleozoic carbonates represent a portion of the region's prerift stratigraphy and are potential reservoirs and candidates for future hydrocarbon exploitation. Core samples from Roberval K-92 (3578 – 3582 m and 3870 – 3873.5 m), Gudrid H-55 (2676 – 2680 m), and Indian Harbour M-52 (3952 – 3958 m) were collected for petrographic investigations and geochemical analyses. Two main types of carbonates are recognized: 1) a wackestone with limited dolomitization (Indian Harbour M-52) and 2) a dolostone (Roberval K-92 & Gudrid H-55). Three dolomite phases (D1, D2 and D3) were identified petrographically and geochemically and correlated between wells. Their crystal sizes range from dolosparite to saddle dolomite, ranging from 20 to 700 µm, with Fe content 499 - 16607 ppm and Mn 75 - 1262 ppm. Using distribution coefficients for Sr

in dolomite ( $D1_{Sr} = 0.015$  and  $0.06$ ), the calculated Sr/Ca molar ratios for the earliest dolomitizing fluid ( $0.0010 - 0.0060$ ) suggest that initial dolomitization (D1) resulted from mixing marine and non-marine (meteoric) waters. The petrography, fluid inclusion microthermometry and stable isotope geochemistry suggest that D2 (50 to 300  $\mu\text{m}$ ) and D3 (250 to 750  $\mu\text{m}$ ) are derived from hydrothermal fluids. From petrographic examination, visual estimates of porosity vary among wells and range from  $< 1$  to 20%. Pores are either interstitial or of the vuggy type. Interstitial porosity likely developed during early dolomitization. Several phases of dissolution and late calcite cementation subsequently led to the creation and destruction of vuggy porosity.  $^{87}\text{Sr}/^{86}\text{Sr}$  sampled from calcite and dolomites, ranged from 0.708897 to 0.709264. Pristine micritic (C1) cements suggest that deposition likely started in the Early to Mid-Ordovician with early dolomitization occurring no later than this time. The  $\delta^{13}\text{C}$  signatures of the dolomicrite also match the global values documented for the preserved Ordovician carbonates.

### 3.1 INTRODUCTION

The Labrador Shelf is located northwest of the Mesozoic petroleum rich Grand Banks of Newfoundland (**Fig. 3.1**). The Hopedale Basin contains Paleozoic carbonates and Mesozoic-Cenozoic clastic sediments, which were deposited during tectonic stages of synrifting, postrifting syndrifting, and postdrifting, respectively. Prerift carbonates, the focus of this study, represent a small and irregular portion of the regions stratigraphy.

The Paleozoic Era is defined by compressional tectonics whereby a series of major orogenic events, initiated by the Taconic Orogeny, produced the Appalachians, several economically important passive margin basins (e.g. Anitcosti Basin), and ultimately, the supercontinent Pangea. Paleozoic basins, particularly those along the Laurentian Margin, contain petroleum-rich, carbonate reservoirs (cf. **Chapter 1; Fig. 1.8**)

The Hopedale Basin carbonates are represented by dolomites and limestones, and were investigated in cores from three exploration wells: Indian Harbour M-52, Gudrid H-55, and Roberval K-92. Gas has been successfully tested in Gudrid H-55 well (8.1 MMcf/d; C-NLOPB; Atkinson & Fagan, 2001) The other 3 wells had no hydrocarbon reservoir in Paleozoic carbonates.

Preliminary petrographic investigations of the pre-rift carbonates in the region have been provided by McWhae et al., (1980) and Bell & Howie (1990). However, no previous detailed studies have focused on the relationships between early and late diagenetic events and porosity evolution in those carbonates. The age of carbonate sediments has not been constrained further than the geological period. Within the Paleozoic in the Gudrid H-55 well, palynomorphs are thought to be Carboniferous

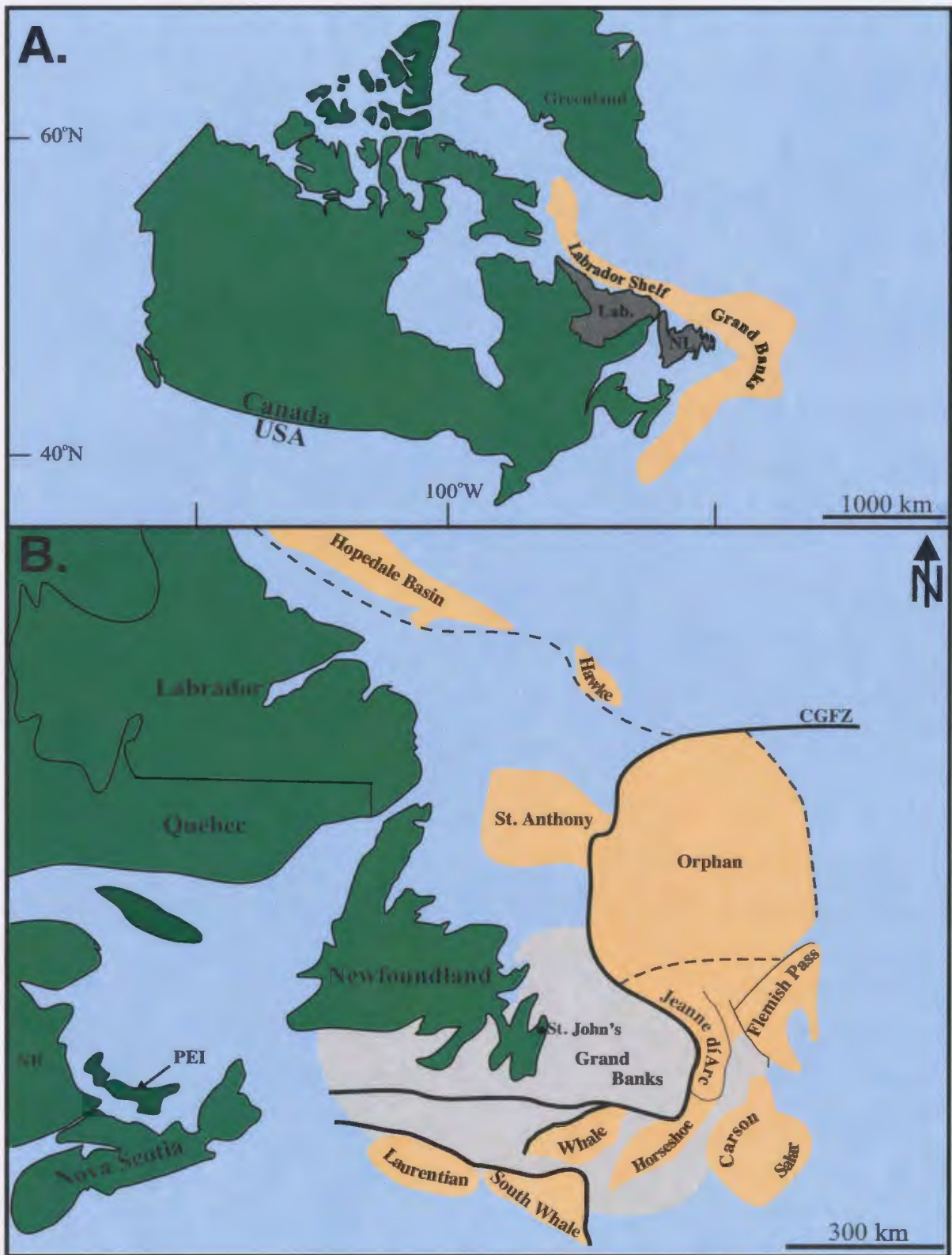


**Fig. 3.1.** *A.* Map of Canada highlighting Newfoundland and Labrador (dark grey) and the offshore sedimentary basins (yellow). *B.* Mesozoic sedimentary rift basins (all the way to 300 m water depth; yellow) of Newfoundland and Labrador (after Enachescu, 1992).

contaminants, as they are not representative with the diagenetic textures of the rocks (Bell & Howie, 1990). Therefore, a detailed study to properly characterize the reservoir at the micro-scale, with further age assessment, would be of great value to the Labrador Shelf in general and for the Hopedale Basin in particular.

The main objectives of this paper are: (1) to identify and characterize the calcite and dolomite phases of the pre-rift carbonates; (2) to investigate their geochemical attributes; (3) to study the influence of diagenesis, particularly the dolomitization, on porosity evolution; and (4) to shed light, if possible, on the age of these carbonate sediments.

### **3.2 TECTONIC AND GEOLOGICAL FRAMEWORK**

The Labrador Shelf, like all other Mesozoic rift basins surrounding modern-day Atlantic, forms part of the North America passive margin. The actual shelf formed during the complicated Mesozoic diachronous rifting of the North American and Europe/Moroccan margins, with the Labrador margin representing the final stage of rifting in the eastern North Atlantic between North America and Greenland during the Early Cretaceous (Berriasian) (McWhae et al., 1980; Balkwill, 1987; Sørensen, 2006). This led to the development of the Hopedale and Saglek basins on the Labrador Shelf, which correlate with the Lady Franklin Basin on the Greenland conjugate margin. These basins were filled with syn-rift to syn-drift (Mesozoic-Cenozoic) sediments (**Fig. 3.2**).

Paleozoic pre-rift carbonates are unconformably situated below Mesozoic-Cenozoic sediments (**Fig. 3.2**), and rest unconformably on top of older igneous and metamorphic basement highs (**Fig. 3.3**). Carbonates along the “Appalachian trend” in

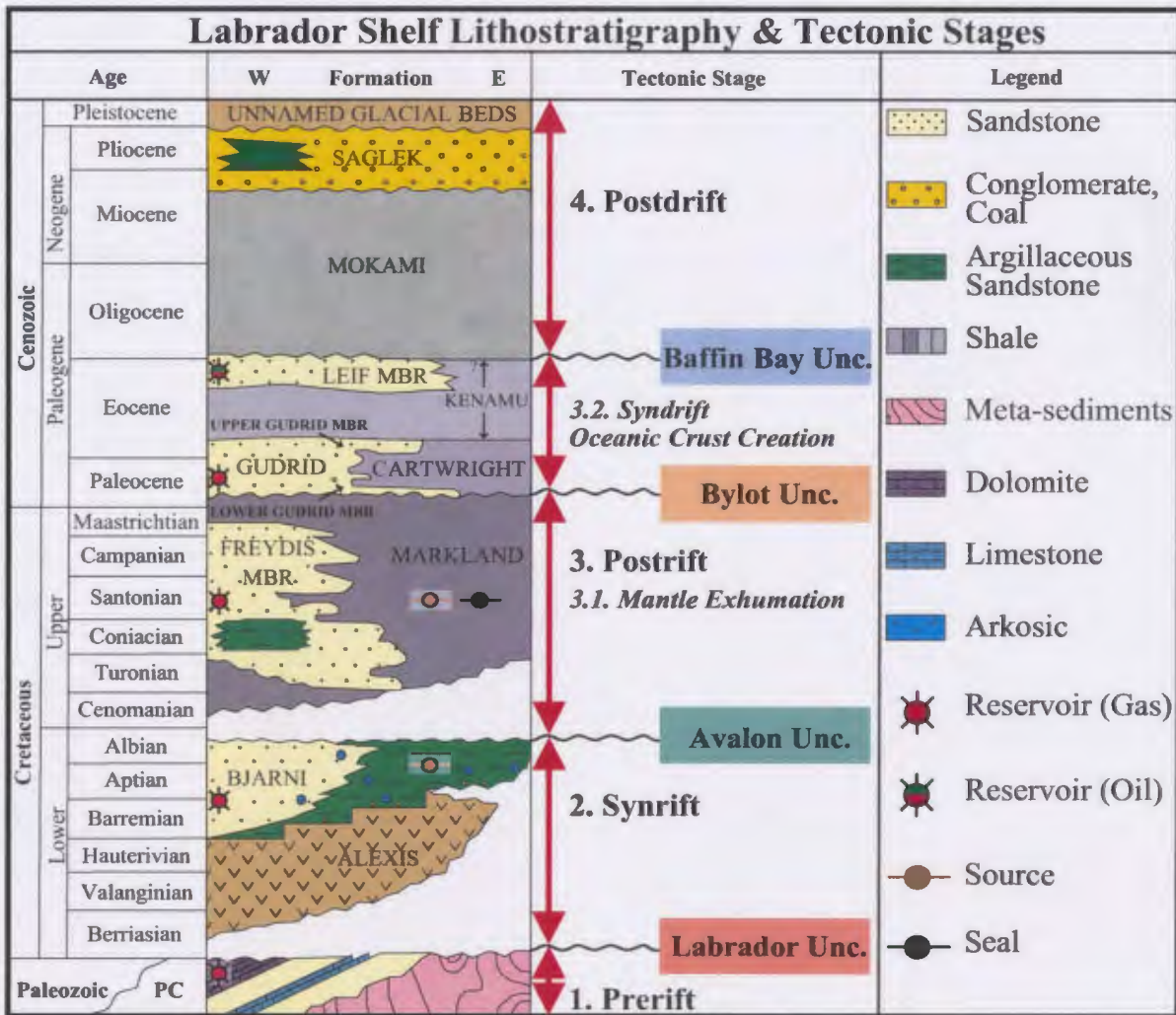


**Fig. 3.2.** Stratigraphy and tectonic evolution of the Labrador Shelf, including major unconformities (Modified after Enachescu, 2006).

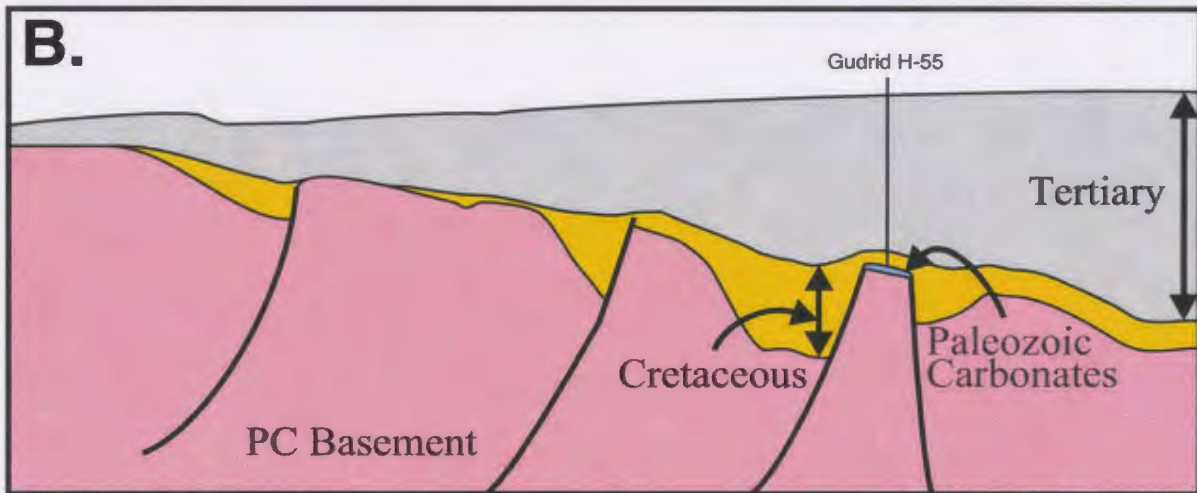
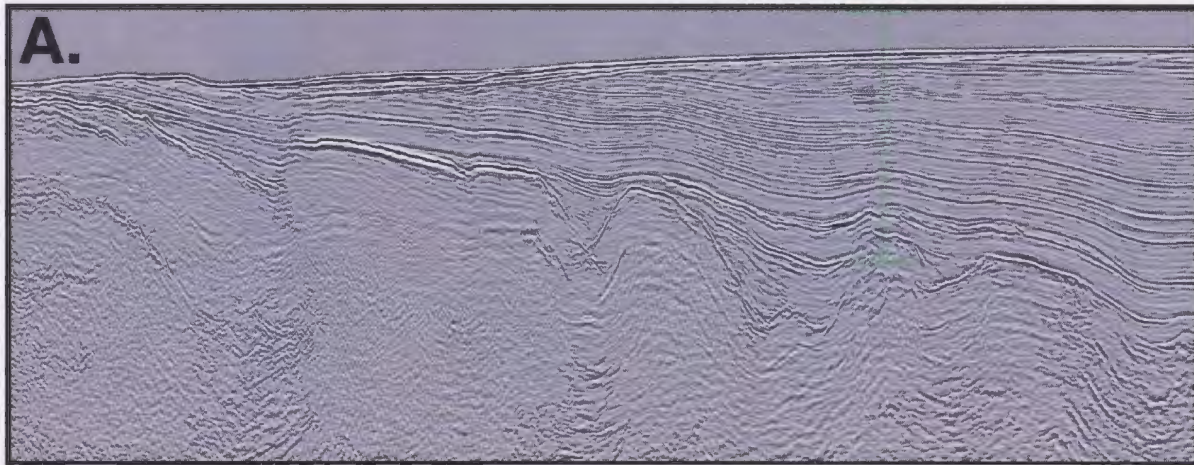


**Fig. 3.3.** *A.* Partial image of the original dip seismic line crossing Gudrid H-55 discovery well. *B.* Generalized interpreted schematic cross-section through Gudrid H-55 well exemplifying Paleozoic carbonates reservoir resting on top of a Pre-Cambrian horst block. Seismic courtesy of GSI.

nearby western Newfoundland were deposited as peritidal-dominated passive margin or shallow subtidal foreland basin units on the continental margin of the Iapetus and Rheic oceans (Atkinson & Fagan, 2001). This occurred either 1) prior to syn-continental Ordovician accretion (Taconian orogeny), or 2) during the Carboniferous invasion of the Windsor Sea on Laurussia, prior to final closure of the Rheic Ocean and the Permian formation of Pangea. However, it is still unclear which scenario is most likely for deposition of these carbonates.

### **3.3 METHODS**

Carbonate cores of three exploration wells from the Hopedale Basin (**Fig. 3.4**), Roberval K-92, Gudrid H-55 (gas discovery), and Indian Harbour M-52 were provided by the Canada-Newfoundland and Labrador Offshore Petroleum Board (CNLOPB, 2007). A total of 12.2 m of core was sampled based on visual variations in diagenetic textures (**Plate 3.1; Fig. 3.5**). Thin-sections were cut and stained with alizarin red-s and potassium ferricyanide solutions (Dickson, 1966), while the mirror-image slabs were used for microsampling. They were examined using a standard polarizing (PL) microscope (Nikon Eclipse E600W POL) and a cold ELM 3F Cathodoluminoscope (CL) at Memorial University of Newfoundland. The mirror-image slabs were polished, cleaned, sonicated in deionized water and dried overnight at 50 °C. Microsamples were extracted from the clean polished slabs under a binocular microscope using a low-speed microdrill.

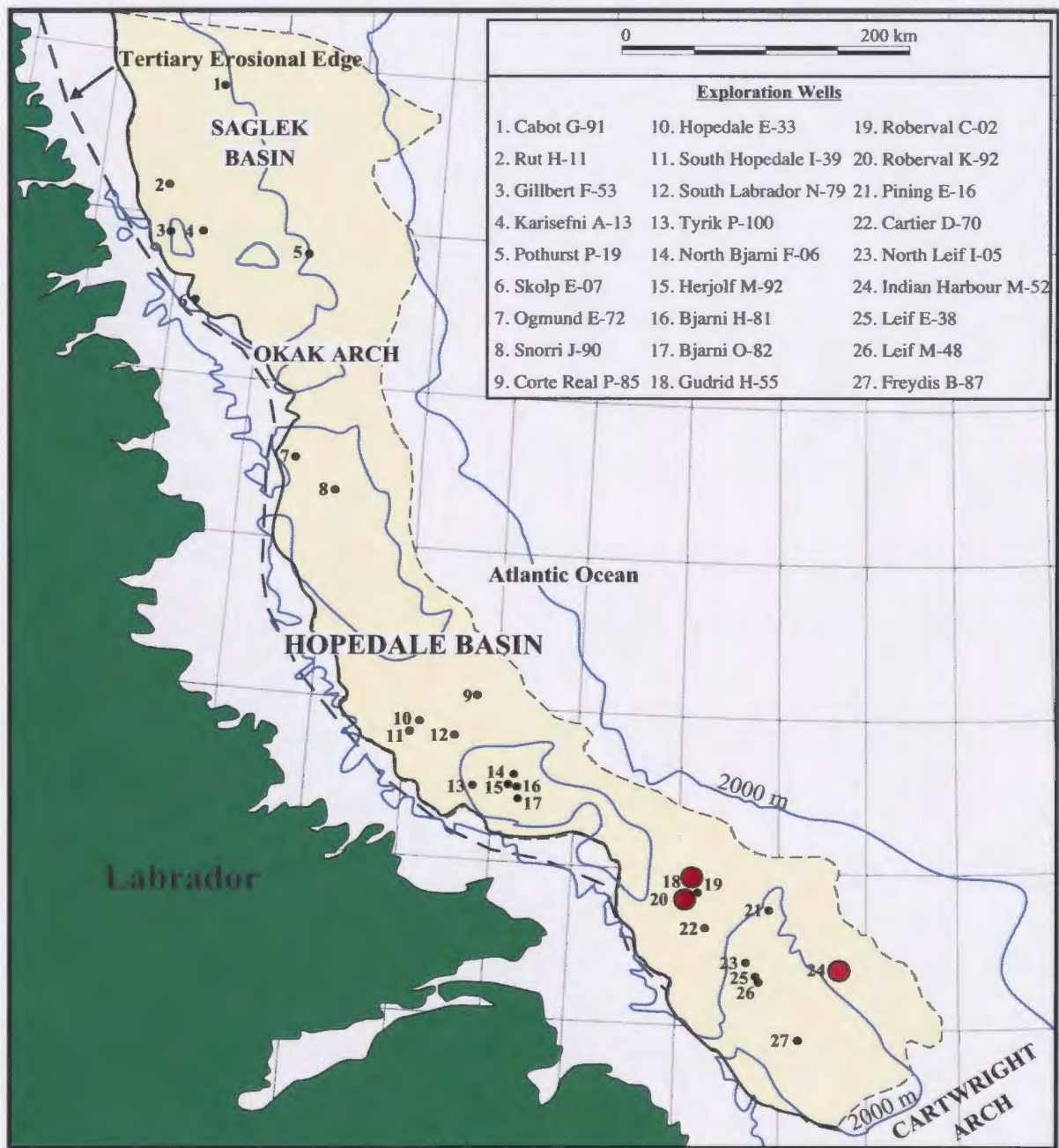


**Fig. 3.4.** Exploration wells in the Hopedale and Saglek Basins, Labrador Shelf. Larger red dots indicate carbonate wells studied. Modified after Atkinson & Fagan, 2001.

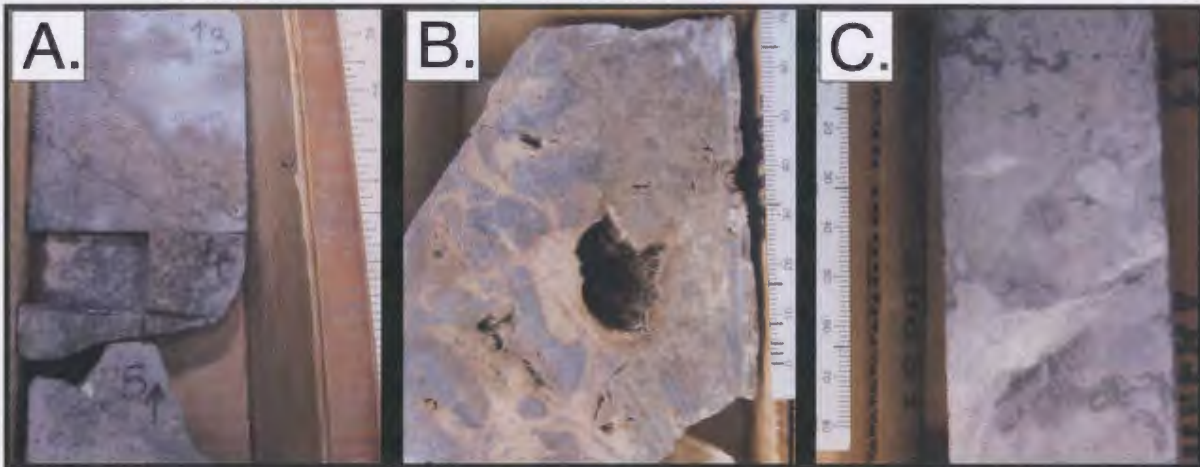


**Plate 3.1.** Core images from, A. Gudrid H-55 (~2679.0 m), B. Roberval K-92 (~3871.5 m), and C. Indian Harbour M-52 (3954.6 m - 3955.2 m). Photo's courtesy of Matthew Harvey.

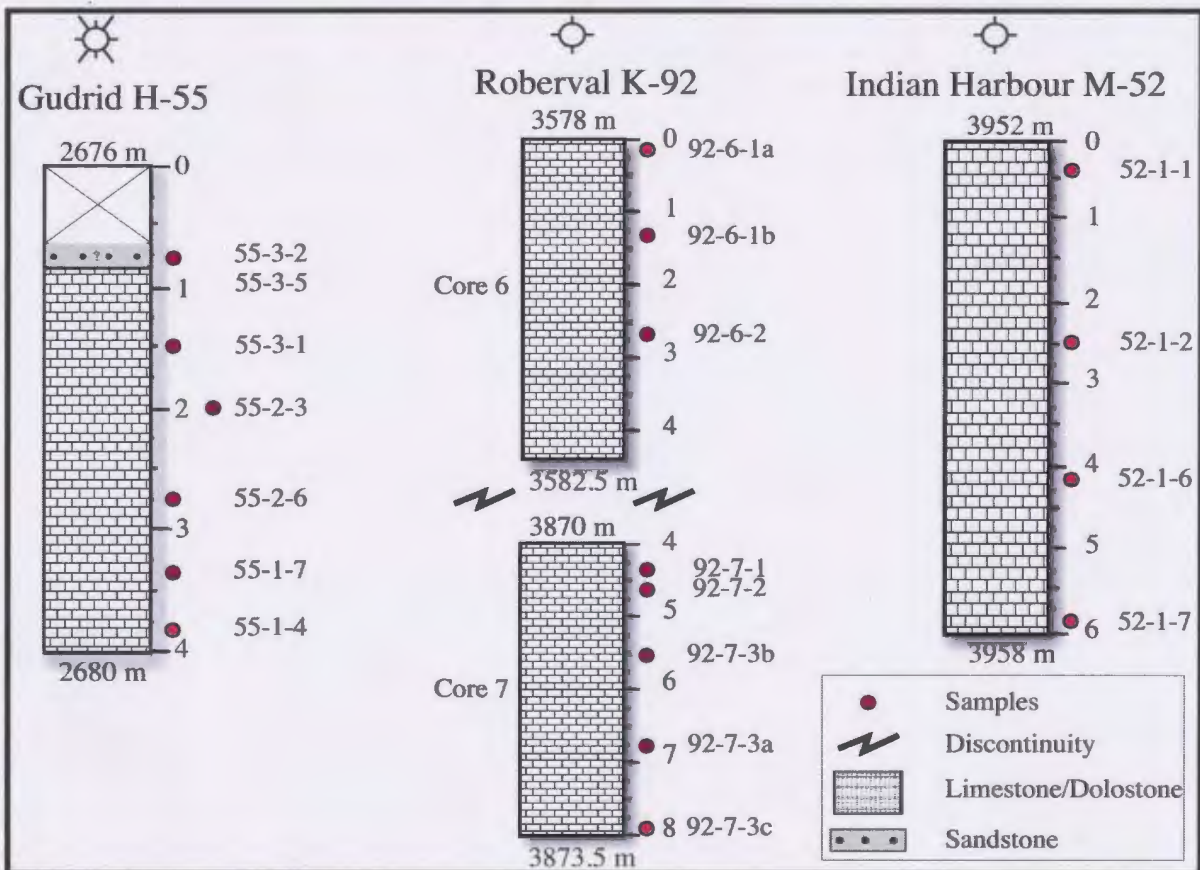


**Fig. 3.5.** Sample locations, numbers, and depths of studied core from Gudrid H-55, Roberval K-92, and Indian Harbour M-52. Note that between Roberval K-92 core 6 and 7 there is a break of approximately 312.5 m.

Geochemical analysis was performed following the analytical protocol outlined in Azmy et al. (1998; 2001; 2006). The C- and O- isotope measurements were made using a ThermoFinnigan Delta V PLUS Isotope Ratio Mass Spectrometer (IRMS) connected to GasBench II. About 200  $\mu\text{g}$  of powder sample was reacted in inert atmosphere with ultrapure concentrated (100%) orthophosphoric acid at 70°C. The  $\text{CO}_2$  produced was automatically flushed through a chromatographic column and delivered to the source of the IRMS. The gas was ionized in a stream of helium and measured for isotope ratios. The analytical uncertainty was better than 0.1‰ ( $2\sigma$ ), determined by repeated measurements of NBS-19 ( $\delta^{18}\text{O} = -2.20$  ‰ and  $\delta^{13}\text{C} = +1.95$  ‰ V-PDB) and L-SVEC ( $\delta^{18}\text{O} = -26.64$  ‰ and  $\delta^{13}\text{C} = -46.6$  ‰ V-PDB) standards during each run of samples.

For trace element analyses, about 5 mg of sample powder was digested in 5% (v/v) acetic acid for 70–80 min and the clear solution was decanted. The solution was evaporated and the precipitate was re-dissolved in nitric acid and analyzed for Ca, Mg, Sr, Fe, and Mn concentrations (Coleman et al., 1989) using a HP 4500*plus*<sup>p</sup>. The concentrations of elements were recalculated based on 100% carbonates. The relative uncertainties of measurements were better than 5%.

For Sr isotope analyses, approximately 4 mg of sample powder was dissolved in 2.5N ultrapure HCl. After HCl evaporation, Sr was extracted with quartz glass ion exchange columns filled with Bio Rad AG50WX8 resin. Approximately 75–100 ng Sr was loaded on Re filaments using a  $\text{Ta}_2\text{O}_5\text{--HNO}_3\text{--HF--H}_3\text{PO}_4$  solution. Measurements were performed with a Finnigan MAT 262 multi-collector mass spectrometer at the Institut für Geologie, Mineralogie und Geophysik, Ruhr Universität, Bochum, Germany

(cf. Diener et al., 1996). Sr isotope ratio measurements were completed using two standard reference materials, NIST (NBS) 987 and USGS EN-1, which gave mean  $^{87}\text{Sr}/^{86}\text{Sr}$  values over the analyses interval of  $0.710236 \pm 0.000008$  and  $0.709151 \pm 0.000008$ , respectively.

Primary, pseudoprimary, and secondary fluid inclusions were distinguished based on the criteria set by Goldstein & Reynolds (1994), using a Nikon microscope with a 40x Nikon objective lens. Only primary inclusions, identified by their growth relationship to the crystal edges, were used for microthermometry. A Linkam THMS-600 heating-freezing stage was used for microthermometry and the calibration was checked using  $T_{\text{mCO}_2}$ ,  $T_{\text{mH}_2\text{O}}$  and  $T_{\text{hH}_2\text{O}}$  (-56.6, 0.0 and 374.1 °C). Accuracy in measurements around 0 and 100 °C is estimated between 0.1 and 0.2 °C, respectively.

### 3.4 PETROGRAPHY

The petrographic nomenclature used for carbonate phases is summarized in **Table 3.1** and the trends in dolomite crystal sizes for the studied wells are shown in **Figure 3.6**.

Samples consist of various more or less dolomitized limestone and dolostone facies. The limestone samples (from Indian Harbour M-52) consist mainly of lime mudstone with a wackestone texture; the facies is represented by fossiliferous micritic lime mud, (C1), with algal aggregates and shell fragments. Diagenetic elements consist of calcite filling molds after shells, localized clusters of dolomites (D1), stylolites, and coarse calcite cement (C3) filling various cross-cutting fractures. C1 appears dull and

Cement	Abbreviation	Petrographic Description
Dolomite 1	D1	Dolosparite
Dolomite 2	D2	Medium to coarse grained
Dolomite 3	D3	Coarse grained; Saddle dolo.
Calcite 1	C1	Micritic limemud; original depositional fabric preserved
Calcite 2	C2	Intercrystalline, vug-filling
Calcite 3	C3	Intermediate to deep; intercrystalline and vug-filling

**Table 3.1.** Nomenclature used for naming dolomites (e.g., Azmy et al., 2001).

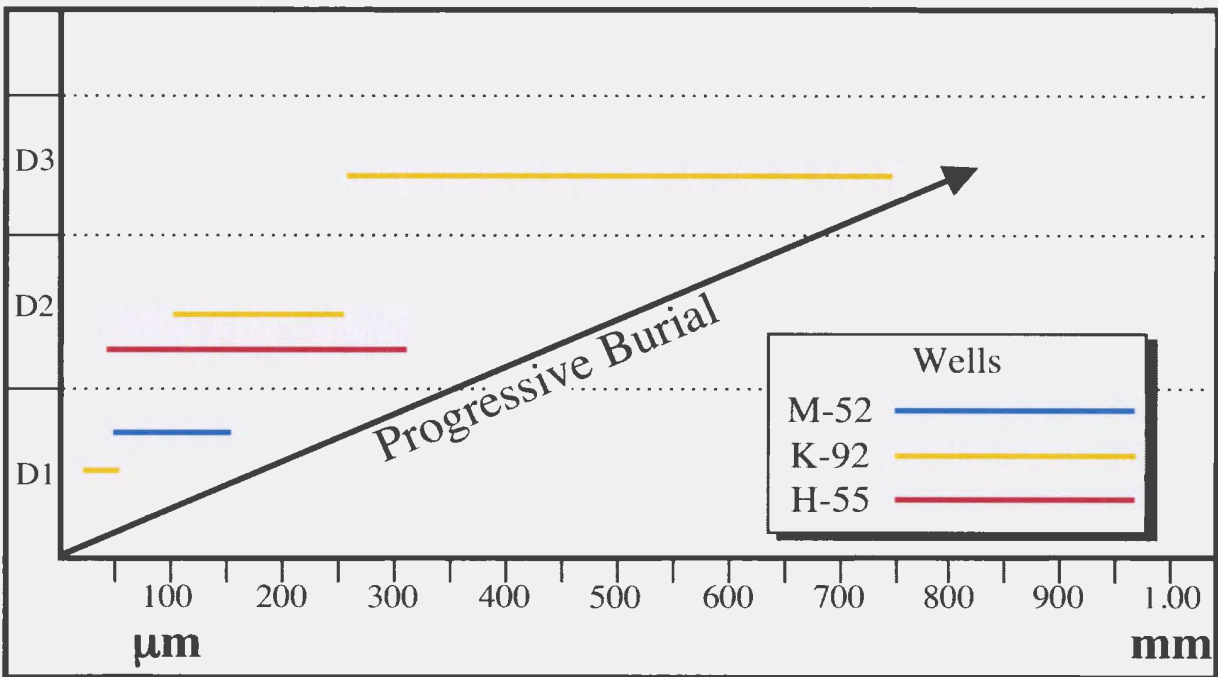


**Fig. 3.6.** Dolomite generations (D1, D2, & D3) in each well plotted against crystal size.

unzoned under cold cathodoluminoscope, while C3 contains thinly zoned bright sector zoning.

Dolostones (samples from Roberval K-92 and Gudrid H-55) are pervasive and do not preserve any of the original limy elements. Multiple phases of dolomite and calcite cementation are distinguished, along with pyrite and stylolite. Dolomite 1 (D1) is a semi-turbid, xenotopic dolosparite with subhedral crystals ranging from 20 to 150  $\mu\text{m}$ ; the crystals exhibit dull cores with outer brightly zoned luminescence (CL) (**Plates 3.2 & 3.3**). Dolomite 2 (**Plates 3.2 & Plate 3.3**) is a cloudy to clear-zoned, xenotopic dolosparite with sub- to euhedral crystals (20 – 300  $\mu\text{m}$ ); the crystals exhibit dull luminescence. Dolomite 3 (**Plate 3.2**), the latest of the dolomite phase consists of turbid and coarse-grained (250 – 750  $\mu\text{m}$ ) saddle dolomite with faint zonation under cathodoluminescence. Finally, two pore-filling calcite phases, C2 and C3, are recognized clear in plane-polarized light and exhibit zoned CL (**Plates 3.2 & 3.3**).

### 3.5 GEOCHEMISTRY AND MICROTHERMOMETRY RESULTS

**Table 3.2** summarizes the geochemical attributes of the investigated carbonates in the studied cores.

#### 3.5.1 *Major and Trace Elements*

Dolomite 3 contains the highest Fe content with an average of 10127 ppm (**Table 3.2**), with a maximum value of 16607 ppm. In contrast, Fe content in D1 averages 2242 ppm with a maximum content of 5510 ppm (**Table 3.2**). The highest Mn content occurs in D1 (1262 ppm), with an average content of 463 ppm (**Table 3.2**). However, the highest

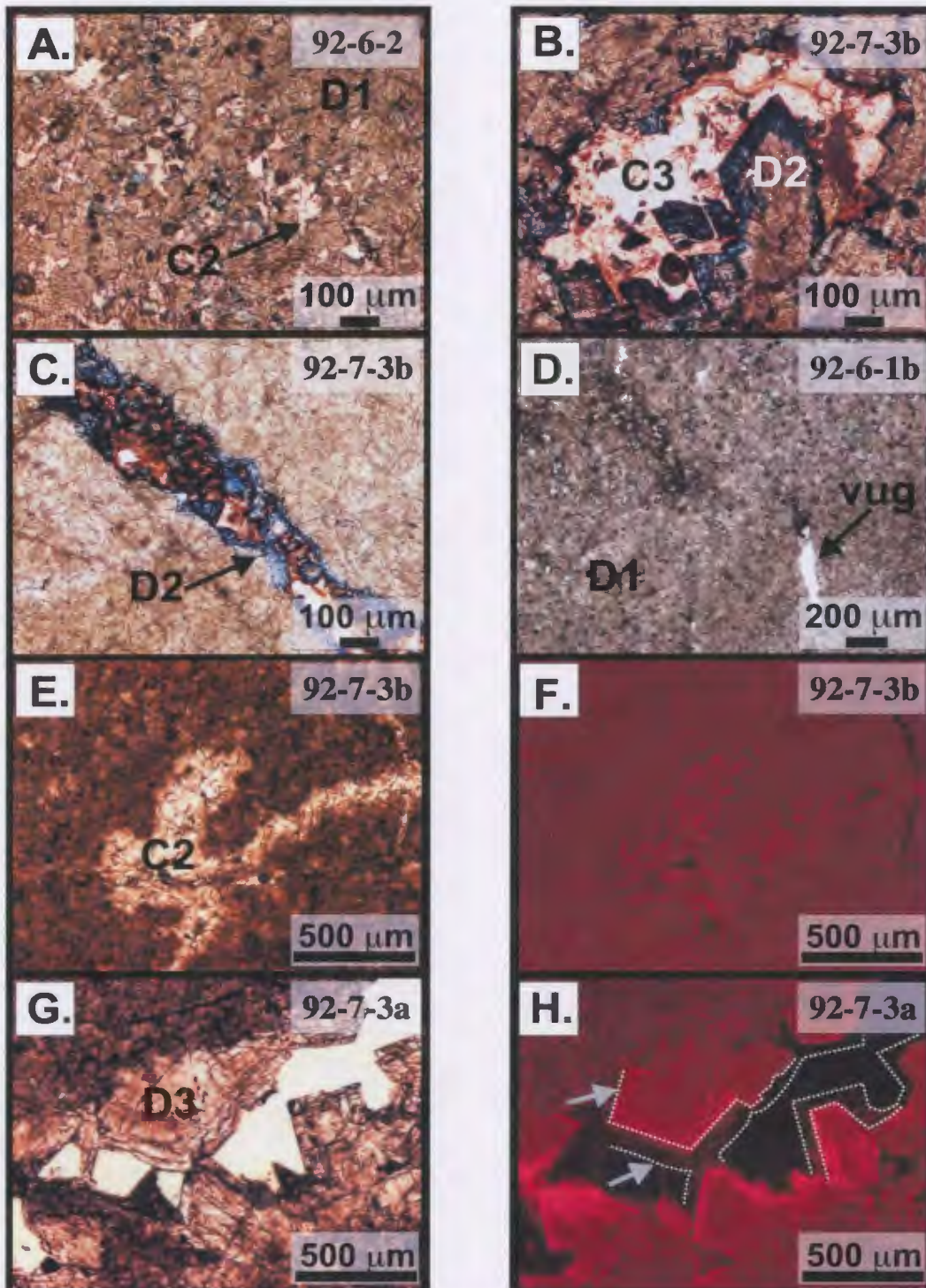


**Plate 3.2.** Plain-polarized light and cathodoluminescence photomicrographs of dolomites from Roberval K-92. *A-C*, Calcite filling intra-crystalline, vuggy, and micro-fracture porosity, respectively, *D*, D1 with interstitial and vuggy porosities, *E - H*, counter-part plain-polarized light and cathodoluminescence (showing zoning and smoothed edges from late dissolution) photomicrographs of dolomite and calcite.

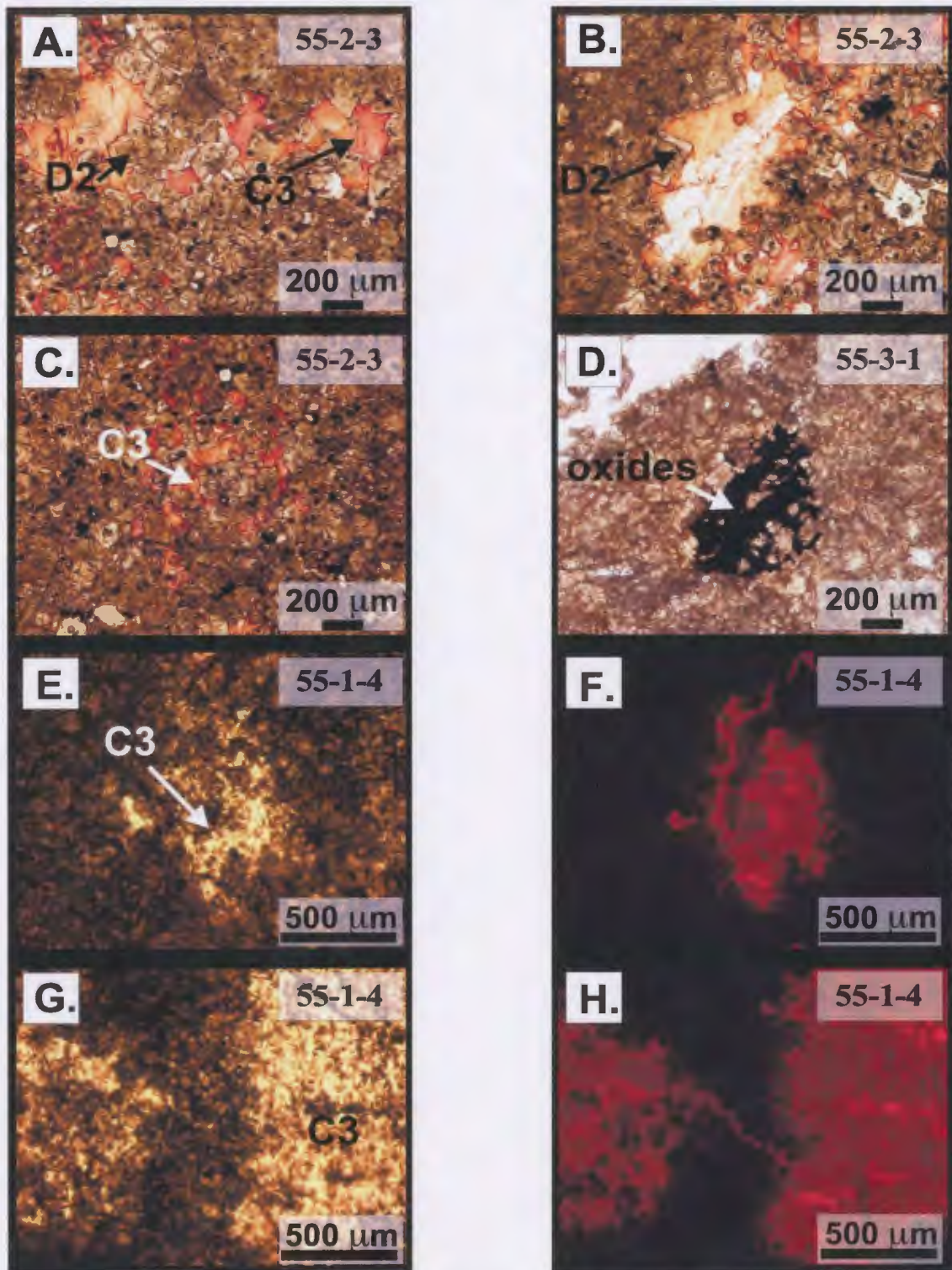


**Plate 3.3.** Plain-polarized light and cathodoluminescence photomicrographs of dolomite and calcite from Gudrid H-55. *A-C*, calcite filling interstitial and vuggy porosity, *D*, oxides in a vug, *E-H*, PL and counterpart CL images showing calcite invading porosities.

average Mn content is found in D3 with 809 ppm (**Table 3.2**). For all three types of dolomite, the average Sr values show little variation (62 to 73 ppm, **Table 3.2**); the highest Sr content (90 ppm) is found in D3.

For calcite, C3 contains higher average concentration of Mn (2965 ppm) and Fe (1286 ppm) compared to C1 (59 and 666 ppm, respectively). The highest Sr content (418 ppm) occurs in C1.

### **3.5.2 Stable Isotopes**

Dolomites 1 and 2 have average  $\delta^{18}\text{O}_{\text{VPDB}}$  values of -5.8 ‰ (N= 14 and 8, respectively; **Table 3.2**). The most  $\delta^{18}\text{O}_{\text{VPDB}}$ -depleted dolomite is D3, with a minimum value of -9.0 ‰ and an average of -7.8 ‰ (N= 4). The  $\delta^{13}\text{C}_{\text{VPDB}}$  values of dolomites have a narrow range from 0.7 to -2.0 ‰, with the lowest mean value in D3 (-1.5 ‰).

Calcite 3 has a mean  $\delta^{13}\text{C}_{\text{VPDB}}$  value of -6.0‰, with minimum and maximum values of -10.5 and -1.3 ‰, respectively (**Table 3.2**), while Calcite 1 has relatively more enriched  $\delta^{13}\text{C}_{\text{VPDB}}$  values, ranging from -0.2 to -0.6 ‰.  $\delta^{18}\text{O}_{\text{VPDB}}$  in C1 and C3 average -9.2 and -7.9 ‰, with minimum values of -9.8 and -9.0 ‰, respectively. Maximum  $\delta^{18}\text{O}_{\text{VPDB}}$  values for C1 and C3 are -8.8 and -5.7 ‰, respectively.

### **3.5.3. $^{87}\text{Sr}/^{86}\text{Sr}$**

$^{87}\text{Sr}/^{86}\text{Sr}$  values taken from calcite and dolomite cements show little variation within wells. Micritic C1 values differ between 0.708897 and 0.708941, with an average of 0.708919 (**Table 3.3**). D1 averages 0.708992 and contains the largest range (0.708864 to 0.709366), while D2 averages 0.709076, ranging from 0.708922 to 0.709264. Overall  $^{87}\text{Sr}/^{86}\text{Sr}$  values average at 0.709007, ranging between 0.708864 and 0.709366.

Generation		CaCO <sub>3</sub> (%)	MgCO <sub>3</sub> (%)	Sr (ppm)	Fe (ppm)	Mn (ppm)	δ <sup>18</sup> O	δ <sup>13</sup> C	<sup>87</sup> Sr/ <sup>86</sup> Sr
Dolomite 1	mean	42.3	57.7	68	2242	344	-5.8	-0.8	0.709084
	max	44.7	60.8	89	5510	1262	-3.4	0.7	0.709366
	min	39.2	55.3	53	499	75	-8.6	-2.0	0.708883
	s.d	2.8	2.8	12	1564	339	1.9	0.9	0.000243
Dolomite 2	mean	40.2	59.8	62	1969	342	-5.8	-0.8	0.709025
	max	40.8	60.5	83	2602	903	-5.1	-0.5	0.709264
	min	39.5	59.2	37	1201	67	-6.6	-1.3	0.708864
	s.d	0.7	0.7	13	493	356	0.6	0.4	0.000201
Dolomite 3	mean	41.7	58.3	73	10127	509	-7.8	-1.5	
	max	44.1	59.5	90	16607	809	-6.9	-1.1	
	min	40.5	55.9	55	7070	360	-9.0	-2.0	
	s.d	0.01	0.01	19	4495	208	0.9	0.4	
Calcite 1	mean	98.0	2.0	363	666	59	-9.2	-0.3	0.708919
	max	98.8	2.8	418	1379	104	-8.8	-0.2	0.708941
	min	97.2	1.2	311	259	37	-9.8	-0.6	0.708897
	s.d	0.01	0.01	53	490	31	0.4	0.1	0.000022
Calcite 3	mean	88.5	11.5	217	1286	2965	-7.9	-6.0	
	max	93.2	17.3	266	1755	4012	-5.7	-1.3	
	min	82.7	6.8	149	1054	2125	-9.0	-10.5	
	s.d	0.05	0.05	59	319	783	1.5	3.9	

**Table 3.2** Trace element, stable isotope, and strontium geochemical data from sampled dolomite and calcite generations from Roberval K-92, Gudrid H-55, and Indian Harbour M-52.

Cement	Average $^{87}\text{Sr}/^{86}\text{Sr}$	Range $^{87}\text{Sr}/^{86}\text{Sr}$	Overall Average $^{87}\text{Sr}/^{86}\text{Sr}$
Micrite (C1)	0.708919	0.708897 - 0.708941	
Dolosparite (D1)	0.708992	0.708864 - 0.709366	0.709007
Dolosparite (D2)	0.709076	0.708922 - 0.709264	

**Table 3.3.** Averages, ranges, and overall  $^{87}\text{Sr}/^{86}\text{Sr}$  average for each cement sampled.

Generation	$T_h$ °C
D2	117.9
	120.9
	123.1
	123.7
<b>mean</b>	<b>121.2</b>
<b>max</b>	<b>123.7</b>
<b>min</b>	<b>117.9</b>
<b>s.d</b>	<b>2.6</b>

**Table 3.4.** Homogenization temperatures from D2 cements, taken from Roberval K-92 and Gudrid H-55.

### **3.5.4. *Microthermometry of Fluid Inclusions***

**Table 3.4** summarizes the homogenization temperature results of the primary fluid inclusions from D2 cements. Note that no sample from D1 or D3 or calcite cements provided measurable primary fluid inclusions. At approximately 3  $\mu\text{m}$  diameter, inclusions were too small to measure melting temperatures. They contained only one phase ( $\text{H}_2\text{O}$ ). Homogenization temperatures ( $T_h$ ) of D2 single-phase inclusions range from 117.9 to 123.7°C, with an average of 121.2°C.

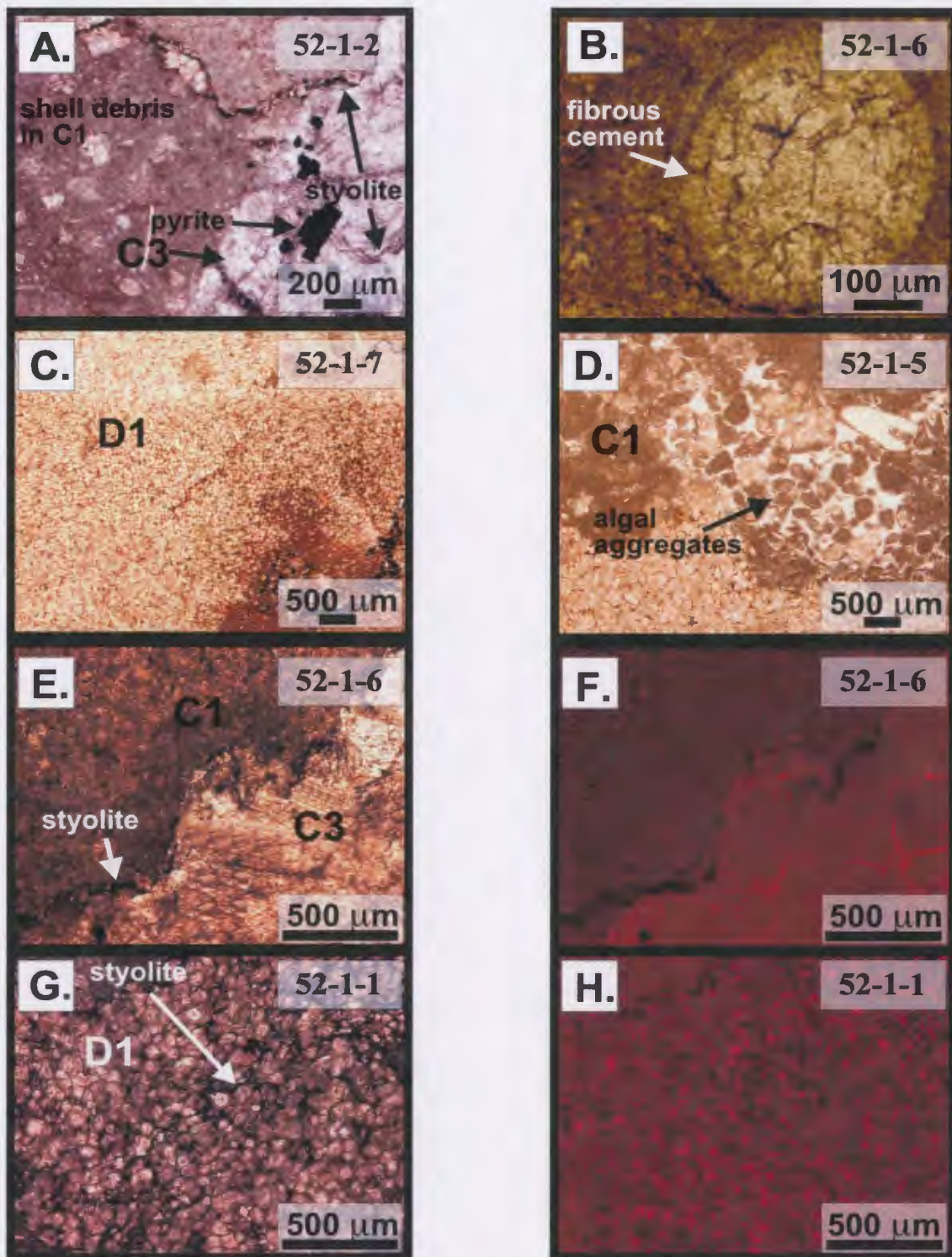
### **3.6 Diagenesis and Paragenetic Sequence**

Figure 3.7 presents the paragenetic sequence based on the above petrographic observations, as well as various cross-cutting relationships between depositional and diagenetic fabrics, pyrite precipitation, and stylolitization events. Four diagenetic environments have been recognized: marine, meteoric, shallow to intermediate, and deep.

Algal aggregates, fibrous cements and micrite lime mud, were precipitated in the marine environment, and comprise the initial carbonate framework (**Fig 3.7; Plate 3.4**). With sedimentation and burial, dissolution of shell fragments (porosity phase 1) occurred along with calcite cementation (C2), resulting in some vugs filled and others left devoid of C2 cements during meteoric diagenesis (**Fig 3.7; Plate 3.2**). With progressive burial calcite cementation continued and dolomicrite (D1) was formed during shallow burial resulting in development of pore spaces (porosity phase 2), which are at times filled with C2. The development of this porosity may be a result of the difference in molar volume

Petrographic Features	Burial Environments			
	Marine	Meteoric	Shallow - Intermediate	Deep
<i>Micrite (C1)</i>	--- --			
<i>Fibrous Cement</i>	--- --			
<i>Algal Aggregates</i>	--- --			
<i>Fossil Fragments</i>	--- --			
<i>Porosity Phase 1 (shell dissolution)</i>		--- --		
<i>Calcite 2 (C2)</i>		--- --		
<i>Dolomite 1 (D1)</i>			--- --	
<i>Porosity Phase 2 (inter-crystalline)</i>			--- --	
<i>Styolites</i>			--- --	
<i>Dolomite 2 (D2)</i>				--- --
<i>Dolomite 3 (D3)</i>				--- --
<i>Calcite 3 (C3)</i>				--- --
<i>Pyrite</i>				--- --
<i>Porosity Phase 3 (late dissolution)</i>				--- --

**Fig. 3.7.** Paragenetic sequence of Labrador Shelf carbonates of studied wells. Events based on petrography and geochemical evidence. Asterisk indicate cements that were unable to be sampled for geochemistry.



**Plate 3.4.** Plain-polarized light and cathodoluminescence photomicrographs of dolomites and calcites from Indian Harbour M-52. *A & B*, micritic and fibrous cements, *C*, dolomite 1, *D*, algal aggregates and micritic cement, *E & F*, calcite 3 invading micritic cements, *G & H*, PPL and CL images of dolomite 1.

between calcite and dolomite (**Fig 3.7**; cf. Warren, 2000). With increasing compaction from burial, low amplitude stylolites cross-cut C1 and D1 cements.

The final stage of dolomitization occurred during deep burial, forming saddle dolomites. Deepest burial C3 cements then filled fractures, vugs, and/or the remaining interstitial pores, also containing pyrite (**Fig 3.7**; **Plates 3.2 - 3.5**). Finally, smoothed or rounded edges of some D3 crystals indicate a third and final phase of porosity developed by dissolution, which occurred during deep burial settings (**Fig 3.7**; **Plates 3.2G & 3.5B, C, D, F**).

### **3.7. Discussion**

The concentrations of Ca in D1, D2, and D3 generations vary between 39.2 mol % and 44.1 mol %, which suggest that these dolomites are non-stoichiometric (**Table 3.2**). The concentrations of Fe and Mn mainly reflect the redox state of the diagenetic environment (e.g., Azmy et al., 2001) and successive dolomite phases from the Labrador Shelf are progressively enriched in these elements, which indicate progressive burial under reducing conditions (**Fig. 3.8A**). The Mn-Sr and Fe-Sr relationships show negative correlations, reflecting the increase in diagenetic alteration (water-rock interaction) with progressive burial (**Figs 3.8B & 3.9A**). However, the trend is more pronounced for the calcite phases likely because it occurred under more open conditions and possibly because of the differences in the distribution coefficients of these elements in dolomites and calcites. The distinctive high Mn concentrations in C3, a reflection of the redox state, suggest that it precipitated at very late stage during deeper burial conditions (**Fig. 3.8A**),

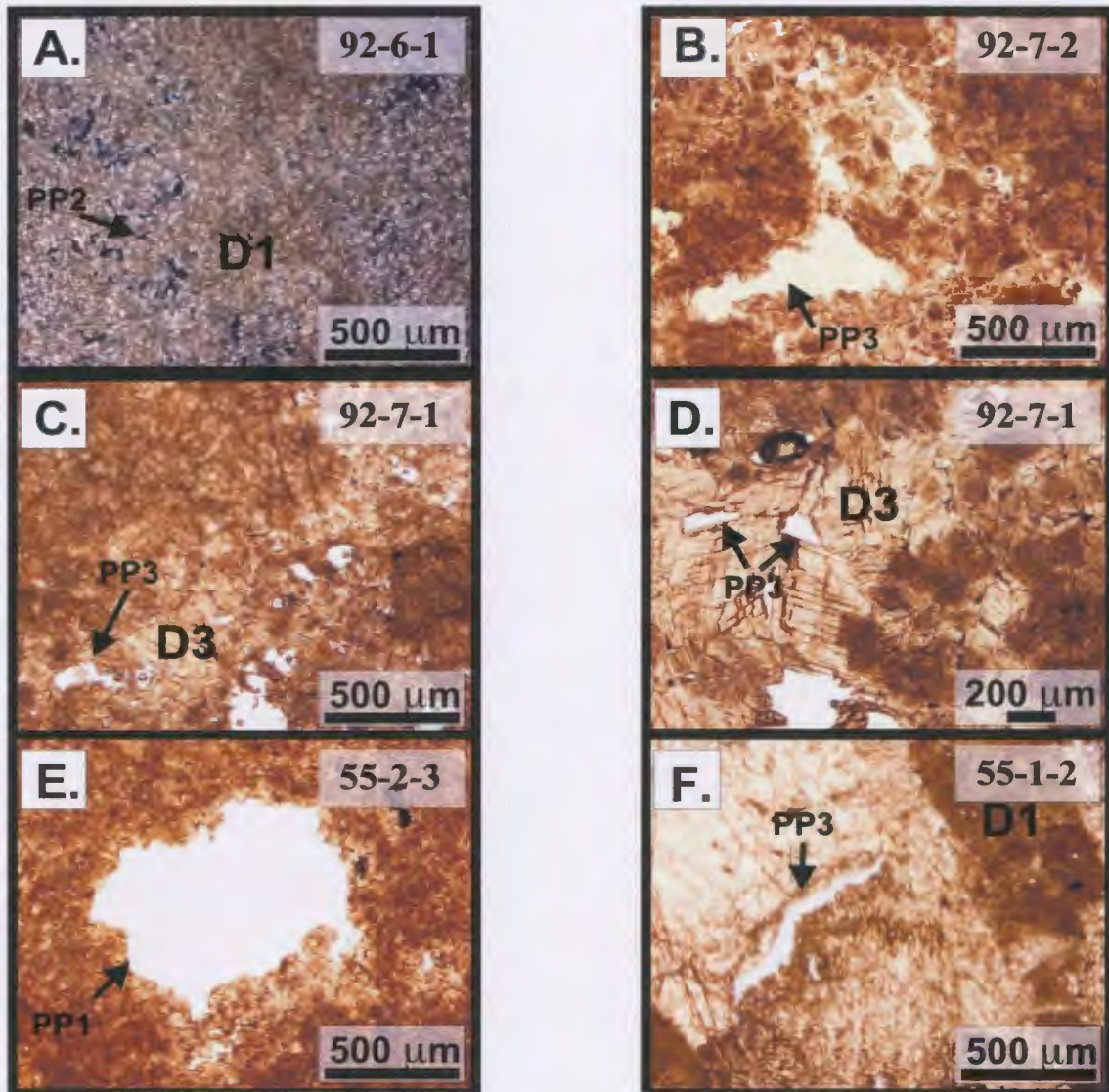


**Plate 3.5.** Photomicrographs showing different phases of porosity development. *A-D*, inter-crystalline and vuggy porosity in Roberval K-92, *E*, vuggy porosity in Gudrid H-55 and *F*, vuggy porosity from PD3. All images taken in plain-polarized light, except *A*, taken in cross-polarized light.

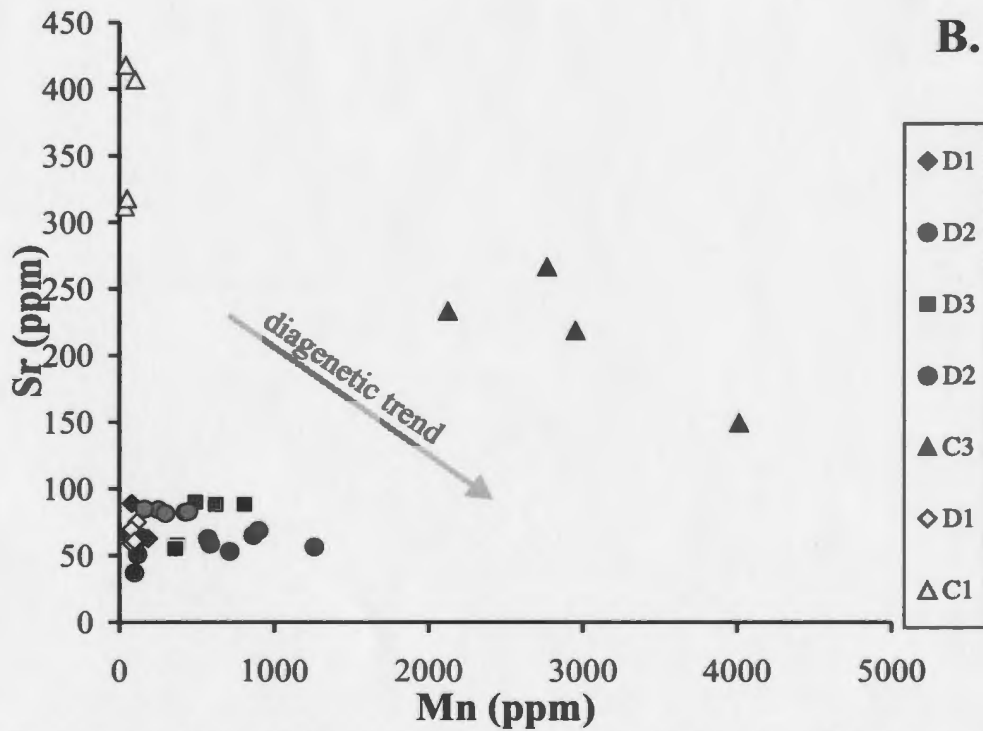
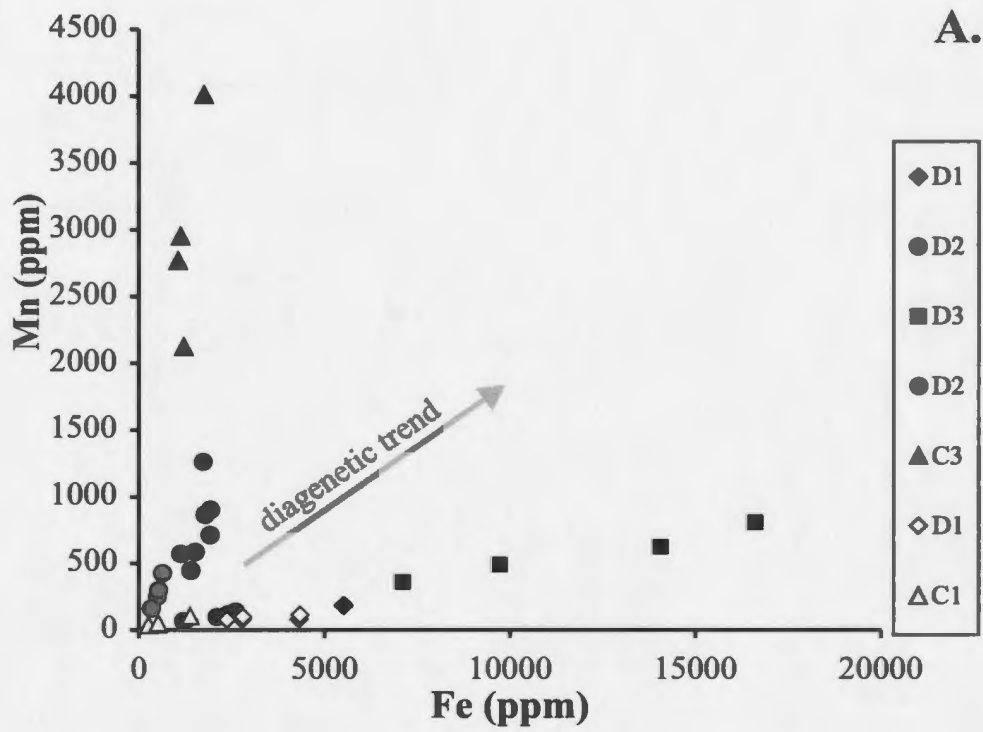


**Fig. 3.8. A.** Fe vs. Mn and **B.** Mn vs. Sr scatter plots of dolomite and calcite cements from Roberval K-92 (black filling), Gudrid H-55 (grey filling), and Indian Harbour M-52 (white fill).

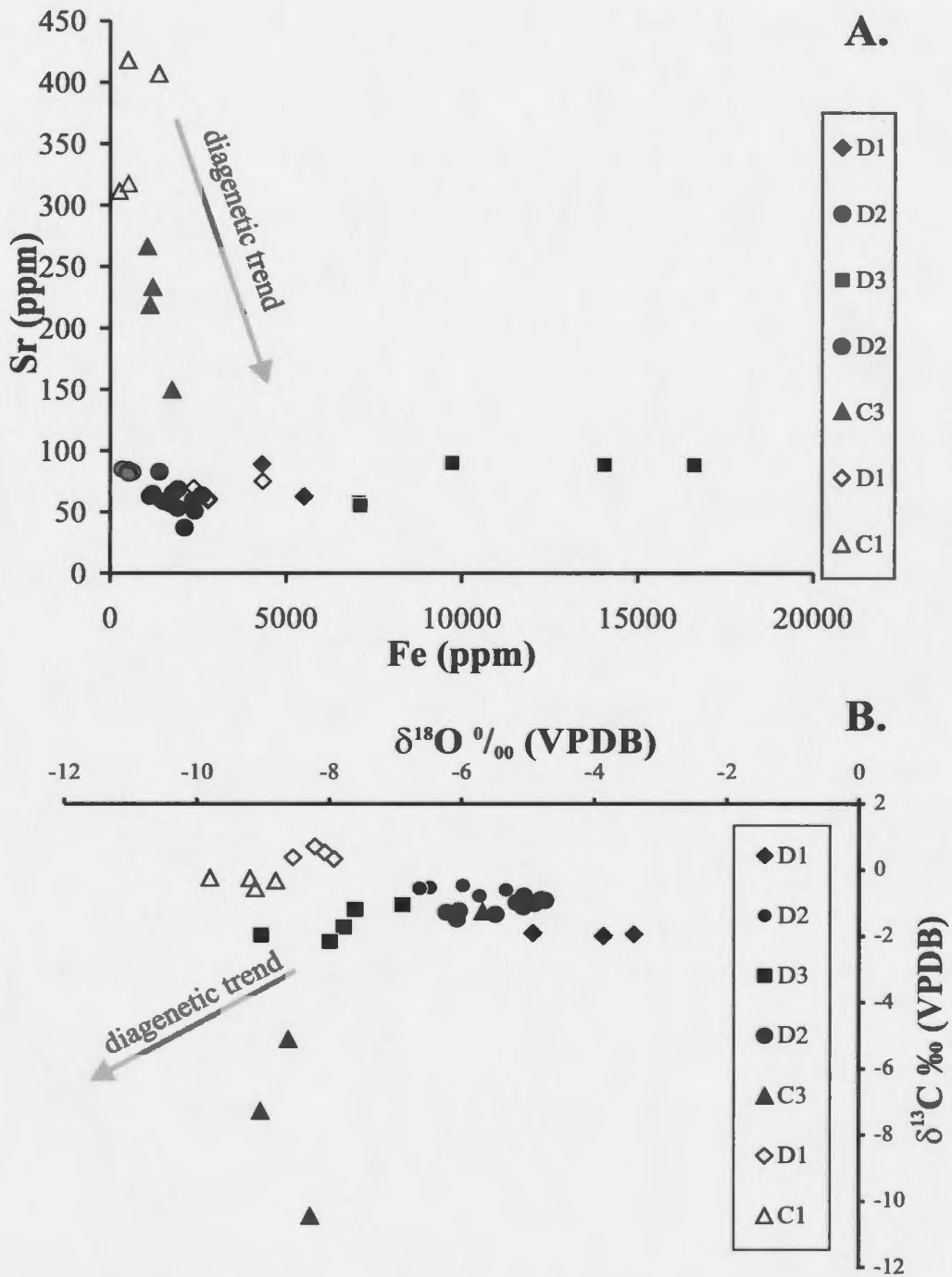


**Fig. 3.9.** *A.* Fe vs. Sr and *B.*  $\delta^{18}\text{O}$  vs.  $\delta^{13}\text{C}$  scatter plots of dolomite and calcite cements from Roberval K-92 (black filling), Gudrid H-55 (grey filling), and Indian Harbour M-52 (white fill).

which is also consistent with its depleted  $\delta^{18}\text{O}$  and  $\delta^{13}\text{C}$  signatures (**Fig. 3.9B**), and the petrographic cross-cutting relationships (cf. Al-Aasm and Azmy, 1996; Lavoie et al., 2005; Lavoie and Chi, 2006). Therefore it is possible that C3 postdates earlier calcite and dolomite cements.

Ideas of the nature of the dolomitizing fluids can be proposed from the Sr concentrations of dolomites (cf. Budd, 1997; Azmy et al., 2001) through the calculation of the Sr/Ca molar ratio of the dolomitizing solution using the equation  $(\text{Sr}/\text{Ca})_{\text{dolomite}} = D_{\text{Sr}}(\text{Sr}/\text{Ca})_{\text{fluid}}$ , where  $D_{\text{Sr}}$  is the distribution coefficient, varying from 0.015 to 0.060 (Budd, 1997). For  $D_{\text{Sr}} = 0.015$ , the calculated Sr/Ca molar ratios of D1 range from 0.0041 to 0.0060, and for  $D_{\text{Sr}} = 0.060$  the ratios range between 0.0010 and 0.0015. The calculated Sr/Ca molar values are lower than values of present-day seawater of 0.0086 (Drever, 1988), thus suggesting that the earliest dolomitization (D1) occurred in the presence of diluted solutions; mixing of marine and meteoric waters is a likely scenario for D1. Furthermore, the low Sr range (53 - 89 ppm; **Table 3.2**) suggests that there are no precursor calcite inclusions, and as a result, the D1 elemental composition arguably reflects the nature of the dolomitizing fluid.

The small crystal size of D1 and lack of two-phase inclusions suggest that it has likely formed in near surface conditions at temperatures ranging between 25 and 30 °C (cf. Goldstein and Reynolds, 1994). To ascertain an age of earliest dolomitization, the assumption is made that Labrador Shelf carbonates belong, or are akin to Ordovician sediments, in affiliation with an extensive passive margin Cambro-Ordovician basin (e.g. Anticosti Basin; cf. Atkinson & Fagan, 2001). Early to Mid-Ordovician seawater values

range from -9.3 and -7.6 ‰ SMOW, with an average of -8.5 ‰ SMOW (Shields et al., 2003). The  $\delta^{18}\text{O}$  value of present-day meteoric water is usually about 4 ‰ lower than that of the seawater (Clark & Fritz, 1997). Assuming that the early Ordovician meteoric and seawaters had similar relative difference in the o-isotopic compositions, the  $\delta^{18}\text{O}$  values estimated for the parent fluids of D1 (**Fig. 3.10**) would fall within the end-members values suggested for the Early to Mid-Ordovician meteoric and seawaters, which is consistent with a possible mixing zone origin.

Generally,  $\delta^{18}\text{O}$  and  $\delta^{13}\text{C}$  signatures of carbonates become progressively depleted with increasing diagenetic alteration and burial depth (Brand & Veizer, 1983; **Fig. 3.9B**). Increased depletion of  $\delta^{18}\text{O}$  and homogenization temperatures of primary fluid inclusions from D2 (**Table 3.4**) suggest formation at deeper burial setting compared to than those of D1, and possibly from hydrothermal fluids. Compared with other cores, the  $\delta^{18}\text{O}$  values of the D1 in Indian Harbour are relatively more depleted (**Fig. 3.9B**) although their trace element contents are still comparable. This is possibly attributed to the depleted  $\delta^{18}\text{O}$  signature of C1, which is likely the precursor of D1 (**Fig. 3.9B**).

Homogenization temperatures of D2 (117.9 – 123.7°C) suggest that the  $\delta^{18}\text{O}$  values for the dolomitizing fluid ranged between 5.5 and 8‰ SMOW (**Fig. 3.10**), which is consistent with the deep burial fluids that are usually circulated through crustal rocks at high temperature.

Average  $\delta^{13}\text{C}$  values of D1, D2 and C1 are comparable (**Table 3.2**), suggesting that the dolomitizing fluid did not contain much dissolved  $\text{CO}_2$  to reset the c-isotope signature, and dolomitization started at early stages of diagenesis, which is consistent

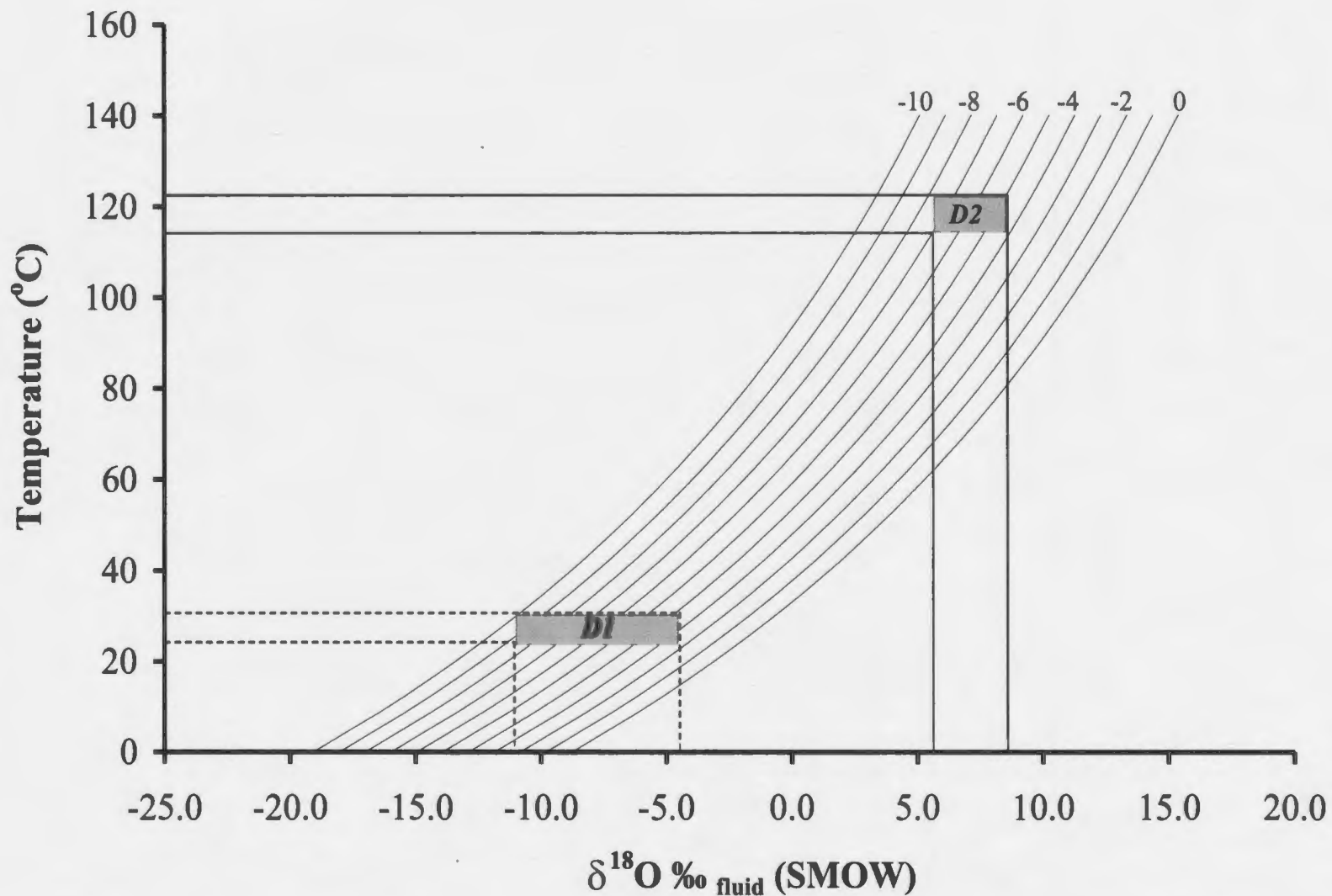


**Fig. 3.10.** Temperature vs.  $\delta^{18}\text{O}_{\text{diagenetic fluid}}$  for various  $\delta^{18}\text{O}_{\text{dolomite}}$  values that were reconstructed from the equation  $10^3 \ln \alpha = 3.2 \times 10^2 T^{-2} - 3.3$  (Land, 1983). The vertical bars indicate the ranges for  $\delta^{18}\text{O}_{\text{fluid}}$  based on the most enriched and depleted sample for the given dolomite generation, while shaded areas mark the preferred temperature ranges.

with the calculated D1 Sr/Ca molar ratios. However, the distinct depletion in the  $\delta^{13}\text{C}$  values of C3 is consistent with deep burial settings as well as a possible influence of organic matter during cementation (**Fig. 3.11**).

### ***3.7.1 Porosity Evolution***

Visual estimates of porosity from thin section range from 1 to 20% and include interstitial and vuggy pores, suggesting that the total porosity in the Labrador Shelf carbonates was controlled by multiple phases of dolomitization and carbonate cementation and dissolution. Dissolution and calcite cementation can be divided into several stages (**Fig. 3.11**), which occurred at different burial depths as a result diverse diagenetic fluid movements. The most critical events leading to porosity generation were initial and latest-stage dolomitization. Conversely, frequent stages of calcite cementation precipitated within pore spaces, particularly from the first and second phases of porosity generation.

The first phase of porosity resulted in moldic pores from dissolution of shell debris, which resulted in elongated and unconnected vugs, ranging from 200 to 400 $\mu\text{m}$  (**Plate 3.2D**) The subsequent phase of porosity generation (intercrystalline) was associated with early dolomitization, a mineralogical-scale phenomenon where porosity was created by volume changes in the crystal lattice from  $\text{CaCO}_3$  to  $\text{MgCa}(\text{CO}_3)_2$  (Warren, 2000). These pores are well to poorly connected, ranging from 50 $\mu\text{m}$  to 200 $\mu\text{m}$  (**Plate 3.2**). The precipitation of C3 cements during deep burial resulted in fractures, and some of the interstitial and vuggy pores occlusion (**Plates 3.3E, G**). Therefore, the deep burial fractures played a minor role in the overall final reservoir. The third event of

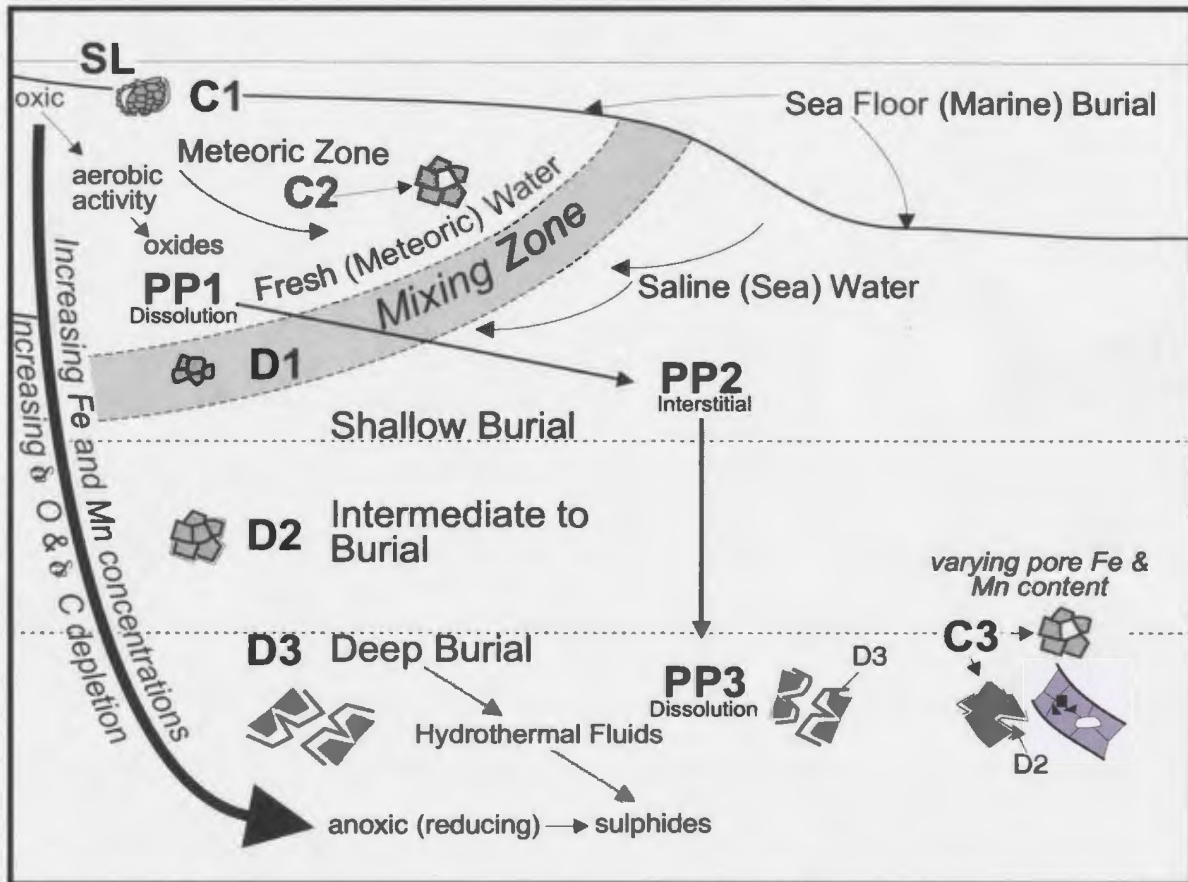


**Fig 3.11.** Schematic diagram of the diagenetic burial environments in a generalized platform carbonate setting. Dolomite, calcite, and porosity phase ("PP") are placed in their interpreted burial realms based on petrography and geochemistry (see text for abbreviations).

porosity generation occurred as very late dissolution during the deep burial stage after the precipitation emplacement of C3. As a result, large vugs, poorly- to moderately-connected and ranging from 200 to >1mm, were created in D3 and C3 cements (**Plates 3.5B-D, F**). However, vugs associated with C3 represent a very small portion (<1%) of the total visual porosity estimates in all samples.

Porosity preservation is determined by the porosity type and by the different diagenetic fluids that have flushed through the system during dolomitization. Calcite cement (C2) was precipitated in open-conditions (e.g. meteoric), periodically filling some pores and pore networks in intercrystalline D1. Vuggy pore spaces can be occluded and filled during this process possibly due to the lack of connectivity and open-system conditions (**Plate 3.2A, B, D**). D2 cements are associated with late stage calcite (C3) whereby intercrystalline and vuggy pores are generally completely filled; suggesting pore omission was a result of well-connected pore networks (Plate 3.3). Again, isolated pores (vugs) associated with D3 (**Plates 3.2G and 3.5B, C, D, F**) may suggest isolation from any deep burial fluids.

### ***3.7.2 Sr-isotopes and implications for age***

The age of the Hopedale Basin carbonates have remained unresolved to date. Dolomites in Gudrid H-55 are assigned to the LPWC2 palynological zone (Westphalian-Stephanian; CNLOPB website, 2007; GSC Labrador Atlas, 1989) and Roberval K-92 dolomites additionally containing Westphalian spores (Balkwill et al. 1990). The Indian Harbour M-52 well is devoid of any palynological material (GSC Labrador Atlas, 1989)

but Jenkins (1984) has dated conodonts in basal core with an Arenigian-Early Llanvirnian age. Additional authors (e.g., Barss, 1979; Bell & Howie, 1990 and Atkinson & Fagan, 2001) suggest that Paleozoic carbonates might be Early to early Late Ordovician.

The  $^{87}\text{Sr}/^{86}\text{Sr}$  values (ranging between 0.708864 and 0.709366) from micrites (**Plate 3.4**) in the Indian Harbour M-52 well match the primary values documented for the Early to Mid-Ordovician oceans (Veizer et al., 1999 and more references therein). Dolosparites in both Roberval K-92 and Gudrid H-55 wells also yielded Sr-isotope ratios within a similar range (Table 3.3) indicating that dolomitization started early, shortly after inception of burial. Thus, the Labrador Shelf platform carbonates, in the Hopedale Basin, were likely deposited during Early to Mid-Ordovician (**Fig. 3.12**) rather than during the Carboniferous, as suggested by Westphalian-Stephanian spores and thus, strengthening the claim (Jenkins, 1984) that these spores may be contaminants. It is also unlikely that  $\delta^{13}\text{C}$  values retrieved from micritic (C1) cements have been altered, and reset, giving an Ordovician age. Instead,  $^{87}\text{Sr}/^{86}\text{Sr}$  values were obtained from pristine C1 cements, and hence, Ordovician seawater. This is also consistent with their distinctive depleted  $\delta^{13}\text{C}$  values (**Fig. 3.12**) relative to those of their Carboniferous counterparts (cf. Veizer et al., 1999). However, this does not rule out the possibility of Carboniferous carbonates occurring somewhere along the margin although, it is quite probable that the Westphalian-Stephanian spores in Gudrid H-55 and Roberval K-92 were contaminants.

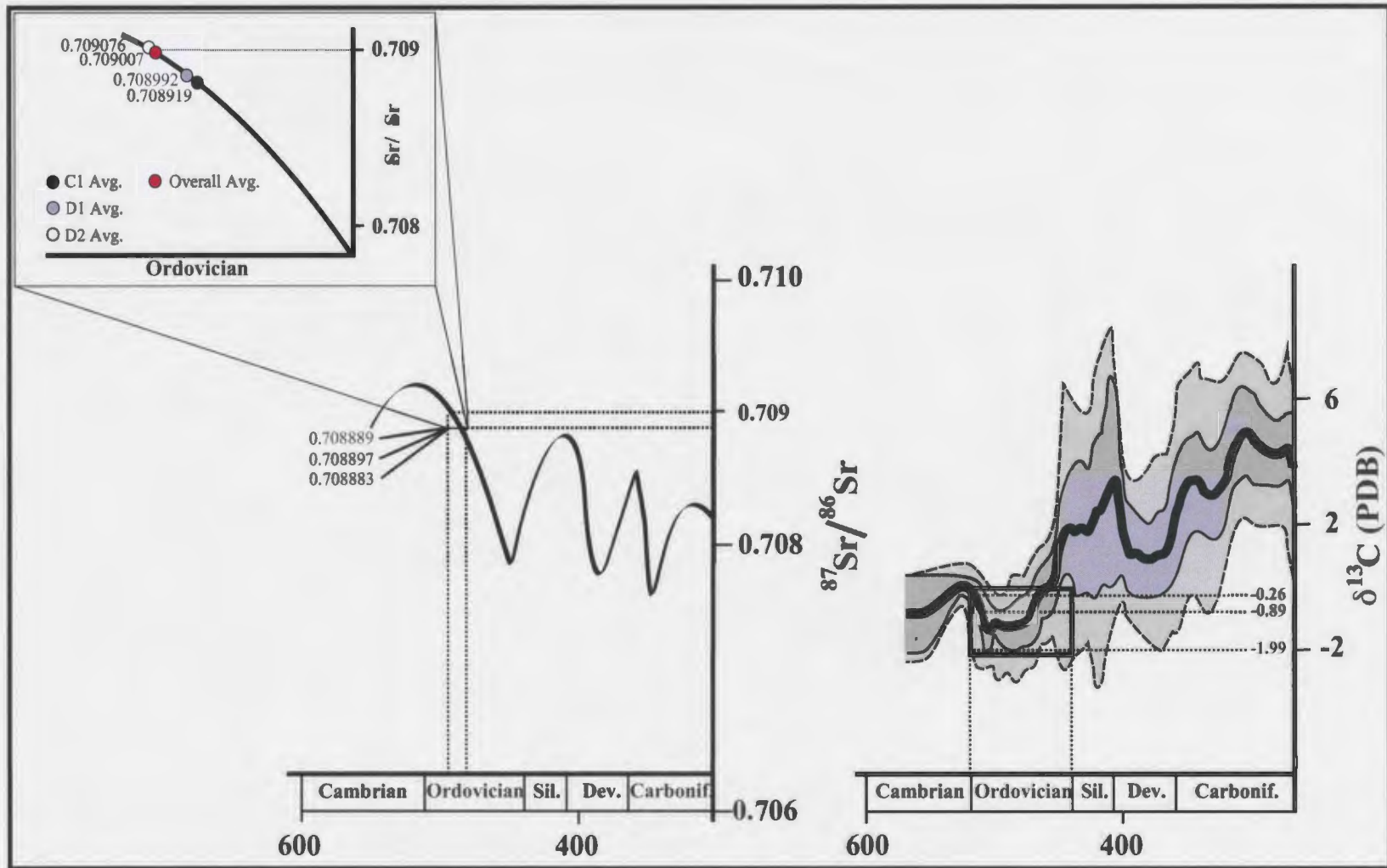


**Fig. 3.12.** Average  $^{87}\text{Sr}/^{86}\text{Sr}$  and  $\delta^{13}\text{C}$  values from calcite and dolomite cements compiled with Veizer et al. (1999) reference  $^{87}\text{Sr}/^{86}\text{Sr}$  and  $\delta^{13}\text{C}$  curves.

### 3.8 CONCLUSIONS

Labrador Shelf carbonates investigated in three cores, Roberval K-92, Gudrid H-55, and Indian Harbour M-52 have been influenced by multi-phase dolomitization and calcite cementation throughout their burial history. Roberval K-92 and Gudrid H-55 carbonates were more extensively dolomitized than Indian Harbour M-52, while calcite cementation is predominant in all studied core.

Dolomites can be classified, based on petrography and CL images, into three generations with distinct petrographic properties, including:

- 1) D1, anhedral to subhedral dolosparite (20 – 150 $\mu$ m);
- 2) D2, subhedral to euhedral dolosparite (50 – 300 $\mu$ m);
- 3) D3, euhedral saddle dolomite (250 – 700 $\mu$ m);

Of the three generations of dolomites, D1 is relatively more abundant in Roberval K-92 and Indian Harbour M-52 core, while D2 is abundant in Roberval K-92 and Gudrid H-55. Finally, the latest dolomite D3 is mostly found in Roberval K-92.

Trace elements, stable isotope geochemistry, and fluid inclusions support petrographic classifications and suggest distinct populations of dolomites. The calculated Sr/Ca molar ratios the earliest dolomite (D1) indicates that the dolomitizing fluid was likely of mixing zone origin.

Porosity evolution is strongly linked to dolomitization, diagenetic dissolution, and late fracture-filling calcite cementation. Initial dolomitization and dissolution created interstitial and vuggy porosity, respectively. Progressive burial was associated with deep burial calcite cements, occluding porosity, although very late stage dissolution had some

recovery effect. Deep burial fractures had insignificant contribution to the reservoir porosity. Ultimately, porosity preservation is controlled by effective porosity whereby pore types and pore networks allow diagenetic fluids to enter and precipitate calcite during progressive burial.

The  $^{87}\text{Sr}/^{86}\text{Sr}$  values and  $\delta^{13}\text{C}$  signatures of the investigated carbonates are consistent with those globally documented for Early to Mid-Ordovician seawater and not that of enriched Carboniferous  $\delta^{13}\text{C}$  values. Therefore, it is suggested that these carbonates were deposited on the continental shelf of Iapetus, prior to continental accretion during the Mid to Late Ordovician and not as passive margin sediments, during the formation of the Appalachians in the Carboniferous.

### **3.9 Acknowledgments**

This project was supported by the Pan-Atlantic Petroleum Systems Consortium (PPSC) funds to Drs. Michael Enachescu and Karem Azmy. Special thanks to Dr. Dieter Buhl at Ruhr University, Bochum, Germany and Dr. Denis Lavoie at the Geological Society of Canada (Quebec). We would like to extend our thanks to Alison Pye, Pam King and Wilfredo Diegor. Core viewing and sampling was permitted by CNLOPB with the help of Dave Mills and Jason Newell. Core pictures are courtesy of Matthew Harvey (ConocoPhillips). Seismic images are courtesy of GSI. Cathodoluminescence imaging was provided by Dr. John Hanchar at Memorial University. Many other thanks go to people who have helped one way or another throughout the process: Allison Cocker, Erin Gillis, Angie Dearin, Michelle Martin, Mike Greene, Jordan Stead, Christopher

Phillips, Nicola Tonkin, Leon Normore, Dr. Mark Wilson (Memorial University), and Dr. Rudi Meyer (University of Calgary).

**CHAPTER 4  
(MANUSCRIPT 2)**

**PETROGRAPHY, DIAGENETIC EVOLUTION AND IMPLICATIONS  
FOR RESERVOIR QUALITY OF THE BJARNI FORMATION  
SANDSTONE, HOPEDALE BASIN, LABRADOR SHELF**

**SCHWARTZ, S.S.<sup>1</sup>, MEYER, R.<sup>2</sup> AND ENACHESCU, M.E.<sup>1</sup>**

<sup>1</sup>Department of Earth Sciences, Memorial University of Newfoundland, St. John's, NL,  
Canada A1B 3X5

<sup>2</sup>Department of Geoscience, University of Calgary, Alberta, Canada, T2N 1N4

**ABSTRACT**

The Labrador Shelf is a Mesozoic extensional margin containing the Saglek and Hopedale Basins, with separation between North America and Greenland occurring approximately 70 Ma (Louden, 2002). The Hopedale Basin, a site for of past and present petroleum exploration, is located north of the Orphan Basin and is situated between two basement highs, the Okak and Cartwright Arches. In total, five significant hydrocarbon discoveries have been made in the Hopedale Basin, which include the Snorri, Hopedale, North Bjarni, Bjarni, and Gudrid fields. Estimates of reserves are 22 trillion cubic feet with approximately 4.2 Tcf of natural gas and 123 million barrels of NGL (CNLOPB). Reservoir types include Early to Mid Cretaceous synrift alluvial to fluvial sandstones (i.e. Bjarni Formation) and unnamed prerift Paleozoic carbonates preserved on the top of basement highs. Six exploration wells from different stratigraphic depths and locations within the Hopedale Basin, containing approximately 31 m of Bjarni Formation sandstone, were logged, sampled, and petrographically analyzed from intervals that include Bjarni H-81 (2157 – 2164 m), Ogmund E-72 (2234 – 2240 m), North Bjarni F-06

(2452 – 2458 m), Herjolf M-92 (2632 – 2640 m), Roberval K-92 (3095 – 3112.5 m), and North Leif I-05 (3110 – 3113.5 m).

Detrital compositions of sandstones vary from samples at inter-well and intra-well locations and encompass a broad range of framework clast compositions, ranging from  $Q_{90.5}F_{2.0}L_{7.7}$  to  $Q_{38.5}F_{39.0}L_{22.5}$ . Detrital minerals are generally anhedral to subhedral, ranging between 20 and 1050 $\mu$ m, poorly sorted, and include mono- and polycrystalline quartz, potassium feldspars and minor plagioclase, with intrusive igneous lithic clasts, and accessory minerals that include biotite, orthopyroxene, and sillimanite. The main diagenetic minerals include iron oxides (e.g. hematite), chlorite, ferroan and non-ferroan calcite cements, kaolinite, and quartz overgrowths. Inter- and intragranular porosities are recognized and developed as a function of sediment provenance and burial dissolution of potassium feldspars, respectively. The total porosity, a sum of intergranular and intragranular porosities, varies between 7.0 and 60.0 point counts per sample, with the highest total porosity observed at Bjarni H-81 (47.0). Both porosities are partially occluded by diagenetic minerals, reducing overall porosity. Feldspar dissolution occurred simultaneously during ferroan and non-ferroan calcite cementation, from shallow to deep burial, suggesting that it may have played a role in calcite and kaolinite precipitation. It is suggested here that the diagenetic evolution of the Bjarni Formation sandstone is intimately related to its tectonic setting. Sediment maturity is reflected in the varying inter- and intra-well compositions, driven by chemical weathering, which lead to changes in pore water chemistry, influencing the destruction of potassium feldspars and co-precipitation of diagenetic minerals.

#### 4.1 INTRODUCTION

The petroleum potential of the Labrador Shelf has been investigated for more than 40 years. The first exploration wells were drilled in the 1970's. Located fewer than 600 km northwest of the Orphan Basin (Fig. 4.1), the Labrador Shelf contains 27 exploration wells, divided amongst the Saglek and Hopedale basins (Fig. 4.2). Gas and gas condensate were identified in five exploration wells: Snorri J-90, Hopedale E-33, North Bjarni F-06, Bjarni O-82, and Gudrid H-55. Reserves are estimated at 4.2 Tcf of natural gas and 123 million barrels of NGL (C-NLOPB; Atkinson & Fagan, 2001). Play types include both siliciclastic (e.g. Bjarni Formation) and carbonate reservoirs (unnamed Paleozoic dolomites). North Bjarni has reserves at 2.2 Tcf of gas and 82 million barrels of NGL (C-NLOPB; Atkinson & Fagan, 2001), and Gudrid H-55 has tested gas rates of 8.1 MMcf/d (C-NLOPB; Atkinson & Fagan, 2001).

Siliciclastic sediments form almost exclusively the Mesozoic-Cenozoic basin fill of the Labrador basins (cf. Umpleby, 1979; McWhae et al., 1980; Balkwill et al., 1990; Enachescu, 2006; Martin, 2007). The effects of diagenesis on siliciclastic sediments and its relationship to petroleum geology have been extensively documented (cf. Hurst, 1981; Saigal et al., 1988; Bjørlykke, 1998; Midtbø et al., 2000; Storvoll et al., 2000; Lima & De Ros, 2002; Lee et al., 2003). From an economical hydrocarbon-bearing perspective, understanding diagenetic alteration of sediments is extremely important because diagenesis can be either detrimental or beneficial to reservoir quality, classification, and development of reservoirs.

The main objectives of this paper are: (1) to identify and petrographically classify the Bjarni Formation sandstones in the Hopedale Basin from core samples; (2) to

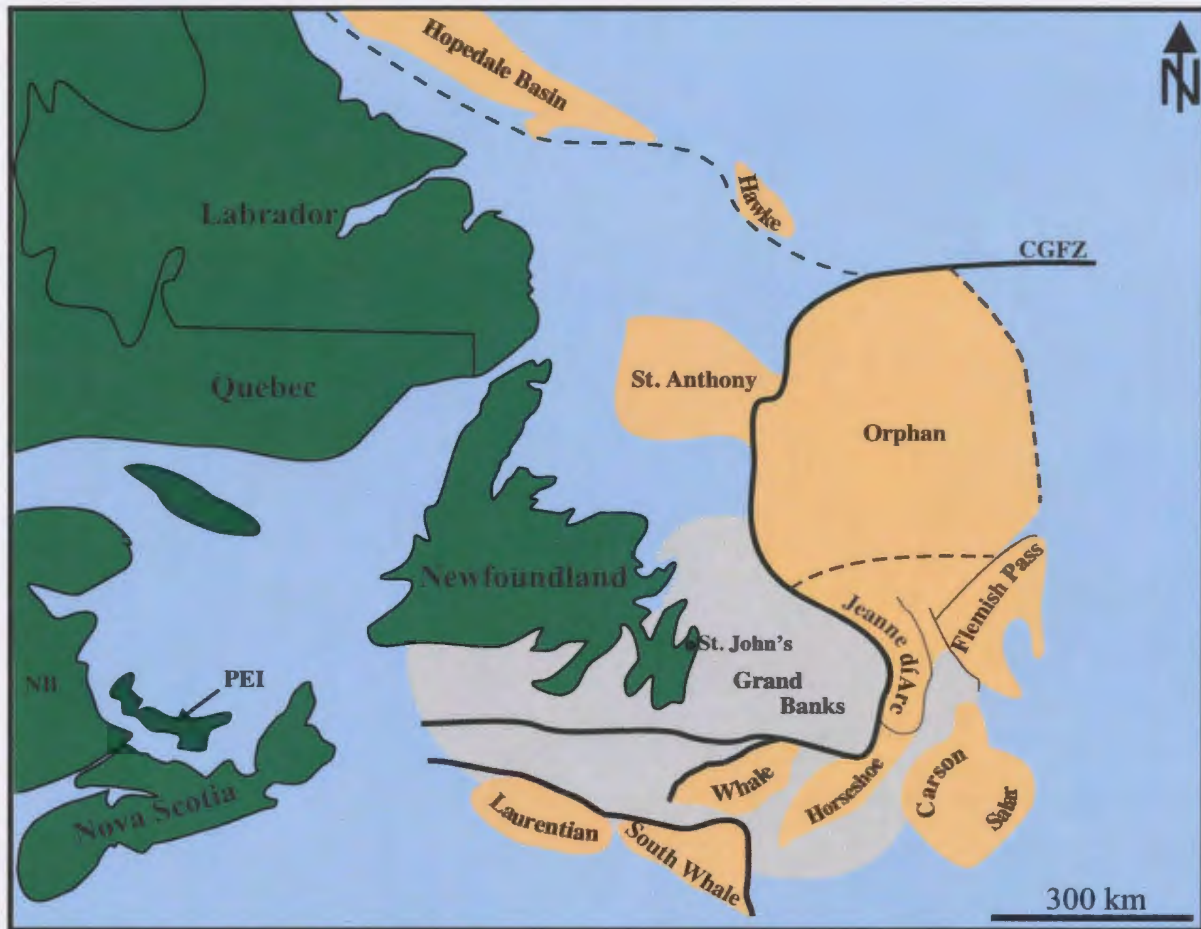


**Fig. 4.1.** Map of Eastern Canada highlighting the offshore Mesozoic sedimentary basins (yellow) and Grand Banks (grey). Modified after Enachescu, 1992.

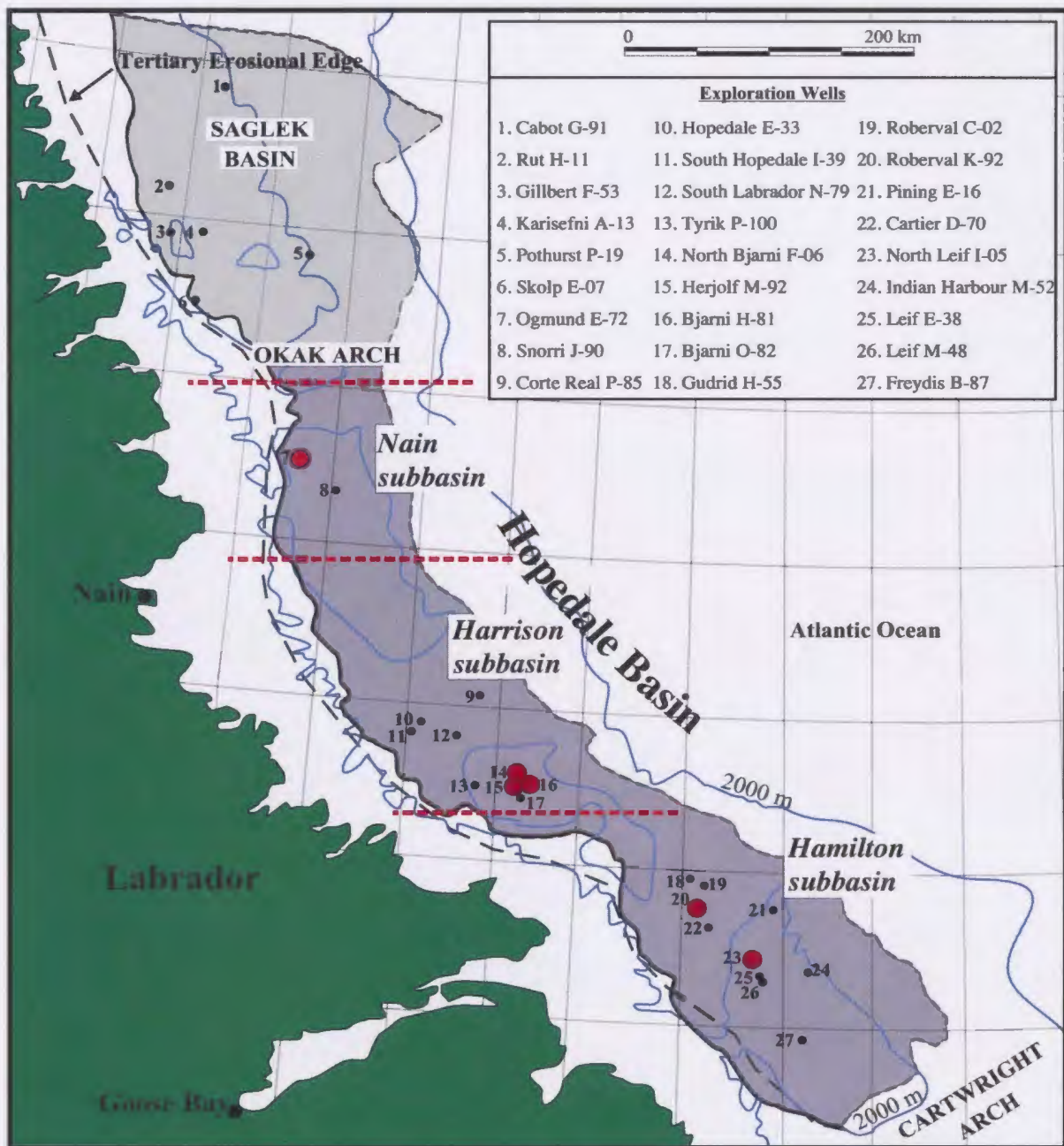


**Fig. 4.2.** A map showing the locations of the exploration wells in the Hopedale (dark grey) and Saglek (light grey) basins, Labrador Shelf. Included are Enachescu (2006) subbasins (between dashed red lines). Larger red dots indicate wells studied. Modified after Atkinson and Fagan, (2001).

petrographically document and investigate main authigenic minerals and diagenetic events; (3) investigate the effects and controls of diagenesis on porosity development, relating to reservoir quality, and; (4) describe any similarities or differences in diagenetic alteration based on well location and stratigraphic depth within the basin.

## **4.2 TECTONIC & GEOLOGICAL FRAMEWORK**

Labrador Shelf was formed through continental extension during the Late Mesozoic, preceding a cycle of basin closure and multiple orogenic events during the Paleozoic. The opening of the Labrador Sea, and the creation of the Saglek and Hopedale basins, represent a single and relatively simple rifting stage when compared with multiple events occurring to the south along the Newfoundland-Ireland and Newfoundland-Iberian margins (Louden, 2002; Enachescu et al., 2005). Labrador margin rifting commenced during the Early Cretaceous (Berriasian) and ended upon Labrador-Greenland break-up during the Late Cretaceous (McWhae et al., 1980; Balkwill, 1987; Louden, 2002; Sørensen, 2006).

As a result, the regional stratigraphy is composed of Mesozoic-Cenozoic sediments, filling the Hopedale and Saglek Basins and overlying remnants of Paleozoic carbonates. The stratigraphy has been separated as corresponding to five distinct tectonic stages (Enachescu, 2006; Enachescu and Martin, 2007; **Fig. 4.3**) containing prerift, synrift, postrift (predrift), drift and postdrift sediments. For the interest of this paper, only the hydrocarbon-bearing synrift Bjarni Formation will be discussed.

### ***4.2.1 Early Cretaceous Synrift and The Bjarni Formation***

The second litho-tectonic stage of the Labrador margin formation is represented by Early to Mid Cretaceous sediments (**Fig 4.3**), deposited above the Labrador

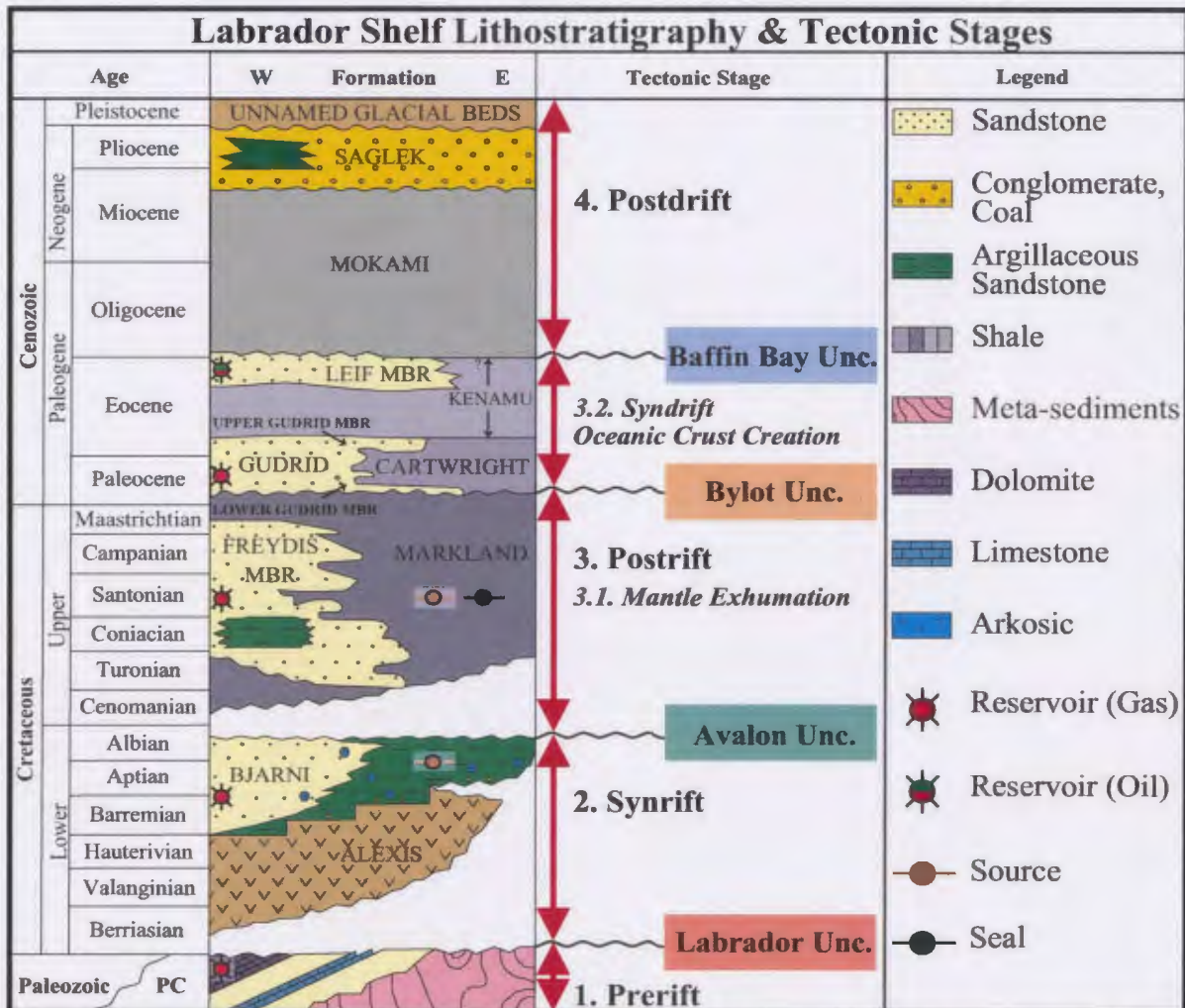


**Fig. 4.3.** Stratigraphy and tectonic evolution of the Labrador Shelf, including major unconformities (Modified after Enachescu, 2006).

Unconformity during intra-cratonic rifting in a climate thought to be warm-humid, tropical to sub-tropical (Douma, 1987). Rifting is indicated by the presence of the volcanic-epiclastic Alexis Formation, containing Neocomian (Berriasian-Albian) ages from basalt whole-rock K-Ar analyses (McWhae et al., 1980; Balkwill et al., 1990). However, Oxfordian-Kimmeridgian-dated gabbro dykes located on the Greenland conjugate margin may suggest an earlier initiation of rifting (Balkwill et al., 1990).

The Bjarni Formation type section is located between 3767 m and 2614 m in the Herjolf M-92 well (Umpleby, 1979). The lithology of the lower member is described as conglomeratic, coarse to fine-grained, lithic, feldspathic, coaly, quartzose sandstones interbedded with non-marine shales (cf. McWhae et al., 1980; Balkwill et al., 1990), generally representing a continental depositional setting of alluvial-fluvial sandstones. The upper member of the Bjarni Formation consists of finer grained carbonaceous feldspathic sands with some marine, but predominantly nonmarine shales (Balkwill et al., 1990), possibly indicating fluvial to marginal marine deposition with some marine shales.

Preliminary petrographic investigations of the syn-rift Bjarni Formation have been briefly documented by Umpleby (1979), McWhae et al. (1980), and Balkwill et al. (1990). The Bjarni Formation is described as containing equal amounts of detrital quartz and feldspar with some clay matrices by Umpleby (1979), who briefly documented the diagenetic affects on the Bjarni Formation sandstones. Feldspar dissolution, calcite cementation, and clay mineralization are described as affecting porosity, which is "...irregularly distributed and appears to be mainly secondary after the dissolution of calcite." (Umpleby, 1979, p. 10). The porosity averages approximately 12 %, consistent with values derived from petrophysical and visual analyses (Umpleby, 1979).

### 4.3 METHODS & DATABASE

Six wells containing cores of the Bjarni Formation from the Hopedale Basin were logged and sampled at the Canada-Newfoundland Offshore Petroleum Board (CNLOPB website, 2007) core facilities in St. John's, Newfoundland. Following documentation of lithologies, sedimentary structures, diagenetic textures, and ichnofabrics, samples were cut from core and prepared for petrographic thin sections (**Table 4.1**). Sample spacing was based on core quality, percentage of core recovered and preserved, and presence of diagenetic textures. Thin sections were impregnated in blue-dyed epoxy, mounted on glass slides, cut to 30  $\mu\text{m}$ , and stained for feldspars using 55% hydrofluoric acid and sodium cobaltinitrite, while calcite cements were stained using Alizarin Red S (cf. Dickson, 1966).

Thin sections were analyzed using a *Nikon Eclipse E600* petrographic microscope. Total point counts, ranging from 200 to 370, were recorded for each thin section and then plotted on ternary diagrams for sandstone classification. Authigenic minerals and any other diagenetic features (e.g. feldspar dissolution) were also counted during this process. The point counting method used in this study ('Line Method') entails counting individual grains by the intersection of the cross hairs amongst equally spaced linear traverses along thin sections (Galehouse, 1969, 1971). However, it is important to note that point counting of detrital and diagenetic minerals assume that grains are equally spaced and are of similar, if not, equal size. Framework grains were automatically normalized to 100% when plotted on ternary diagrams using Excel<sup>®</sup> (i.e. *Ternplot*) and point count abundances of diagenetic minerals (and porosity) were represented as a fraction of a sample as well as an average abundance per well.

Well	Fm	Core	Top (m)	Base (m)	Gross (m)	Rec. (m)	Rec. (%)	Thin sections
BJARNI H-81	Bjarni	1	2157.0	2164.0	7.0	2.4	34%	2
N. BJARNI F-06	Bjarni	1	2452.0	2458.0	6.0	1.5	25%	3
HERJOLF M-92	Bjarni	1	2632.0	2640.0	8.0	7.6	95%	10
NORTH LEIF I-05	Bjarni	1	3110.0	3113.5	3.5	3.5	99%	5
OGMUND E-72	Bjarni	2	2234.0	2240.0	6.0	5.3	88%	3
ROBERVAL K-92	Bjarni	2	3095.0	3112.5	17.5	10.5	60%	3
<i>TOTAL</i>						<b>30.8</b>		<b>26</b>
<i>AVG.</i>						<b>5.1</b>		

**Table 4.1.** Core numbers, thicknesses, thin-sections, and well names used to study the Bjarni Formation sandstone.

Finally, sandstones were classified and normalized to 100% using QFL ternary diagrams (modified from Pettijohn, 1975; Folk, 1968) to graphically represent compositions based on three end member framework grains; Quartz (Q), Feldspar (F), and Lithics (L). The greatest stability and the sum of monocrystalline quartz, chalcedony grains, polycrystalline quartzite, and chert is represented by Q. Feldspar grains (F) that are the most abundant of the unstable single-crystal grains. L is the sum of all the unstable grains (lithic or rock fragments), including sedimentary, igneous, and metamorphic grains.

#### **4.4 BJARNI FORMATION CORE DESCRIPTIONS**

##### ***4.4.1 Ogmund E-72***

Ogmund E-72 well, drilled to a total depth (TD) of 3094 m, is the most northerly-drilled exploration well in the Nain subbasin (Enachescu, 2006) within the Hopedale Basin (**Fig. 4.2; #7**), and is here interpreted as a alluvial to fluvial sandstone. Ogmund E-72 contains both the Bjarni Formation (core 2) and Markland Formation (core 1). Average porosity values for core 2 are 18.7 % (CNLOPB basins webpage).

Core 2 contains coarse to very coarse grained, green-yellow sandstone, with laminae and beds (2 to 12 cm) that are generally intercalated with black shale laminae (**Fig. 4.4**). Shale laminae appear irregular, lenticular, commonly scoured by overlying sandstone beds. The only sedimentary structures present are planar and inclined laminations. A subrounded igneous (granitic) boulder, approximately 20 cm in length is present at approximately 75 cm from the base of the core (**Plate 1A**).

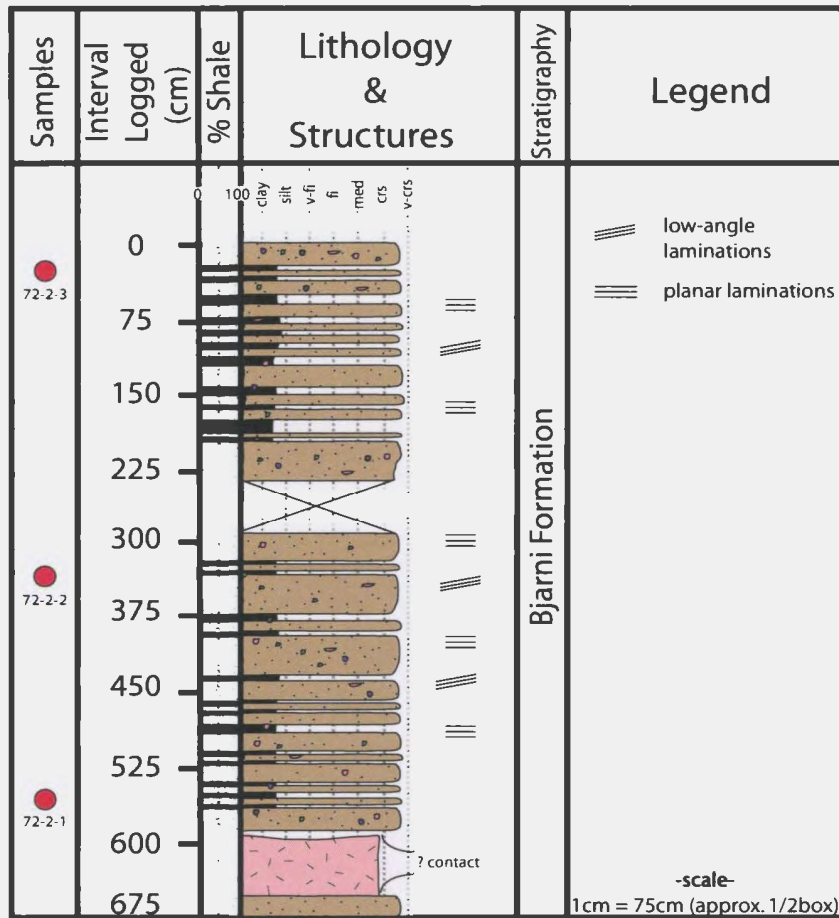
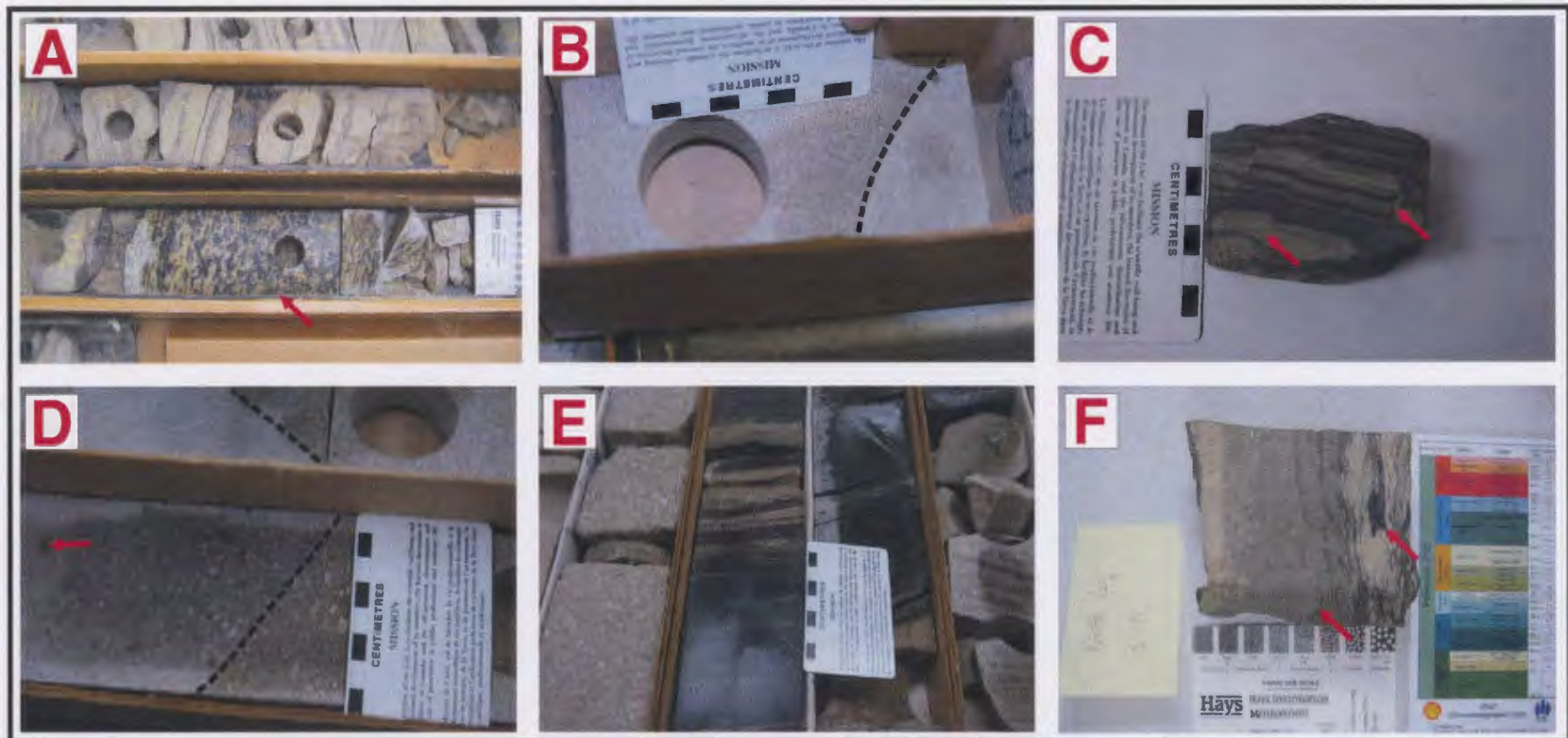


Fig. 4.4. Bjarni Formation core logged from well Ogmund E-72.



**Plate 4.1.** Images of Bjarni Formation core taken from the six wells studied. **A.** Ogmund E-72, core 2 (~2240 m - 2237 m) with possible random igneous boulder (arrow) amongst flaser to wavy laminations; **B.** North Bjarni F-06, core 1 (~2451.5 m) with dashed line indicating a calcite cemented horizon and arrow pointing to pyrite; **C.** Bjarni H-81, core 1 (~2156 m) indicating small scale faulting of wavy laminations (arrow); **D.** Herjolf M-92, core 1 (~2632 m - 2633 m) with dashed lines indicating cemented horizons and an arrow indicating pyrite; **E.** Roberval K-92, core 2 (~3097 m - 3100 m) with conglomeratic sandstone and inclined lenticular to wavy laminations; and **F.** North Leif I-05, core 1 (~3110.5 m) with arrows showing coal stringers and fragments.

#### **4.4.2 Herjolf M-92**

The Herjolf M-92 well is located towards the middle of the Hopedale Basin (Harrison subbasin) and was drilled to a TD of 4086.1 m (**Fig. 4.2; #15**). Four cores were retrieved during exploration drilling: cores 1 and 2 (Bjarni Formation), core 3 (Alexis Formation), and core 4 (basement). Core 2 was omitted from this study because it dominantly contains mudstone facies, and not sandstone. Cored samples from Herjolf M-92 yield an average porosity of 15.9 % in core 1 (CNLOPB basins webpage).

Core 1 dominantly consists of beige-grey, granular to fine grained, conglomeratic sandstone (**Fig. 4.5**). Only a few mudstone beds and laminations are present towards the base of the core. Within the sandstones there are a few intervals that coarsen-upward (525 – 540 cm and 1300 cm) and some that fine upward (600 – 750 cm). Two fine-grained calcite cemented horizons are present towards the top of core 1 along with disseminated pyrite (**Fig. 4.5; Plate 1D**). Sedimentary structures are rarely visible and only include planar laminations and minor inclined laminations. These sandstones are interpreted to represent fluvial deposition via braided or meandering rivers.

#### **4.4.3 Bjarni H-81 and North Bjarni F-06**

Core from Bjarni H-81 and North Bjarni F-06 exploration wells combine for approximately 4 m of core (**Table 4.1**). Bjarni H-81 (**Fig. 4.6A**) and North Bjarni F-06 (**Fig. 4.6B**) wells are located in the Harrison subbasin of the Hopedale Basin (**Fig. 4.2; #16 & #14**) with TD's of 2515.2 m and 2813 m, respectively.

The wells are located in different fields but relatively close to each other; they are discussed together because of the relative very poor core recovery of 34% and 25%, respectively. Porosity analyses in North Bjarni F-06 average 16.7 % (CNLOPB basins

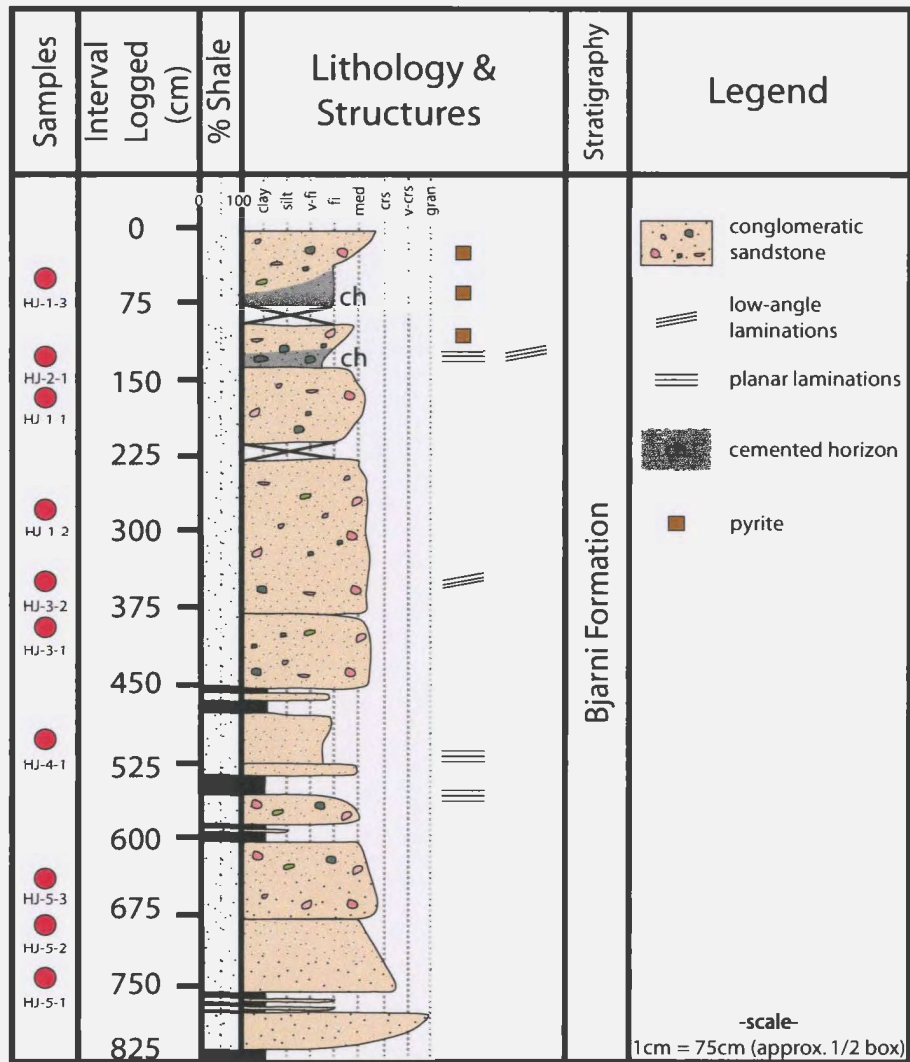


Fig. 4.5. Bjarni Formation core logged from well Herjolf M-92.

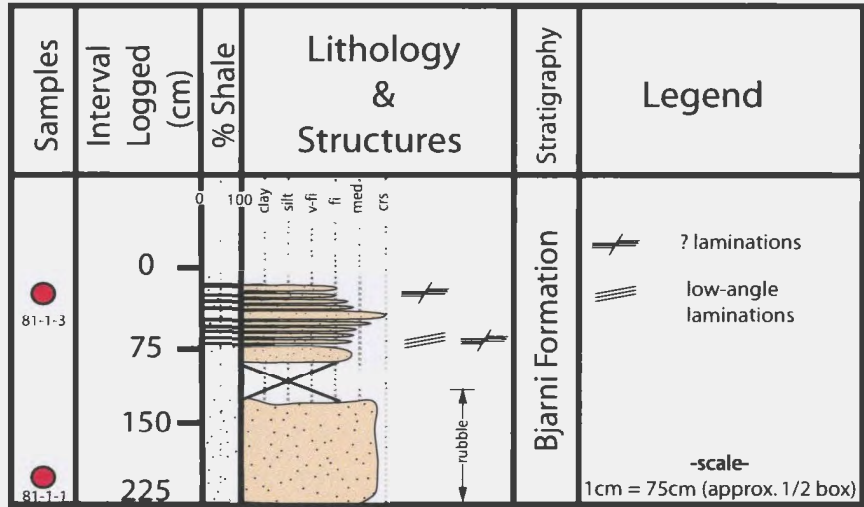


Fig. 4.6A. Bjarni Formation core logged from well Bjarni H-81.

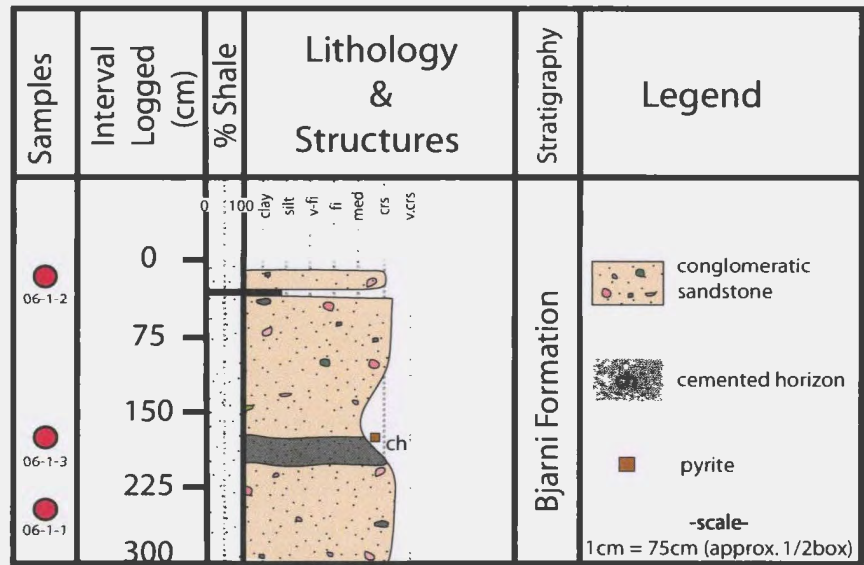


Fig. 4.6B. Bjarni Formation core logged from well North Bjarni F-06.

webpage).

Between 225 cm and approximately 100 cm of core is rubble; granule to cobble-sized fragments of beige medium to coarse grained sandstone (**Fig. 4.6**). The ‘consolidated’ remainder of the core is comprised of regularly intercalated mud and fine to medium grained sandstone laminae, with the exception of a small coarse interval of sandstone at approximately 75 cm. Some mud and sandstone lamina contain micro-faulting (**Plate 1C**), while the coarser sandstone intervals are generally structureless with very faint, possibly inclined laminae.

The North Bjarni F-06 core is substantially better preserved than that of Bjarni H-81. It is composed of beige-grey, medium to coarse conglomeratic sandstone. Feldspar and quartz clasts range from granule- (1mm) to pebble- (10mm) size and are subangular to rounded. Approximately 125 cm from the base of core 1 is a calcite-cemented horizon (**Plate 1B**), similar to that observed in Herjolf M-92, however, only a minor occurrence of pyrite is observed at the cemented boundary. The cemented zone is beige to grey in colour and thus, is distinctly different from the rest of the core. No sedimentary structures were observed in the North Bjarni F-06 core. Again, cores from both wells are interpreted as fluvial sandstones.

#### **4.4.4 Roberval K-92**

Roberval K-92 well is located in the Hamilton subbasin, less than 10 km southeast of the Gudrid H-55 field and The Roberval K-92 well, TD is 3874 m (**Fig. 4.2; #20**). The Bjarni Formation is encountered in core 2 of a total of 7 cores taken, with approximately 10.5 m recovered. However, nearly one full box is empty (~150 cm) and the remainder of the core is approximately 600 cm long. The preserved intervals do not combine for the

10.5 m quoted by CNLOPB and it is possible that some of the core has been misplaced during storage history, or that there was an error recording the original amount recovered.

Core 2 contains grey silty mudstone laminae and beds, interbedded with fine to coarse, and locally conglomeratic sandstone (**Fig. 4.7**). The overall textures of silt-mud to fine-coarse sandstone ranges from lenticular to wavy laminations (e.g. 150 to 470 cm). Within this interval, escape structures and possible bioturbation traces are visible. These traces are approximately 2 cm long vertical burrows cross-cutting laminations and, circular sandstone-filled, horizontal burrows, approximately 5 mm in diameter. Angular coal fragments of various sizes (e.g. 1 to 20 mm) and inclined laminations are also present in core 2 (**Plate 1E**). Roberval K-92 sandstones represent fluvial deposition with some possible associated lacustrine shales.

#### ***4.4.5 North Leif I-05***

The North Leif I-05 well is located in the southern region of the Hopedale Basin (Hamilton subbasin; **Fig 4.2; #23**). With a TD of 3513 m, North Leif I-05 is the only well that tested oil on the Labrador Shelf, with porosities averaging 11.4 % (Atkinson & Fagan, 2001; CNLOPB basins webpage).

Core 1 (3110 – 3113.5 m) lithologies include interbedded and interlaminated sandstone and shale (**Fig. 4.8**). The sandstone is fine to medium grained, grey-brown, and contains possible subangular to rounded quartz and feldspar pebbles (e.g. 1 to 7 mm), with normal graded bedding. Coal fragments and stringers are abundant and variable in size, ranging from 1 mm to several centimeters in length (**Plate 1F**) and both planar and inclined laminations are also present. Core studied from North Leif I-05 are interpreted to be marginal marine sandstones.

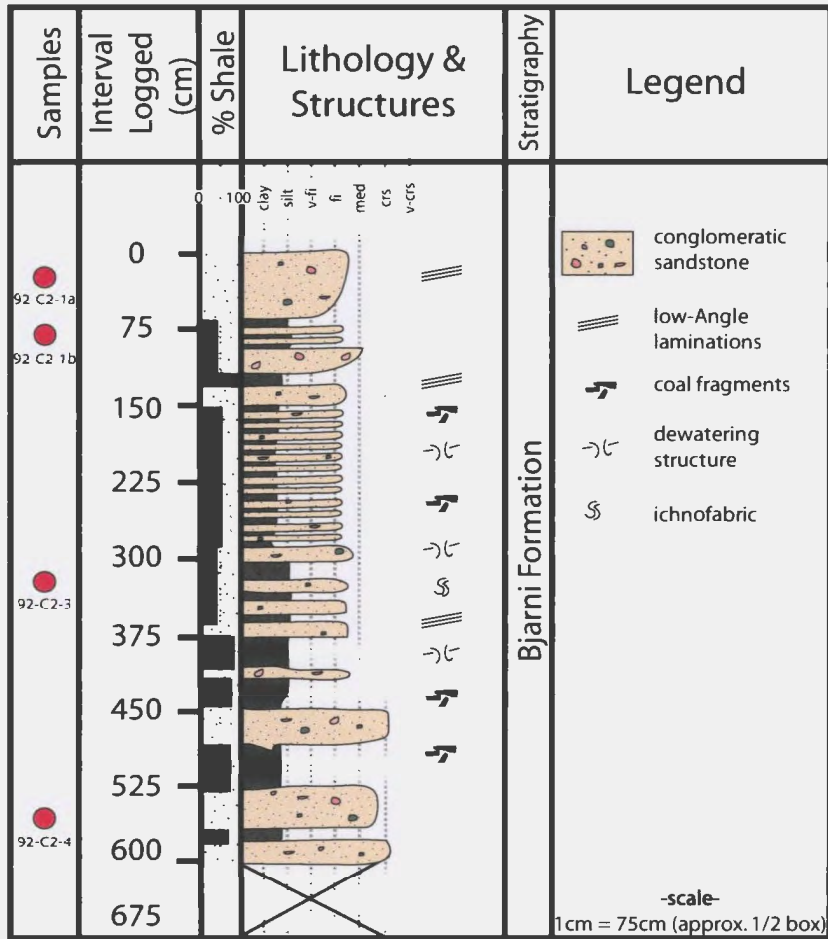


Fig. 4.7. Bjarni Formation core logged from well Roberval K-92.

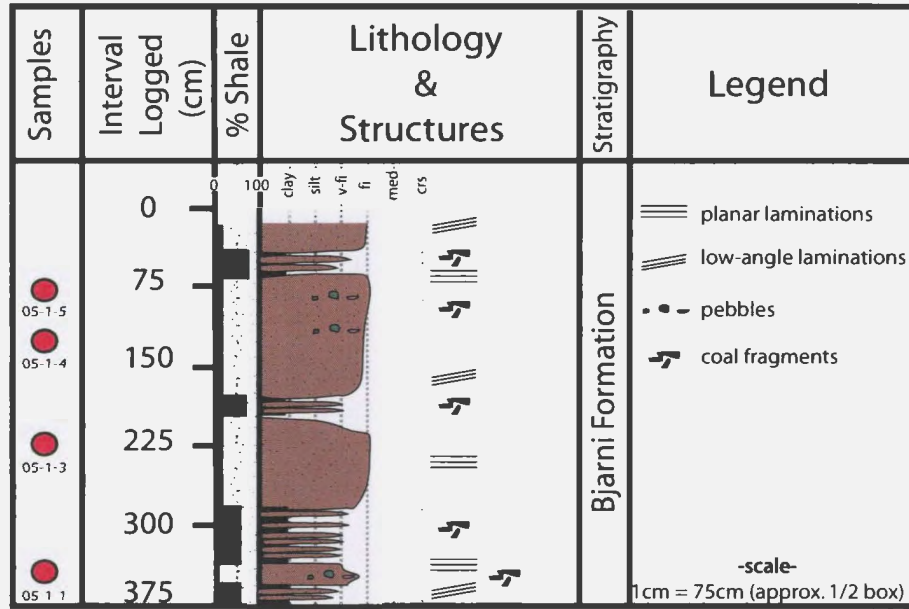


Fig. 4.8. Bjarni Formation core logged from well North Leif I-05.

## 4.5 PETROGRAPHY AND POINT COUNT RESULTS

### 4.5.1 Detrital Mineralogy

Normalized point counts of framework grains from all samples and wells plot in several different compositional areas that range from quartz arenite to arkosic and lithic arenites (**Fig. 4.9A**; **Fig. 4.10**). Samples are also plotted on a Dickinson et al. (1983) tectonic setting ternary diagram, fall within four tectonic environments, with the majority in the recycled orogenic field (**Fig. 4.9B**).

#### 4.5.1.1 Quartz

Quartz occurs as both monocrystalline and polycrystalline grains in all samples (**Plate 4.2**). Monocrystalline quartz grains commonly have undulose and straight extinctions and frequently contain abundant fluid inclusions, while polycrystalline quartz generally contain three or more sub-grains. Both grain-types vary in size, ranging from 50  $\mu\text{m}$  to 300  $\mu\text{m}$  and have varying crystal habits from angular to subrounded. Quartz grains range from poorly to moderately sorted in all samples.

Quartz accounts for the majority of framework grains in all samples, ranging from  $Q_{90.5}$  in North Leif I-05 to  $Q_{38.5}$  in Bjarni H-81 (**Table 4.2**).

#### 4.5.1.2 Feldspar

Feldspars in the studied Bjarni Formation range from  $F_{43.5}$  to  $F_{1.0}$  (**Table 4.2**) and include both plagioclase and potassium-rich end members. Plagioclase feldspars range from clear to cloudy in plain polarized light and often exhibit albite and simple twinning in cross-polarized light (**Plate 4.3C-C'**), while potassium feldspars exhibit microcline, and cross-hatch twinning in cross-polarized light (**Plate 4.3A-A', B-B'**), staining yellow in plain-polarized light. Similar to quartz grains, both plagioclase and potassium feldspars

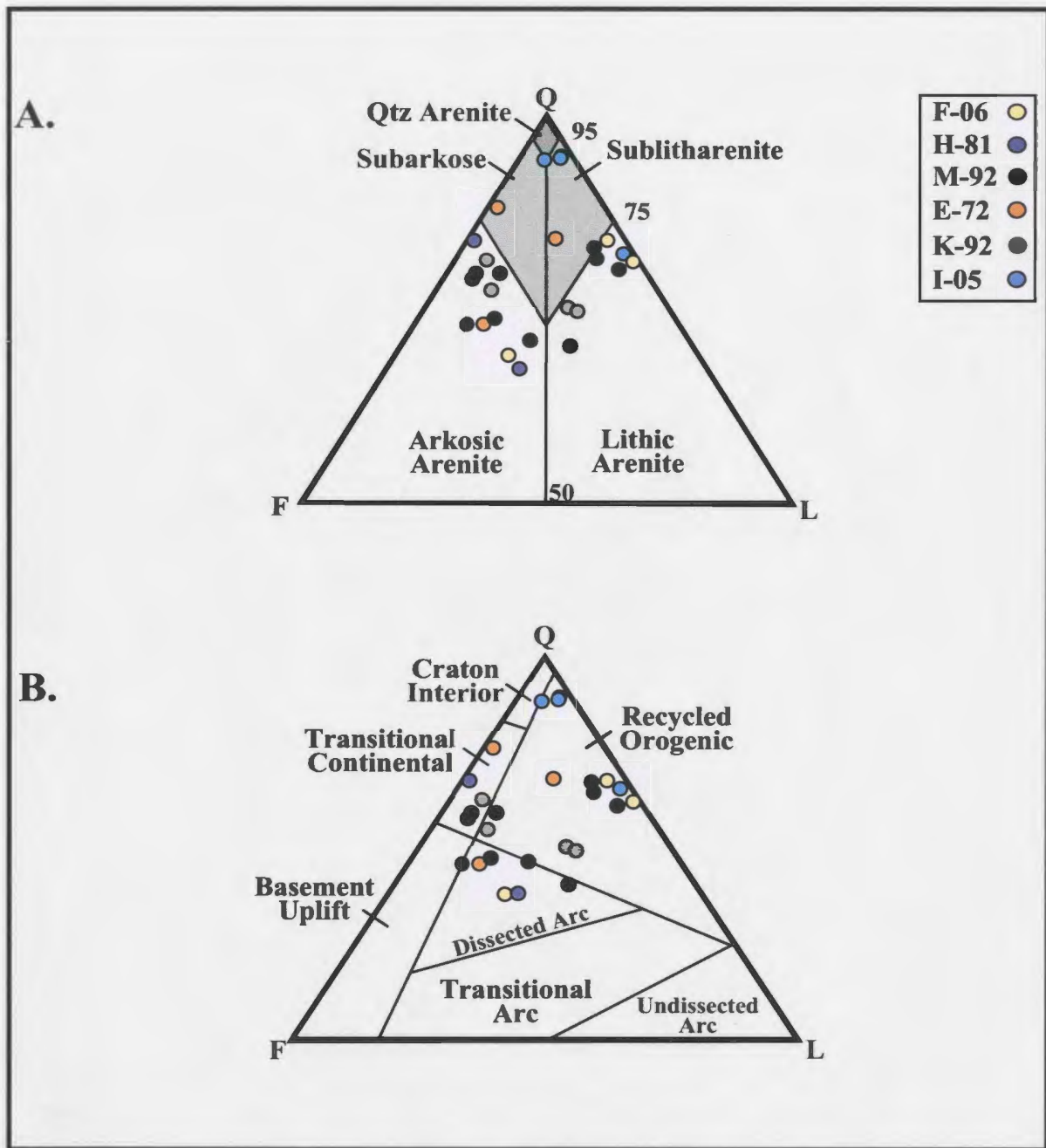


**Fig. 4.9.** Ternary diagrams plotted with individual samples from studied wells containing the Bjarni Formation sandstone. **A.** QFL plot (modified from Pettijohn, 1975; Nichols, 1999); **B.** Tectonic setting QFL ternary plot (modified from Dickinson et al., 1983) and; **C.** QPK plot (quartz, plagioclase, potassium feldspar).

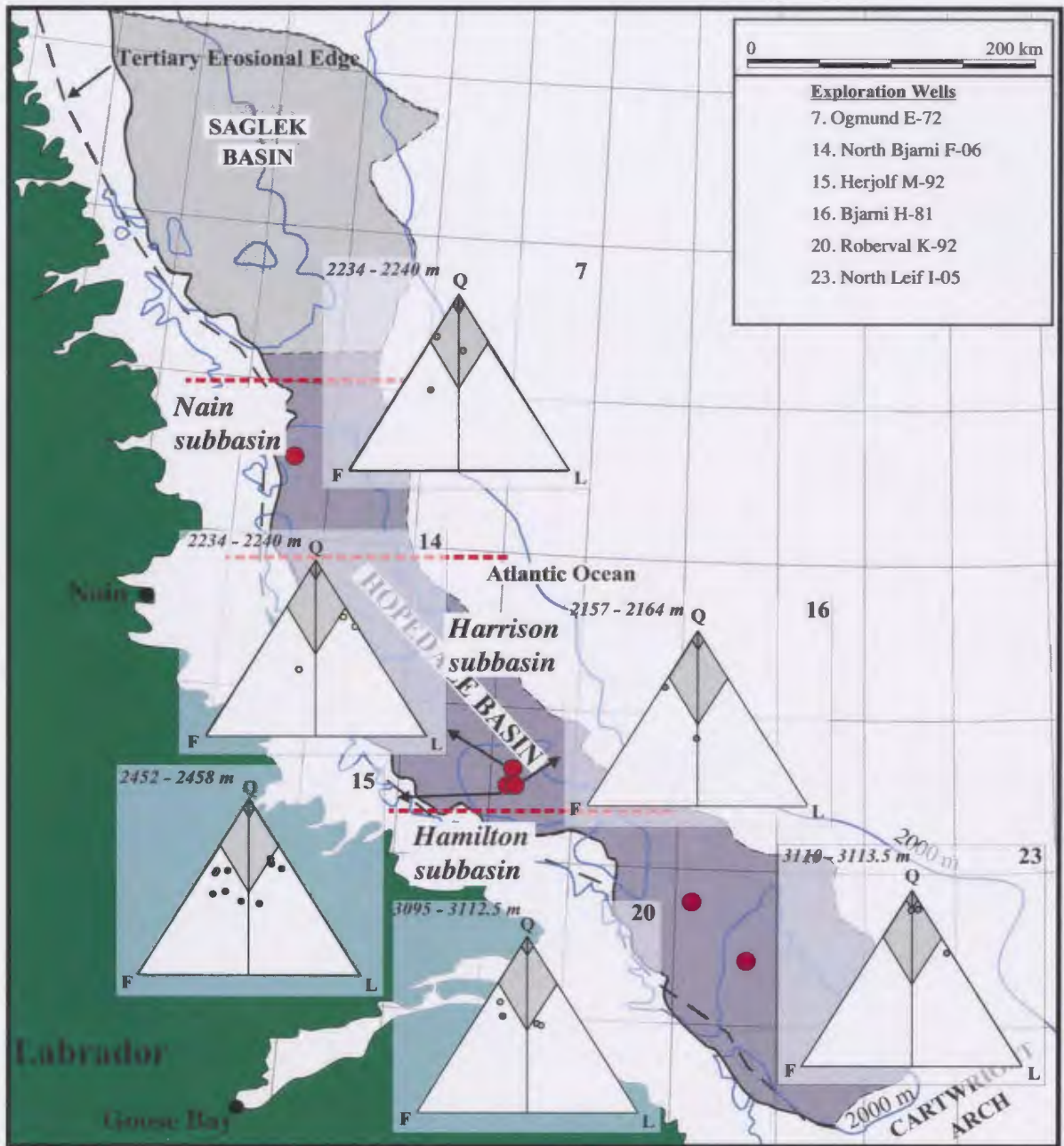


**Fig. 4.10.** Samples plotted on ternary diagrams indicating compositional changes within wells. See Figure 4.9 for QFL compositional names.

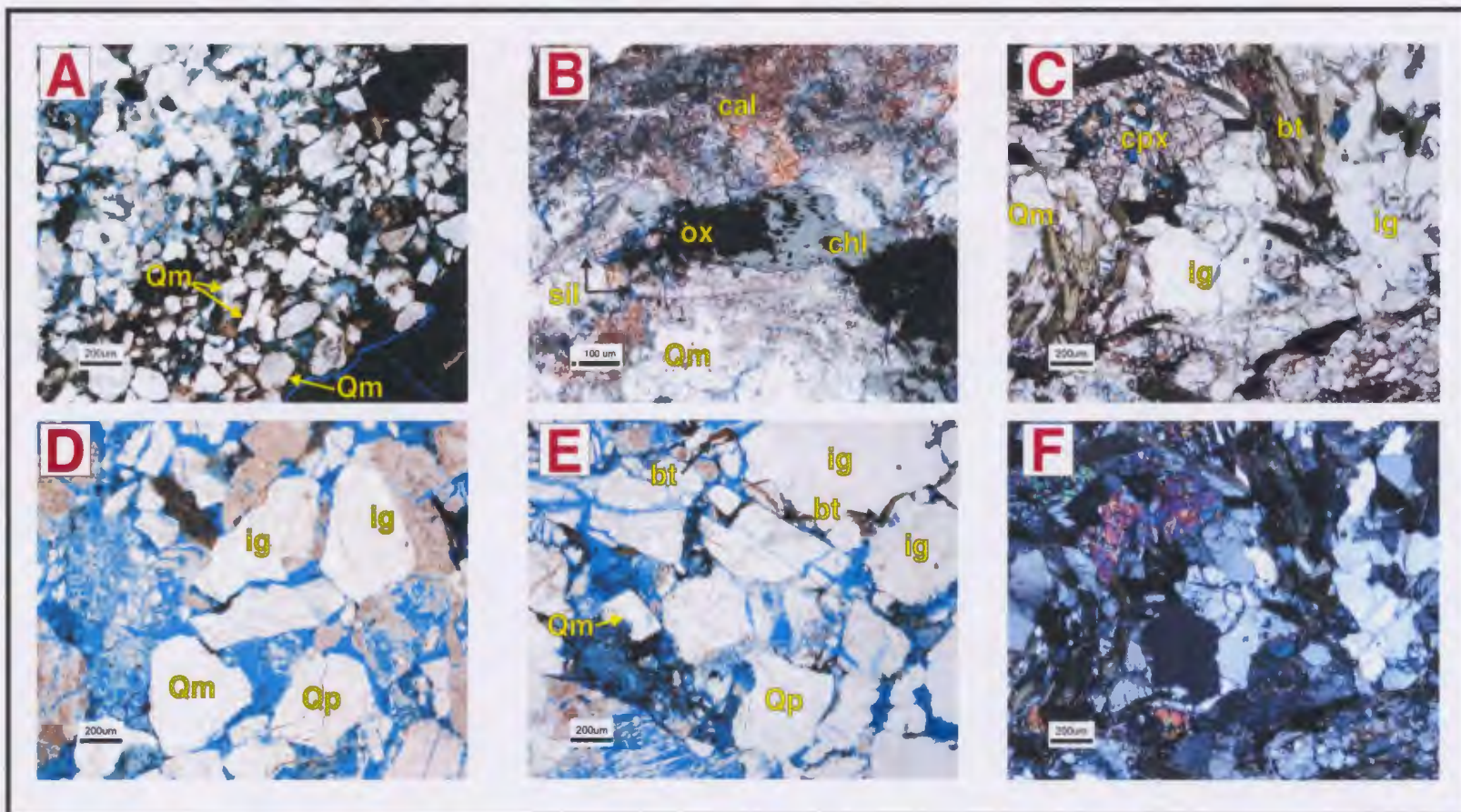


**Plate 4.2.** Photomicrographs of quartz, lithic, accessory, and diagenetic minerals. **A.** (05-1-4), monocrystalline quartz (Qm); **B.** (81-1-1), monocrystalline quartz (Qm), oxides (ox), chlorite (chl), calcite cement (cal), and sillimanite (sil); **C, F (XPL).** (72-2-2), igneous grains (ig), monocrystalline quartz (Qm), biotite (bt), and clinoproxene (cpx); **D.** (72-2-1), igneous grains (ig), polycrystalline and monocrystalline quartz (Qp, Qm) and; **E.** (HJ-1-1), biotite (bt) and polycrystalline quartz (Qp)

Sample	Fm	Subbasin	Depth (m)	Q (%)	F (%)	L (%)	Total Sample & Well QFL Point Counts
81-1-3	Bjarni Formation	Harrison	2156.5	39.6	31.3	29.6	233
81-1-1			2161.0	68.5	31.0	0.5	200
							<b>433</b>
72-2-3		Nain	2233.8	69.0	14.0	17.0	200
72-2-2			2237.2	77.0	22.0	1.0	202
72-2-1			2239.0	46.5	40.0	13.5	200
							<b>602</b>
06-1-2		Harrison	2451.5	38.5	39.0	22.5	200
06-1-3			2451.9	63.0	1.0	36.0	200
06-1-1			2457.3	68.5	3.5	28.0	200
							<b>600</b>
HJ-1-3		Harrison	2633.0	48.0	37.0	15.0	200
HJ-1-2			2633.7	46.5	43.5	10.0	200
HJ-1-1			2633.9	60.0	30.0	10.0	200
HJ-2-1			2635.4	60.0	35.0	5.0	200
HJ-3-2			2636.0	41.0	25.0	34.0	200
HJ-3-1			2636.2	58.5	36.5	5.0	200
HJ-4-1			2637.2	61.0	4.9	34.2	205
HJ-5-3			2638.2	42.3	32.7	25.0	220
HJ-5-1			2638.3	63.8	8.1	28.1	210
HJ-5-2	2638.5		66.7	7.1	26.2	210	
							<b>2045</b>
92-C2-1a	Hamilton		3107.0	63.5	31.0	5.5	200
92-C1-1b		3107.7	55.5	34.0	10.5	200	
92-C2-3		3110.2	51.0	20.5	28.5	200	
92-C2-4		3112.0	50.0	19.0	31.0	200	
						<b>800</b>	
05-1-5	Hamilton	3110.5	65.0	2.0	33.0	200	
05-1-4		3111.3	89.5	6.0	4.5	200	
05-1-3		3112.1	90.0	2.5	7.5	200	
05-1-1		3113.1	90.5	2.0	7.5	200	
						<b>800</b>	

**Table 4.2.** Well samples of QFL point count data from the Bjarni Fm sandstones normalized to 100%. Samples are arranged by stratigraphic depth. For subbasin locations, see **Figure 4.2**.

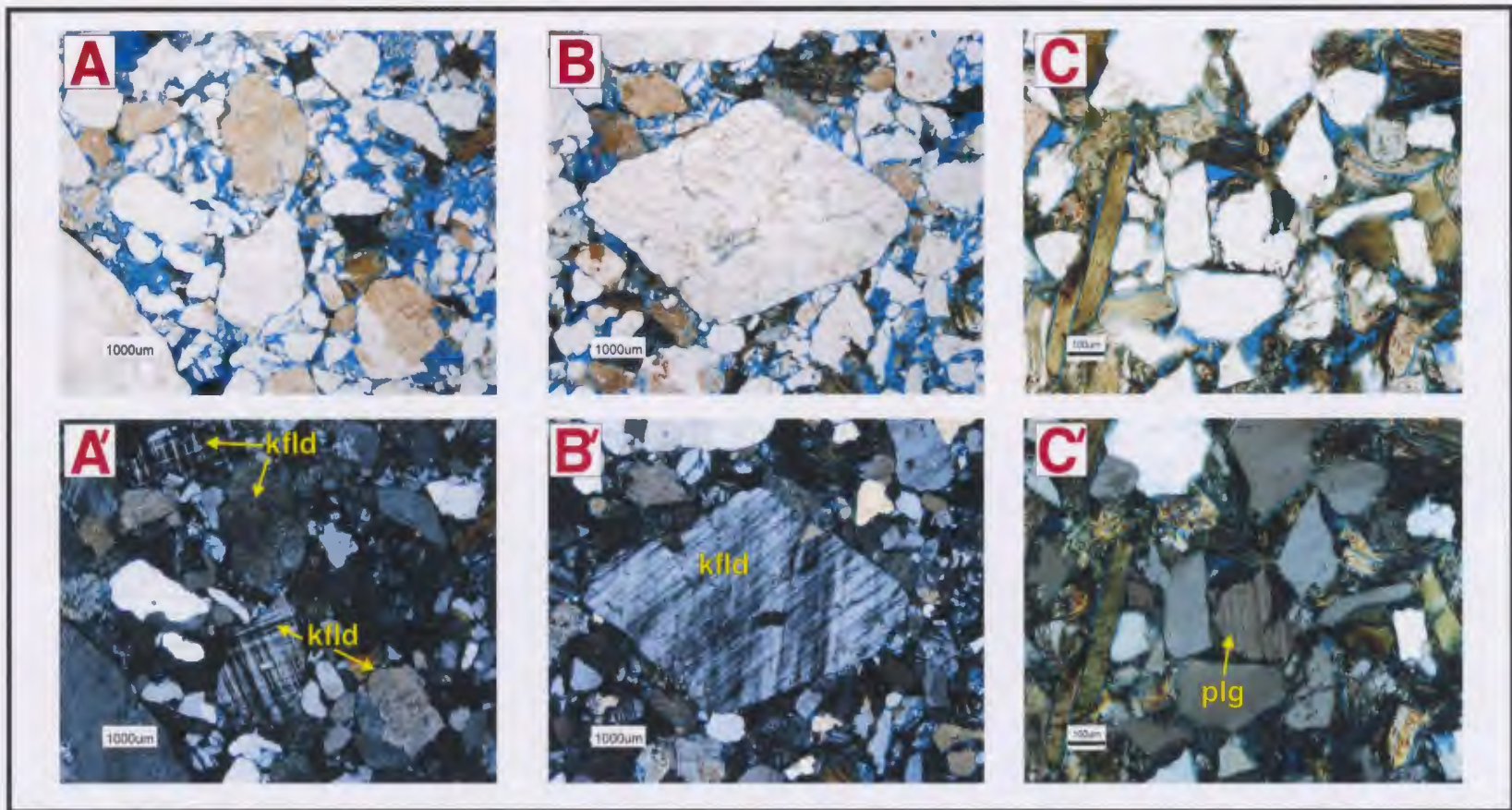


**Plate 4.3.** Plain and cross-polarized light photomicrographs of potassium (kfd) and plagioclase (plg) feldspars. *A-A'* (72-2-1), cross-hatch twinning (*A'*) and (sericite) altered grains (dusty-brown; *A*); *B-B'* (81-1-3), cross-hatch twinning (microcline) and; *C-C'* (HJ-3-1), perthite and simple twinning.

have varying sizes (40 to 300  $\mu\text{m}$ ) and crystal habits (angular to subrounded; **Plate 4.3**) and range from poorly to moderately sorted. Relative plagioclase to potassium feldspar abundance (P/K), ranges in samples from 0 to 1.0, with an average value of 0.29 (**Table 4.3**).

#### **4.5.1.3 Lithics & Accessory Minerals**

Lithic rock components in the Bjarni Formation samples consist of mainly intrusive igneous clasts and minor metamorphic clasts, while accessory minerals include biotite, clinopyroxene, and sillimanite (**Plate 4.2B, C, F**). Biotite grains are green-brown and pleochroic in plain-polarized light. Crystal habits are usually elongate or tabular, and are often deformed between neighbouring grains, ranging from 50 to 200  $\mu\text{m}$ .

Igneous and metamorphic rock fragments generally occur as large (250 $\mu\text{m}$  to 1mm) angular to sub-rounded grains, usually containing quartz and feldspar sub-crystals.

The highest percent of lithic content (L<sub>36.0</sub>) is observed in North Bjarni F-06, while the lowest percentage of lithic content is noted in Ogmund E-72 (L<sub>1.0</sub>).

#### **4.5.2 Authigenic Mineralogy**

Six main authigenic minerals, oxides (e.g. hematite), chlorite, kaolinite, calcite cements (non- and ferroan), pyrite, and quartz overgrowths have been observed in the studied well samples (**Fig. 4.11; Table 4.4**)

##### **4.5.1.1 Oxides**

Oxides generally occur as isolated patches or in areas of altered biotite or chlorite (**Plate 4.2 - 4.5**). Oxides are the most common authigenic phase in all samples, observed in all samples (and burial depths) studied (**Table 4.4**), ranging between 5.0 and 70.0 point counts, with the minimum and maximum averages both in North Leif I-05. Samples

Sample	Fm	Subbasin	Depth (m)	Plagioclase (P) Feldspar Counts	Potassium (K) Feldspar Counts	P/K
81-1-3	Bjarni Formation	Harrison	2156.5	19	54	0.4
81-1-1			2161.0	25	37	0.7
						<b>0.51</b>
72-2-3		Nain	2233.8	11	35	0.3
72-2-2			2237.2	11	35	0.3
72-2-1			2239.0	10	70	0.1
						<b>0.26</b>
06-1-2		Harrison	2451.5	9	69	0.1
06-1-3			2451.9		2	0.0
06-1-1			2457.3		7	0.0
						<b>0.04</b>
HJ-1-3		Harrison	2633.0	22	52	0.4
HJ-1-2			2633.7	24	63	0.4
HJ-1-1			2633.9	11	49	0.2
HJ-2-1			2635.4	13	57	0.2
HJ-3-2			2636.0	12	32	0.4
HJ-3-1			2636.2	31	42	0.7
HJ-4-1			2637.2	1	13	0.1
HJ-5-3			2638.2	21	51	0.4
HJ-5-1			2638.3	5	12	0.4
HJ-5-2	2638.5		2	13	0.2	
						<b>0.34</b>
92-C2-1a	Hamilton	3107.0	9	53	0.2	
92-C1-1b		3107.7	29	39	0.7	
92-C2-3		3110.2	4	37	0.1	
92-C2-4		3112.0	4	37	0.1	
					<b>0.28</b>	
05-1-5	Hamilton	3110.5		4	0.0	
05-1-4		3111.3		12	0.0	
05-1-3		3112.1		3	0.0	
05-1-1		3113.1	2	2	1.0	
					<b>0.25</b>	
<b>Overall Avg.</b>						<b>0.29</b>

**Table 4.3.** Plagioclase and potassium feldspar point count ratios (P/K). Well averages are in bold text.

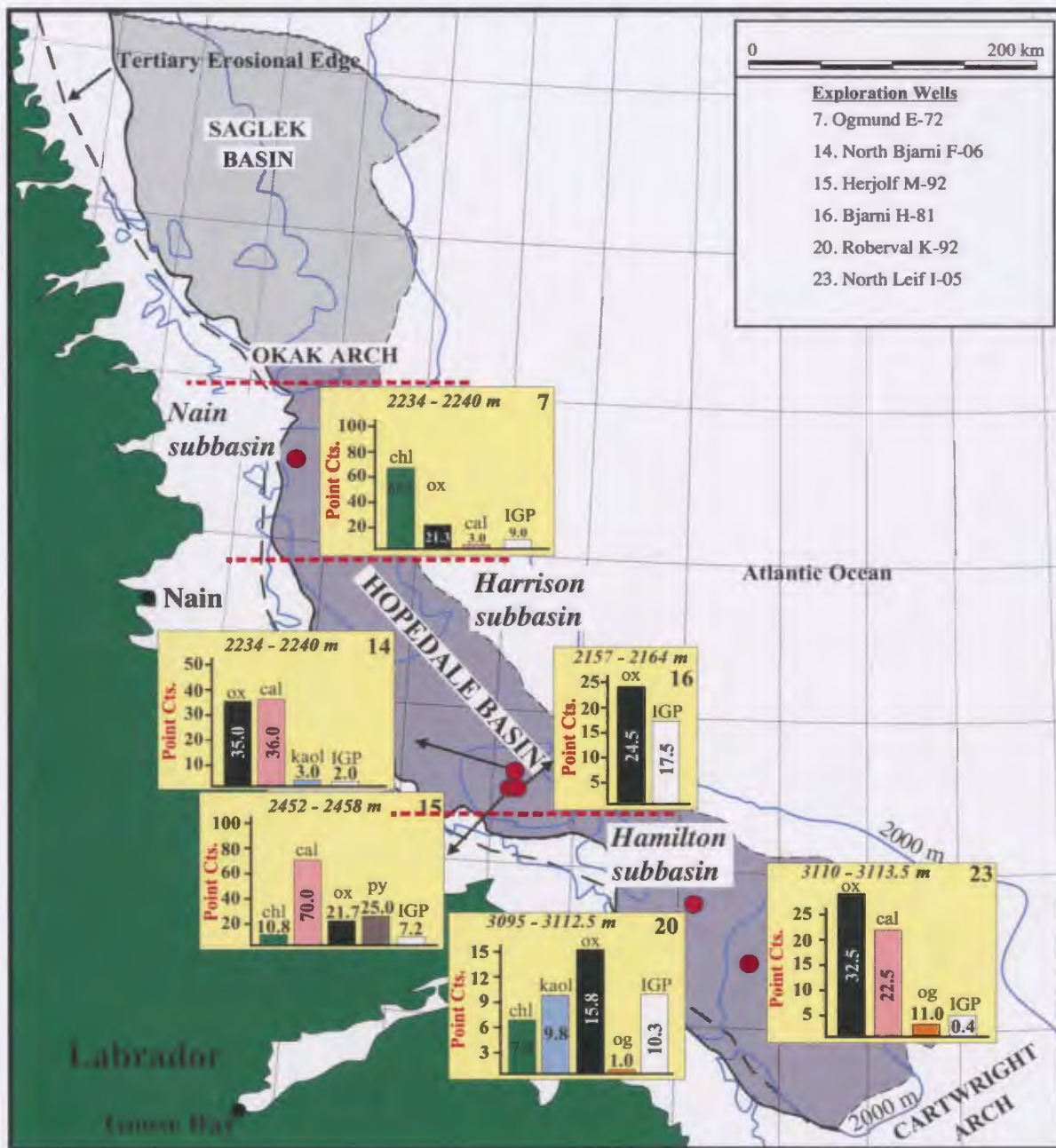


**Fig. 4.11.** Total well authigenic minerals and intragranular porosity point count (Point Cts.) histograms of the sandstone from the studied Bjarni Formation core intervals; oxides (ox), calcite cement (cal), kaolinite (kaol), pyrite (py), quartz overgrowths (og), and intragranular porosity (IGP). Well numbers are located in the upper right corner of histograms. Modified after Atkinson & Fagan, 2001.

Sample	Diagenetic Minerals & Features								
	Depth (m)	Counts	Chlorite	Oxides	Calcite	Pyrite	Kaolinite	OG	IGP
81-1-3	2156.5	303		11.0					21.0
81-1-1	2161.0	308		38.0					14.0
<b>avg</b>				<b>24.5</b>					<b>17.5</b>
72-2-3	2233.8	300	54.0	38.0					
72-2-2	2237.2	312	77.0	8.0	3.0				2.0
72-2-1	2239.0	294		18.0					16.0
<b>avg</b>			<b>65.5</b>	<b>21.3</b>	<b>3.0</b>				<b>9.0</b>
06-1-2	2451.5	307		8.0	89.0				2.0
06-1-3	2451.9	267		47.0	11.0		3.0		
06-1-1	2457.3	263		50.0	8.0				2.0
<b>avg</b>				<b>35.0</b>	<b>36.0</b>		<b>3.0</b>		<b>2.0</b>
HJ-1-3	2633.0	282	10.0	20.0		20.0			12.0
HJ-1-2	2633.7	274		17.0		30.0			4.0
HJ-1-1	2633.9	258	5.0	20.0					8.0
HJ-2-1	2635.4	293		10.0	70.0				3.0
HJ-3-2	2636.0	242		23.0					1.0
HJ-3-1	2636.2	248		20.0					11.0
HJ-4-1	2637.2	275	18.0	20.0					15.0
HJ-5-3	2638.2	308	7.0	41.0					11.0
HJ-5-1	2638.3	292	10.0	21.0					4.0
HJ-5-2	2638.5	298	15.0	25.0					3.0
<b>avg</b>			<b>10.8</b>	<b>21.7</b>	<b>70.0</b>	<b>25.0</b>			<b>7.2</b>
92-C2-1a	3107.0	311	9.0	22.0			15.0	1.0	21.0
92-C2-1b	3107.7	280	7.0	10.0			12.0		10.0
92-C2-3	3110.2	247	10.0	11.0			10.0		4.0
92-C2-4	3112.0	246	2.0	20.0			2.0		6.0
<b>avg</b>			<b>7.0</b>	<b>15.8</b>			<b>9.8</b>		<b>10.3</b>
05-1-5	3110.5	205		5.0					
05-1-4	3111.3	259		17.0	23.0			12.0	
05-1-3	3112.1	315		38.0	22.0			10.0	5.0
05-1-1	3113.1	308		70.0					
<b>avg</b>				<b>32.5</b>	<b>22.5</b>			<b>11.0</b>	<b>5.0</b>

**Table 4.4.** Total and well-average (bold) diagenetic point counts. OG = quartz overgrowths; IGP = intragranular porosity

observed from the North Bjarni F-06 well has the highest average point counts of oxides (35.0).

#### ***4.5.1.2 Chlorite***

Chlorite dominantly appears as an intergranular authigenic mineral (**Plate 4.2B**) as altering biotite (Eggleton and Banfield, 1985) or is observed as a thin coating around detrital grains. Chlorite is identified in three of the six wells studied and has the highest sample point count average and well average in Ogmund E-72 (77.0 and 65.5, respectively). Chlorite is absent from three wells, Bjarni H-81, North Bjarni F-06, and North Leif I-05 (**Table 4.4**).

#### ***4.5.1.3 Kaolinite***

Kaolinite appears as very fine-grained, microporous pore-filling cement with a vermicular- or stacked texture (**Plate 4.4A-C**), occurring only in two wells (Roberval K-92 and North Bjarni F-06). It has the well highest point count average in Roberval K-92 (9.8), while it is only has 3.0 point counts in North Bjarni F-06 samples (**Table 4.4**).

#### ***4.5.1.4 Calcite Cementation***

Calcite generally occurs as a pervasive red (non-ferroan) or mauve-to violet-stained (ferroan), inter- and intragranular filling cement (**Plate 4.3C, E**). It also occurs in isolated intergranular clusters (**Plate 4.2B**) in minor quantities and replacing feldspar grains (**Plate's 4.4C and 4.5E**). Non-ferroan and iron-poor calcite cements are observed in Ogmund E-72 and North Leif I-05, while ferroan calcite cements are noted in Herjolf M-92 and North Leif I-05 (**Table 4.4**). North Bjarni F-06 contains the most point counts of calcite cement in a sample (89.0) and is the only well where calcite was observed in all samples, with an average of 36.0 point counts. Calcite cement was observed in only one

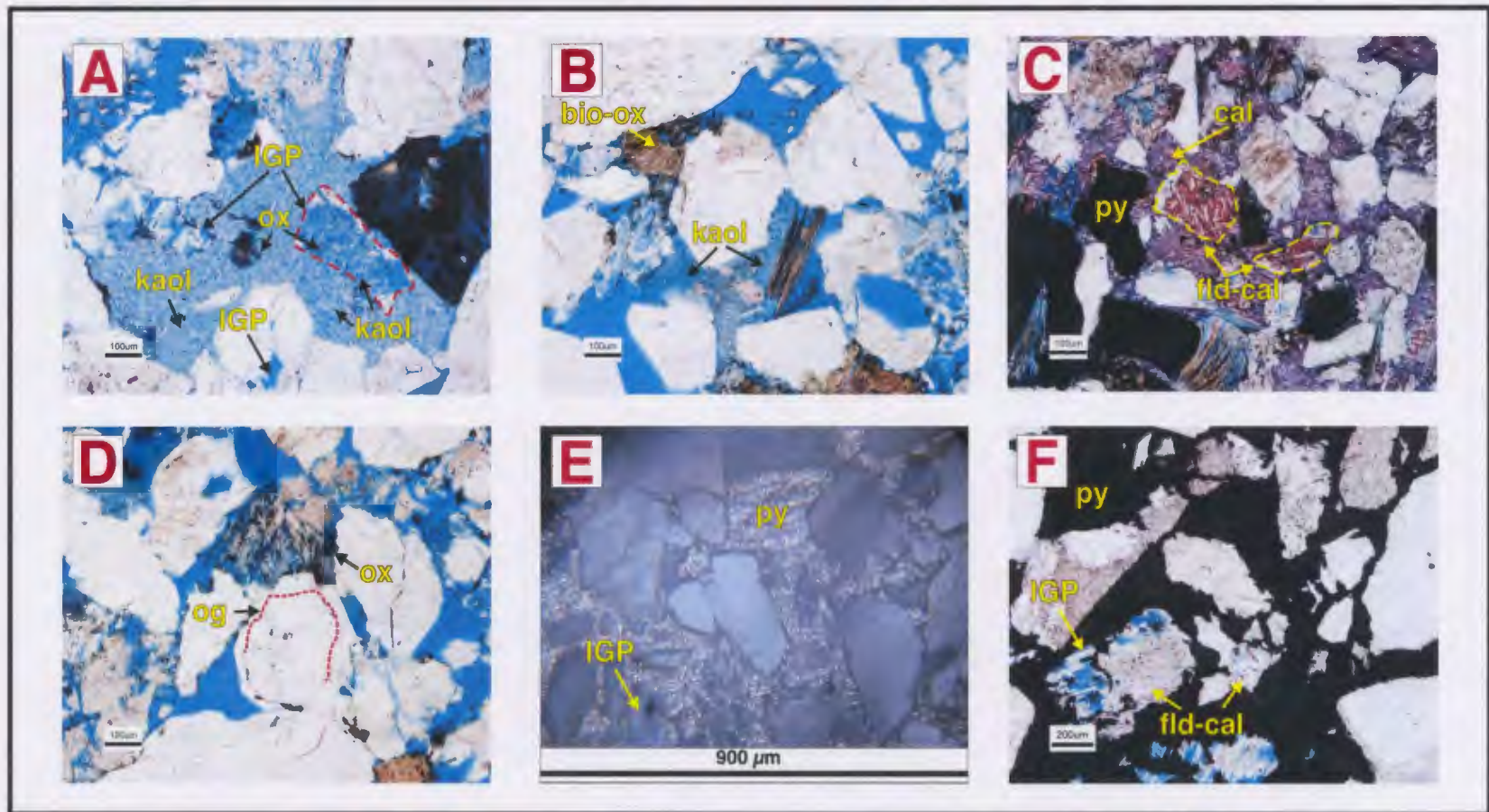


**Plate 4.4.** Photomicrographs of diagenetic minerals. *A. & B.* (92-C2-1a), inter- and intragranular-filling kaolinite (IP, IGP, kaol); *C.* (HJ-2-1), intergranular ferron calcite cement (cal) and filling relict (intragranular porosity) feldspar grains; *D.* (92-C2-1a), quartz overgrowths (Og); *E.* (HJ-5-3), pyrite (py) and intragranular porosity (IGP) in reflected light and; *F.* (HJ-5-3), pyrite (py), intragranular porosity (IGP), and calcite altered potassium feldspar (kfld-cal).

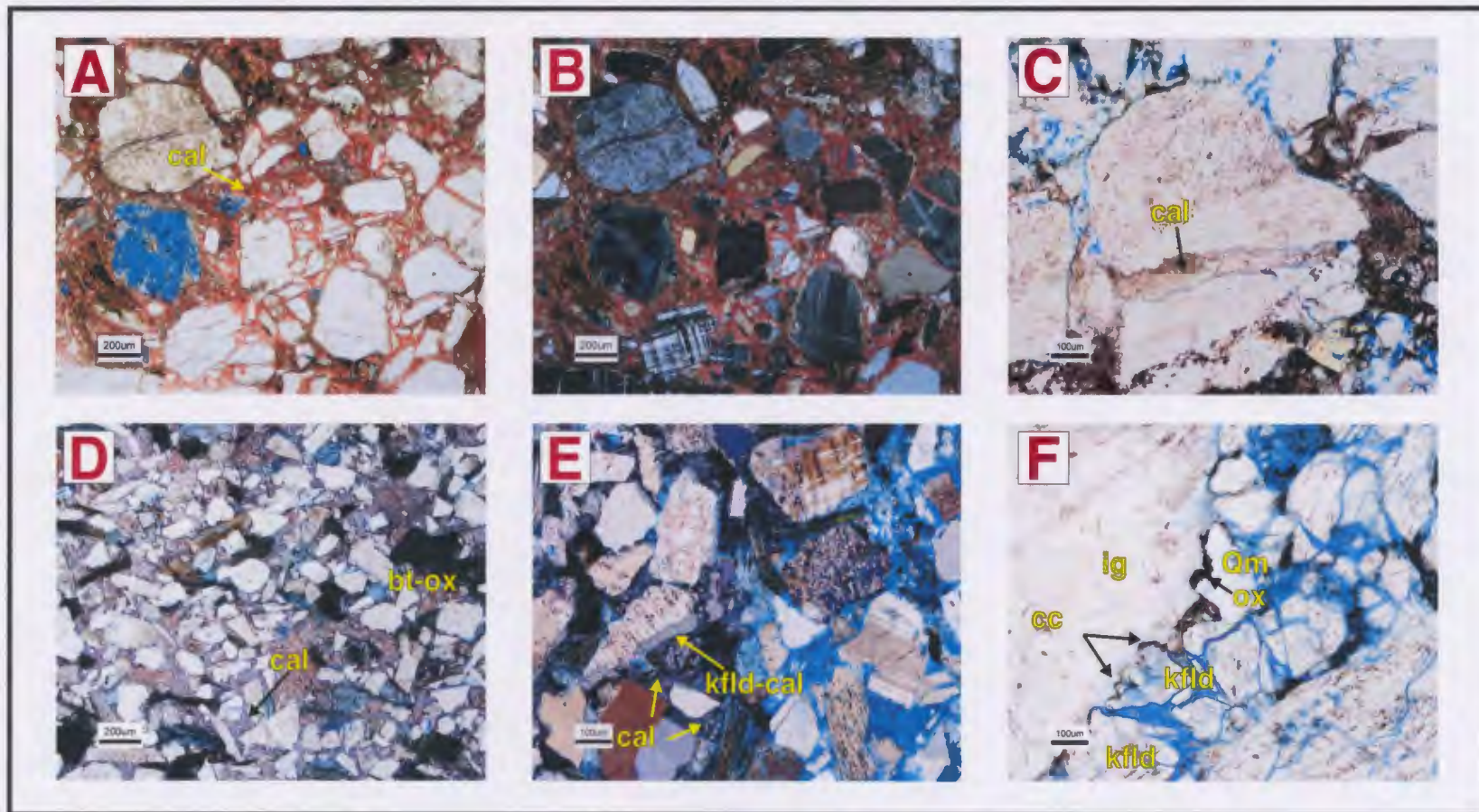


**Plate 4.5.** Photomicrographs of diagenetic minerals. *A* (PL). & *B* (XPL). (06-1-2), intergranular-filling non-ferroan (red-pink) calcite (IGP, cal); *C*. (72-2-2), intragranular- (IGP) filling calcite (cal); *D*. (HJ-2-1), intergranular-filling ferroan calcite (purple) and altered biotite (bt-ox); *E*. (XP; HJ-2-1), intergranular ferroan calcite and calcite altered potassium feldspar (kfld-cal) and; *F*. (HJ-1-2), oxide-rimmed concavo-convex (cc) boundary between a larger igneous grain (ig) and smaller feldspar (fld) and monocrystalline quartz grains (Qm).

sample (Herjolf M-92) with a point count of 70.0.

#### **4.5.1.5 Pyrite**

Pyrite was observed in Herjolf M-92 during point counting representing a well average of 25.0. In PL, pyrite is opaque, occurring in various-sized patches (1 mm to 250  $\mu\text{m}$ ) and fills inter- and intragranular porosities, while in RL, pyrite appears yellow-gold (**Plate 4.4C, E, F**). Pyrite is generally associated with ferroan calcite cementation (**Plate 4.4C, F**).

#### **4.5.1.6 Quartz Overgrowths/Cement**

Quartz overgrowths (or quartz cements) are rare in occurrence, filling only minor intergranular pore space. They are noted in North Leif I-05 with point counts averaging 11.0 and are extremely rare in Roberval K-92 (1.0; **Table 4.4; Plate 4.4C, D**).

#### **4.5.3 Porosity**

Two main porosity-types occur in all studied wells; 1) intergranular porosity and, 2) intragranular porosity. Intragranular porosity is mainly a result of feldspars with varying amounts of dissolution or minor grain fracturing, and also occurs within patches of kaolinite. Porosity percentages are plotted in **Figure 4.12**.

The well with the highest average point counts for total porosity (TP) is Bjarni H-81 (47.0) with the lowest occurring in North Bjarni F-06 (7.0; **Table 4.5**). Average intergranular porosities (IP) for wells range from 29.5 (Bjarni H-81) to 5.7-point counts (North Bjarni F-06; **Table 4.5**). Average well intragranular porosity (IGP) in wells ranges from 2.0 (North Bjarni F-06) to 17.5 point counts (Bjarni H-81). All diagenetic minerals have been observed to occlude intergranular pores (**Plates 4.1 – 4.5**), whereas intragranular porosity is sometimes (partially) filled by minor oxides, kaolinite, and

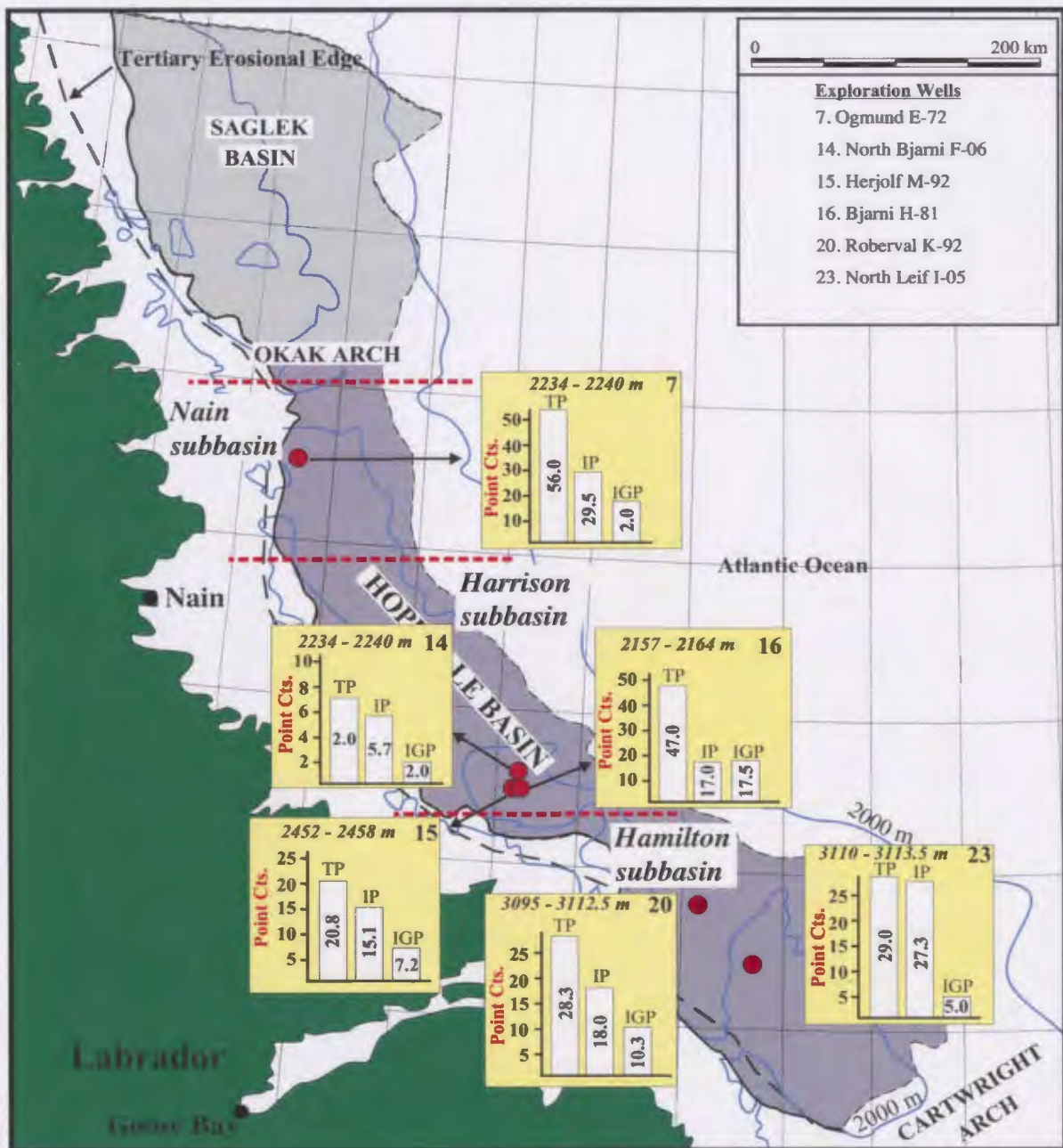


**Fig. 4.12.** Porosity point count histograms of the sandstone from the studied Bjarni Formation core intervals; total porosity (TP), intergranular porosity (IP), and intragranular porosity (IGP), and intragranular porosity (IP). Well numbers are located in the upper right corner of histograms. Modified after Atkinson & Fagan, 2001.

Sample	Depth (m)	Counts	Porosities		
			IP	IGP	TP
81-1-3	2156.5	303	17.0	21.0	38.0
81-1-1	2161.0	308	42.0	14.0	56.0
<b>avg</b>			<b>29.5</b>	<b>17.5</b>	<b>47.0</b>
72-2-3	2233.8	300	8.0		8.0
72-2-2	2237.2	312	18.0	2.0	20.0
72-2-1	2239.0	294	44.0	16.0	60.0
<b>avg</b>			<b>23.3</b>	<b>9.0</b>	<b>29.3</b>
06-1-2	2451.5	307	8.0	2.0	10.0
06-1-3	2451.9	267	6.0		6.0
06-1-1	2457.3	263	3.0	2.0	5.0
<b>avg</b>			<b>5.7</b>	<b>2.0</b>	<b>7.0</b>
HJ-1-3	2633.0	282	8.0	12.0	20.0
HJ-1-2	2633.7	274	19.0	4.0	23.0
HJ-1-1	2633.9	258	17.0	8.0	25.0
HJ-2-1	2635.4	293	7.0	3.0	10.0
HJ-3-2	2636.0	242	17.0	1.0	18.0
HJ-3-1	2636.2	248	6.0	11.0	17.0
HJ-4-1	2637.2	275	2.0	15.0	17.0
HJ-5-3	2638.2	308	18.0	11.0	29.0
HJ-5-1	2638.3	292		4.0	4.0
HJ-5-2	2638.5	298	42.0	3.0	45.0
<b>avg</b>			<b>15.1</b>	<b>7.2</b>	<b>20.8</b>
92-C2-1a	3107.0	311	23.0	21.0	44.0
92-C2-1b	3107.7	280	31.0	10.0	41.0
92-C2-3	3110.2	247	8.0	4.0	12.0
92-C2-4	3112.0	246	10.0	6.0	16.0
<b>avg</b>			<b>18.0</b>	<b>10.3</b>	<b>28.3</b>
05-1-5	3110.5	205			
05-1-4	3111.3	259	7.0		7.0
05-1-3	3112.1	315	35.0	5.0	40.0
05-1-1	3113.1	308	40.0		40.0
<b>avg</b>			<b>27.3</b>	<b>5.0</b>	<b>29.0</b>

**Table 4.5.** Point counts and averages (bold) for different porosity styles, arranged by stratigraphic depth. IP = intergranular porosity; IGP = intragranular porosity; TP = total porosity.

calcite (**Plate 4.5**).

#### **4.5.4 Timing of Major Diagenetic Events (Paragenetic Sequence)**

The relative timing of diagenetic events in the Bjarni Formation from studied core in the Hopedale Basin is summarized in **Figure 4.13**. Two general diagenetic environments have been recognized; 1) early (shallow) and 2) late (deep) burial, occurring between 2100 m - 3200 m.

Earliest diagenesis of the Bjarni Formation is first noted in the form of oxidized grains (e.g. biotite) in all samples, forming iron oxides such as hematite. These either occupy intergranular pores or coat grains (**Plate 4.2A, E**), a consequence of shallow burial in the presence of oxygen. Feldspar dissolution, ranging from slight grain destruction to ghost rhombs, predominant throughout the entire sampled interval and occurred during shallow to deep burial depths. Furthermore, it is possible that feldspar dissolution is initially coeval with all calcite cementation (**Plate 4.5A, D**). If calcite cementation exclusively postdated feldspar dissolution, the liberated ions would have no intergranular pathways to travel through. However, ferroan calcite fills intragranular porosity in some feldspars that are within the cemented area (**Plate 4.4C**), suggesting that at least some calcite cementation post-dates feldspar dissolution. Chlorite precipitation as rims and intergranular pores, commenced at burial depths of approximately 2100 m, indicating shallow burial (i.e. early diagenesis) as they generally predate calcite cementation and quartz overgrowths (Tucker, 2001). Minor kaolinite is first observed at depths of approximately 2450 m, filling inter- and intragranular pores (**Plate 4.4A-C**). Pyrite precipitation and ferroan calcite cementation, resultant from a reducing environment, are noted at approximately 2600 m, filling intergranular porosity. However,

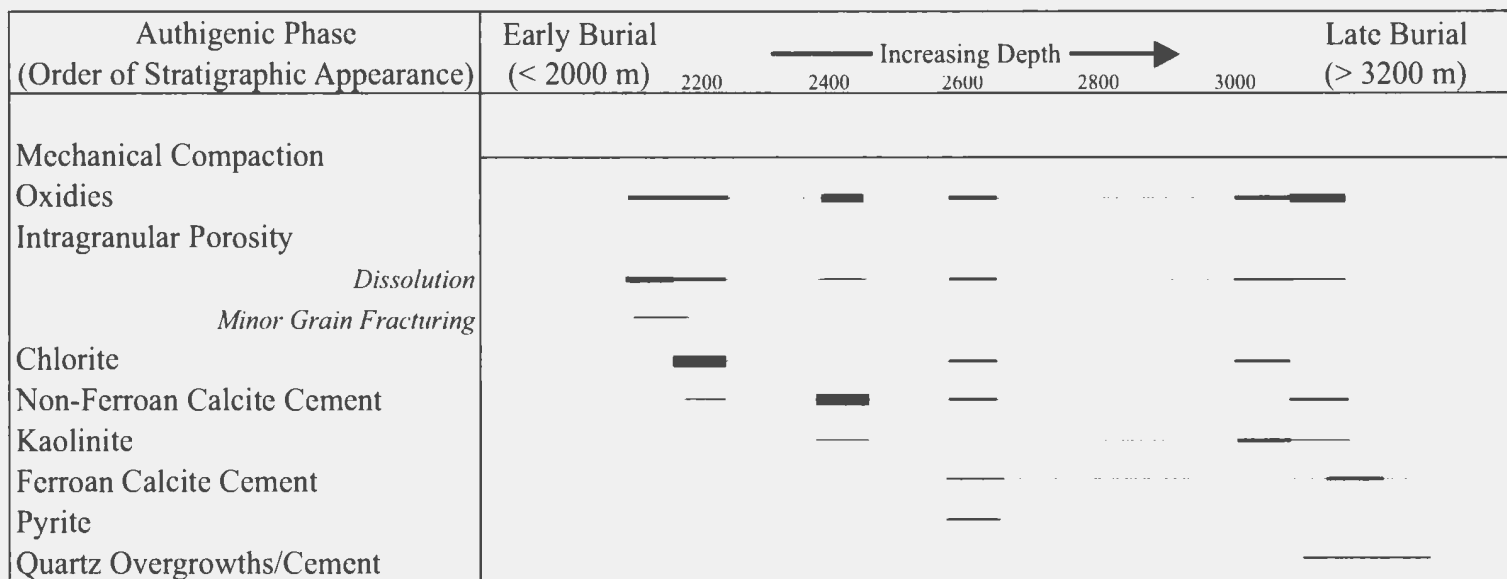


**Fig. 4.13.** Paragenetic sequence of diagenetic events based on petrography, stratigraphic well depth, and order of occurrence. Dashed lines are assumed events and line thickness indicates relative frequency of authigenic phase.

ferroan calcite cements can be absent from intragranular pores such as partially dissolved feldspars, and filling grain fractures (**Plate 4.5C**). Finally, quartz overgrowths in North Leif I-05 that occur at approximately 3100 m represent the latest-formed diagenetic mineral observed in the Bjarni Formation.

## **4.6 DISCUSSION**

The diagenesis of the studied samples from the Bjarni Formation sandstone appear to be inherently related to three main controls: 1) provenance and original mineral composition; 2) pore fluid chemistry, and; 3) burial temperature, all of which are controlled by an active tectonic margin.

### ***4.6.1 Depositional Mineralogy & Provenance***

The variations of inter- and intra-well mineralogy of the Bjarni Formation sandstone (**Fig 4.9; 4.10**), indicate sediment heterogeneity over stratigraphic and geographic intervals, which is related to compositional changes during rift development; a reflection of varying proximities from the sediment source (i.e. rift shoulders, horsts, and rotated blocks). Low P/K ratios may imply a sediment source rich in K-feldspar or a weathering process that has dissolved or altered most of the plagioclase. Therefore, sediment is deemed mature based on the relative instability in soil-forming chemical weathering environments of plagioclase compared to K-feldspar (Nesbitt et al., 1996).

The presence of polycrystalline quartz, various anhedral igneous (plutonic) grains, abundant potassium feldspars, and accessory minerals such as sillimanite, orthopyroxene, and biotite, indicate that the sediment sources, included both granitic and metamorphic terranes, which is consistent with recycled orogenic Labrador Precambrian craton

lithologies described by Umpleby (1979) and Higgs (1978). The presence of highly unstable sillimanite and orthopyroxene, a possible igneous (basement) boulder, and large grain size ranges in Ogmund E-72, may indicate that deposition occurred at a relatively proximal distance from the sediment source in an alluvial setting. By comparison, samples from North Leif I-05 contain the most moderately sorted detrital minerals, composed mainly of quartz arenites, and sublitharenites with less variation in grain sizes. This suggests that the sediment is relatively mature, as a result of a distal location from the source, potentially deposited in a marginal marine setting.

The clay mineral distribution of Mesozoic and Cenozoic Strata of the Labrador Shelf was documented by Douma (1987). Here, the climate is interpreted as being tropical to sub-tropical, during the Early to Mid Cretaceous (Berriasian - Hauterivian and Barremian - Albian), indicating warm and humid conditions. Assuming the sediment source were Precambrian horsts, and were collectively relatively close to the sites of deposition, the climate at the source and at the depositional sites must have been fairly similar, if not the same. In warm and humid climates, kaolinite (not smectite or illite) is the preferred clay mineral precipitated after potassium feldspar alteration (Bjørlykke, 1998). Furthermore, the average P/K ratio of 0.29 indicates that the climate was humid because of the relative depletion of plagioclase potassium feldspars, suggesting that chemical weathering was the dominant process.

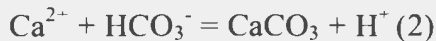
#### ***4.6.2 Pore Fluid Chemistry***

Given the immature, igneous, unstable, and regionally varied composition of the Bjarni Formation sandstones studied, it is possible that pore waters were readily able to attain cations and anions. The presence of altered biotite to oxides (e.g. hematite)

indicates the presence of oxygenated pore waters residing at shallow depth oxidizing  $\text{Fe}^{2+}$ . During this process that biotite was additionally altered, forming authigenic chlorite (cf. Bjørlykke, 1998). Meteoric water may have driven reactions at shallow depth, penetrating deeper into sediments at the time of the synrift stage, when compaction processes and overburden were minimal. Meteoric water, in addition to a bicarbonate source, would contribute to feldspar alteration and kaolinite precipitation (cf. Platt, 1993). However, the destruction of feldspar grains, particularly ones that postdate ferroan calcite cement, pyrite precipitation, and in addition, the observation that feldspars are at several 'stages' of dissolution at different stratigraphic depths and locations in studied samples. This may indicate that dissolution persisted during shallow to deep burial diagenesis and suggests that a deeper burial (basinal) water source may have been responsible for late stage dissolution. It is also possible that there were relatively low temperatures at maximum burial and pore fluids might have been in equilibrium with minerals, in turn implying that sediments were not subjected to the mixing of waters (e.g. marine waters), which would have triggered more cementation, particularly calcite.

With feldspar dissolution, biotite alteration, and possible contributions from meteoric or marine water, pore waters readily contain available cations such as  $\text{K}^+$ ,  $\text{Al}^{2+}$ ,  $\text{Ca}^{2+}$ ,  $\text{Fe}^{2+}$ , and  $\text{Mg}^{2+}$ . These aqueous cations in pore water may have contributed to the precipitation of kaolinite (cf. Jiang & Peacor, 1994). Pore water does not necessarily need to be acidic (i.e. low pH) for kaolinite precipitation. Instead, it must have a low  $\text{K}^+/\text{H}^+$  ratio and silica has to be removed from the system so that it can remain in the kaolinite stability field (Bjørlykke, 1998). However, in a fluvial setting with a warmer climate, such as the environment of deposition for the Bjarni Formation, it is conceivable that

meteoric waters were probably more acidic due to the dissolved atmospheric carbon dioxide and contact with local crystalline igneous (and metamorphic) basement (Hiscott, 1983), leading to the precipitation of kaolinite. During the process of kaolinite precipitation in sandstones, it is common for calcite and quartz to co-precipitate, given bicarbonate is available (Worden & Morad, 2000; Lanson, 2002). It is also conceivable that dissolution of underlying Paleozoic carbonates and basic lava's and dykes, from the Alexis Formation, provided a source of bicarbonate. With that assumption, two general co-reactions can take place (Worden & Morad, 2000):



The above may explain calcite and kaolinite co-precipitation, at different stratigraphic depths and geographic locations, in North Bjarni F-06, Herjolf M-92, Roberval K-92, and North Leif I-05. Reaction (1) would precipitate kaolinite and liberate aqueous silica into pore waters, while reaction (2) would produce calcite cement provided a sufficient supply of bicarbonate (via interaction with basement rocks and/or Paleozoic carbonates), occurring potentially simultaneously with feldspar dissolution.

#### ***4.6.3 Thermal Regime***

Based pm calculations of the organic maturation in wells from offshore eastern Canada, the present-day average, corrected geothermal gradient for exploration wells on the Labrador Shelf is 3.06°C per 100 m of depth (Issler, 1984). The studied well depths approximate a stratigraphic range between 2156 m and 3110 m. Calculating burial temperatures at every 100 m using the average geothermal gradient suggested by Issler (1984), gives a range of 66°C - 95°C (**Table 4.6**). In general, at burial depths greater than

Sample	Fm	Subbasin	Depth (m)	Burial Temperature
81-1-3	Bjarni Formation	Harrison	2156.5	66.0
81-1-1			2161.0	66.1
72-2-3		Nain	2233.8	68.4
72-2-2			2237.2	68.5
72-2-1			2239.0	68.5
06-1-2		Harrison	2451.5	75.0
06-1-3			2451.9	75.0
06-1-1			2457.3	75.2
HJ-1-3		Harrison	2633.0	80.6
HJ-1-2			2633.7	80.6
HJ-1-1			2633.9	80.6
HJ-2-1			2635.4	80.6
HJ-3-2			2636.0	80.7
HJ-3-1			2636.2	80.7
HJ-4-1			2637.2	80.7
HJ-5-3			2638.2	80.7
HJ-5-1			2638.3	80.7
HJ-5-2			2638.5	80.7
92-C2-1a			Hamilton	3107.0
92-C1-1b	3107.7	95.1		
92-C2-3	3110.2	95.2		
92-C2-4	3112.0	95.2		
05-1-5	Hamilton	3110.5	95.2	
05-1-4		3111.3	95.2	
05-1-3		3112.1	95.2	
05-1-1		3113.1	95.3	

**Table 4.6.** Bjarni Formation sandstone sample temperatures. Calculated from 3.06°C per 100m of stratigraphic depth (Issler, 1984)

3-4km and higher temperatures (i.e. >100 - 120°C), illite is the preferentially formed clay mineral. Therefore, with the suggested temperature range, it is possible that kaolinite is the preferred precipitated kaolin.

Aqueous silica will not normally precipitate as quartz at low temperatures (Bjørlykke, 1998). Therefore it is reasonable to indicate that the presence of quartz overgrowths in North Leif I-05 and minor quartz overgrowths in Roberval K-92 is a function of their greater burial depths, as they represent the deepest sediments and highest burial temperatures (~ 95°C) in this study (**Table 4.6**).

#### ***4.6.4 Implications of Diagenesis (Porosity Development)***

Core samples studied from the Bjarni Formation sandstone suggest that the porosity evolution is related to depositional and epigenetic controls, resulting in primary (intergranular) and secondary (intragranular) porosity.

Relatively minor occurrences of mechanical compaction of grain boundaries indicate minimal reduction of intergranular porosity (**Plate 4.5F**), whereas grain fracturing can contribute to intergranular porosity (**Plate 4.1D, E and Plate 4.5F**) when they are not filled with calcite cement (**Plate 4.5C**).

Intergranular porosity is affected by the precipitation of authigenic minerals, reducing pores and pore throat sizes. Minor quantities of intergranular porosity can be attributed to dissolution of biotite grains because they are generally further altered, filling any secondary pores with iron oxides or chlorite. Conversely, during non-ferroan and ferroan calcite cementation, in shallow to deep burial diagenesis, respectively, intergranular porosity is reduced. Intragranular porosity is generally empty in non-ferroan

calcite cements and occluded when associated with ferroan calcite cements (**Plate's 4.5A, B and 4.4C**).

#### 4.7 CONCLUSIONS

The Bjarni Formation sandstones investigated in core from six exploration wells, Bjarni H-81, Ogmund E-72, North Bjarni F-06, Herjolf M-92, Roberval K-92, and North Leif I-05 have been diagenetically altered from authigenic mineral precipitation and grain dissolution, occurring in different diagenetic burial realms. Diagenetic minerals, environments, and occurrences are summarized as:

- 1) **Iron oxides** (e.g. hematite). Represents diagenesis during relatively shallow burial (e.g. biotite alteration), occurring within inter- and intragranular porosity, often replacing biotite, and are the most abundant diagenetic minerals.
- 2) **Chlorite**. Generally intergranular pore-filling and originating from extensively altered detrital biotite, chlorite is observed in shallow to deep buried sediments such as at the Ogmund E-72 and Roberval K-92 locations, respectively, with the highest percentage noted in Ogmund E-72.
- 3) **Kaolinite**. Most abundant in core, at mid to deep burial depths, from well locations in the mid to southern Hopedale Basin (i.e. Harrison and Hamilton subbasins, respectively). It is likely that kaolinite originates from the alteration of potassium feldspar during eogenesis to mesodiagenesis, precipitating in mostly intergranular pores. At the suggested burial depths (>2-3km) illite has not precipitated, with kaolinite being the stable clay mineral.

- 4) **Non-ferroan and ferroan calcite cementation.** The presence of iron in calcite cements suggests that precipitation occurred during deeper burial conditions, whereas iron-free or limited iron calcite cements imply shallower burial; although not *sensu stricto*. The largest percentages of calcite occur in mid to southerly Hopedale Basin locations (i.e. Harrison and Hamilton subbasins). Calcite cementation is associated with reduced total porosity, although it has preserved some intragranular pores when precipitated during shallow burial (i.e. non-ferroan calcite)
- 5) **Pyrite.** The presence of pyrite, dominantly associated with ferroan calcite cementation observed in thin-section and core, further suggest deeper diagenetic burial settings, possibly precipitated from the same fluid, and as a result, preserving some intragranular porosity.
- 6) **Quartz overgrowths/cement.** Minor occurrences of quartz overgrowths in Roberval K-92 and relatively more in North Leif I-05 may be a result of deepest burial and highest temperatures observed in core. The source of aqueous silica may be linked to the destruction of potassium feldspar.

Intragranular porosity was developed mainly through potassium feldspar dissolution, with some additional porosity supplemented by minor grain fracturing and microporous kaolinite precipitation. Since potassium feldspar dissolution occurred at relatively low temperatures where pore fluids are close to equilibrium with minerals, and is observed to be coeval with non-ferroan calcite cementation, vugs are commonly void of authigenic minerals, supplementing the total porosity. The minor porosity created from detrital grain fracturing is generally void, with only minor calcite cementation and oxides

occluding pores. Intragranular porosity of the Bjarni Formation is controlled by feldspar dissolution, minor grain fracturing, and the precipitation of microporous kaolinite, increasing the total porosity in sandstones. In the case of kaolinite precipitation, its microporous nature of this diagenetic mineral may be responsible for increasing total porosity at deeper burial (e.g. Roberval K-92).

Intergranular porosity of the Bjarni Formation sandstone is controlled largely by its provenance. Generally, the largest intergranular pore point counts are observed in wells with the poorest sorting (e.g. Ogmund E-72) and relatively lower number of diagenetic minerals.

Considering the relatively fewer diagenetic minerals and higher total porosity, the best reservoir quality Bjarni Formation sandstone would be located at depths approximately between 2100 and 2250 m (e.g. Bjarni H-81 and Ogmund E-72). Although relatively more diagenetic minerals are present in deeper sediments (2600 – 3110 m), it is possible that, with the higher total porosity point counts observed, these sandstones still may be good potential reservoirs. These recommendations, of course, assume that all the other elements of a petroleum system are in place (e.g. source rock maturity, reservoir connectivity relative to source).

#### **4.8 ACKNOWLEDGMENTS**

This project was supported by the Pan-Atlantic Petroleum Systems Consortium (PPSC) and NSERC funds from Drs. Michael Enachescu (NSERC 204174 and PRAC 204231) and Rudi Meyer (RGP238252). Core viewing and sampling was permitted by CNLOPB with the help of Dave Mills and Jason Newell. Steve Schwartz would like to thank Dr. Rudi Meyer for abundant help with this work. Selected core pictures are courtesy of Matthew Harvey (ConocoPhillips). Thanks to GSI for seismic images. Many additional thanks go to people who have helped one way or another throughout the process: Allison Cocker, Erin Gillis, Angie Dearin, Michelle Martin, Mike Greene, Jordan Stead, Christopher Phillips, Nicola Tonkin, Leon Normore, Dr. Mark Wilson (Memorial University), Simon Haynes (Shell), and Jason Pemberton (Shell).

## **CHAPTER 5 SUMMARY & CONCLUSIONS**

### **5.1 SUMMARY OF APPROACH**

Diagenesis and its implications for porosity development in Early to Mid Ordovician carbonate and Early to Mid Cretaceous Bjarni Formation sandstone hydrocarbon reservoirs, of the Hopedale Basin, Labrador Shelf, have been investigated using petrographic, geochemical, and core analyses. Petrography was used to identify and classify various carbonate and sandstone rock-types based on detrital minerals, along with diagenetic phases, including authigenic minerals as well as associated secondary porosity.

Geochemistry and petrography of dolomite and calcite cements was used to help constrain the diagenetic effects of progressive burial observed in petrography, construct a paragenetic sequence of major diagenetic events, and resolve some of the age ambiguities affecting these sediments. Microthermometry of fluid inclusions provided additional data to identify a depositional setting of carbonate cements.

Point count data was used to compare variations of detrital and diagenetic minerals, along with different porosity types, occurring in Bjarni Formation sandstones between the depths of approximately 2100 to 3100 m.

### **5.2 PETROLEUM SYSTEM IMPLICATIONS**

It is apparent from earlier exploration drilling, that a viable petroleum system exists on the Labrador Shelf. Much subsequent research and documentation has been published on the specific gas discoveries, structural evolution, stratigraphy, shale (source rock)

geochemistry, thermal maturity, and potential play types (McWhae and Michel, 1975; Gradstein and Williams, 1976; Barss, 1979; McWhae et al., 1980; Rashid et al., 1980; Issler and Beaumont, 1987; Bell et al., 1989; Balkwill and McMillan, 1990; Atkinson & Fagan, 2001; Enachescu, 2005; Enachescu and Hogg, 2005; Fowler et al., 2005; Enachescu, 2006; Martin et al., 2006; Martin, 2007 and Stead, 2008).

Recently, new work has been carried-out on the Bjarni Formation and its potential as a host for hydrocarbons. Geophysical data interpreted by Enachescu (2006), Martin (2007) and Stead (2008) suggest that the Bjarni Formation extends much further into the outer shelf and deep water than previously estimated (cf. **Fig. 3.2**). This is a step in the right direction to further spark the interest in this, largely unexplored, frontier region of the North Atlantic. However, with only 27 exploration wells drilled in the entire Canadian Labrador margin, there are still some unanswered questions. One in particular is the reservoir quality and characterization of the remnant Paleozoic carbonates and Bjarni Formation sandstones. These topics were the subject of this thesis and the results of each are summarized below presenting the implications for future hydrocarbon exploration in the Hopedale Basin.

### ***5.2.1 Early to Mid Ordovician Carbonate Reservoirs***

1) Three phases of dolomites and calcite cements are petrographically and geochemically identified in prerift carbonates from Roberval K-92, Gudrid H-55, and Indian Harbour M-52 wells. Cements indicate, through progressive burial, that diagenesis has affected the development of porosity, which was created during early and late dissolution, along with initial dolomitization. Late-stage calcite cementation is the most

destructive calcite phase and has commonly occluded a proportion of secondary porosity and;

2) Paleozoic prerift carbonates have been dated without the aid of biostratigraphic data, using  $^{87}\text{Sr}/^{86}\text{Sr}$  collected from calcite and dolomite cements. An age of Early to Mid Ordovician, with initial dolomitization occurring no later than this time, confirms that none of these sediments are Carboniferous.

#### ***5.2.2.1 Reservoir Characterization***

The sparse and localized nature of the carbonate reservoirs in the Hopedale Basin, combined with the difficulty of their mapping with 2D seismic reflection sections only, make them a secondary target for exploitation. If carbonates are gas charged, the Alexis Formation volcanics that in places rest unconformably above carbonates will provide an adequate seal for hydrocarbons. Alternatively, fine clastics of the post rift sequence should provide an excellent seal.

Initial and secondary porosity types are recognized in association with dolomitization, however, precursor calcite cements occupying all pore types introduce reservoir heterogeneity at the micrometer-scale. The confirmation of an Early to Mid Ordovician age places the Hopedale Basin carbonates amongst the rest of the hydrocarbon-bearing carbonate sequences of the Anticosti and Maritime basins with very little ambiguity.

#### ***5.2.2 Bjarni Formation Sandstone Reservoirs***

1) The cores and thin sections studied from the Bjarni Formation suggest variable detrital and diagenetic compositions within cored intervals from exploration wells in the Hopedale Basin. Detrital variations are likely a reflection of sediment source and

maturity, whereas diagenesis of these sediments is further controlled by burial depth, temperature, and pore water chemistry. The combination of these controls led to the precipitation and co-precipitation of six main diagenetic minerals, while creating secondary porosity;

2) Relatively low primary intergranular porosity development is related to the immature nature of the detrital sediment. In addition, this porosity is frequently occluded by one, or more, of six authigenic minerals recorded;

3) Secondary intergranular porosity is largely created from the destruction of detrital potassium feldspar (intragranular vugs), which is observed as pristine to almost completely dissolved relict grains. This process occurred over diagenetic stages from initial to deep burial. Minor contribution to intragranular porosity is attributed to grain fracturing and microporous kaolinite precipitation and;

4) Calcite cements are the most damaging to porosity of the diagenetic minerals observed. Non-ferroan calcite is possibly coeval with the dissolution of potassic feldspars, and completely occupies intergranular porosity. However, this process appears to have preserved the intragranular pore spaces created from dissolution. In contrast, deeper burial ferroan calcite can post-date feldspar dissolution, resulting in vugs being filled with calcite.

#### ***5.2.2.1 Reservoir Characterization***

Flow rates in Bjarni Formation have been tested in several wells including Bjarni H-81, Bjarni O-82, Hopedale E-33, North Bjarni F-06, North Leif I-05 and Snorri J-90. The initial flow in these wells ranged from 170 000 m<sup>3</sup>/day to 401 860 m<sup>3</sup>/day (CNLOPB). Good porosity values averaging 12 % (Umpleby, 1979; CNLOPB ), which

are confirmed in this petrographic study (cf. **Chapter 4**), also show that the Bjarni Formation has potential to be a successful producing reservoir.

The diagenetic implications for the reservoir quality of the Bjarni Formation appear to be beneficial rather than detrimental in the studied intervals. Although calcite cements have completely destroyed intergranular porosity, it appears that cementation was not pervasive and would not act as barriers to hydrocarbon flow at field scale. Most importantly, the chemical weathering of feldspars has created secondary porosity in virtually all studied intervals, supplementing the total porosity. Compositional and diagenetic mineral variations throughout the studied interval influence porosity. However, point-count estimated porosities as high as 60.0, per sample, remain.

### **5.3 FUTURE WORK**

Additional petrographic and geochemical work needs to be completed on the Paleozoic carbonates and Bjarni Formation sandstones in the Hopedale Basin. When future exploration wells are drilled, additional reservoir intervals need to be analyzed and compared with this study.

Recommendations and questions for future work include:

- 1) Additional geochemical sampling of carbonate and dolomite cements (when there is more carbonate core available) are needed to resolve any statistical uncertainties;
- 2) Geochemical sampling of carbonate cements in the Bjarni Formation sandstones are needed to understand the nature and origin of the diagenetic fluid(s);

- 3) Further quantification of porosity of both reservoir intervals using petrographic digital analysis software (cf. Ehrlich et al., 1984; Antonelli et al., 1994; Layman, 2002);
- 4) An evaluation and correlation of reservoir quality, particularly reservoir heterogeneity and architecture, using petrographic, geochemical, and petrophysical (e.g. wireline) methods must be performed to define petrophysical facies;
- 5) Are there additional diagenetic minerals present in the Bjarni Formation sandstones at greater depth in the Hopedale Basin and their influence on reservoir quality;
- 6) What influence do the inter-bedded/inter-laminated lacustrine shales of the Bjarni Formation have on the diagenesis of the sandstones? Do aid in the production of clay minerals and do they act as barriers or baffles for fluid flow and;
- 7) Is feldspar dissolution, that is, chemical weathering or intrastratal solution, the dominant process in all Bjarni Formation sandstones or just in the intervals studied?

Potential, inner shelf-reservoir sandstones of Tertiary age need to be assessed petrographically and geochemically. These include sandstones from the Gudrid Member (Cartwright Formation) Leif Member (Kenamu Formation), Freydis Member (Markland Formation; cf. **Fig. 1.7**). Similar questions formulated for the Bjarni Sandstone can be addressed for all Tertiary sandstones. During core viewing for this thesis, a number of these sandstones were observed in core. It may be of interest to understand how the

unconsolidated and friable nature of several of these sandstones affects reservoir quality. Some of these sandstones (e.g. Cartwright Formation in Snorri J-90 and Karlsefni A-13) are heavily bioturbated and thus, a core and petrographic-based study on how the bioturbation has affected reservoir quality and porosity would be valuable (cf. Pemberton and Gingras, 2005).

Just as important, all the aforementioned sandstones need to be evaluated in cores from the Saglek Basin and compared to those in the Hopedale Basin. Potential questions may include:

- 1) Are the Saglek Basin Cretaceous and Tertiary sandstones texturally and compositionally similar to those observed in the Hopedale Basin? and;
- 2) Do the Saglek Basin Cretaceous and Tertiary sandstones have a similar diagenetic history, affecting porosity, to those observed in the Hopedale Basin?

It is clear that the Labrador Shelf contains a viable petroleum system with future potential for hydrocarbon discoveries. Hopefully this study and further work on Labrador wells and seismic data, will result in further academic and industry interest.

## REFERENCES

- Al-Aasm, I.S. & Azmy, K. 1996. Diagenesis and evolution of microporosity of Middle-Upper Devonian Kee Scarp Reefs, Norman Wells, Northwest Territories, Canada: petrography and chemical evidence. *AAPG Bulletin*, v. 80, no. 1, pp. 82-100
- Antonellini, M., Aydin, A., Pollard, D.D., and D'Onfro, P. 1994. Petrophysical study of faults in sandstone using petrographic image analysis and x-ray computerized tomography. *Pageoph.* vol. 143. no. 1/2/3. pp. 181-201
- Atkinson, I. & Fagan, P. 2001. *Sedimentary Basins & Hydrocarbon Potential of Offshore Newfoundland and Labrador*. Government of Newfoundland and Labrador, Dept. of Mines & Energy. pp. 31-33
- Ayalon, A. and Longstaffe, F.J. 1995. Stable isotope evidence for the origin of diagenetic carbonate minerals from the Lower Jurassic Inmar Formation, southern Israel. *Sedimentology*. vol. 42. pp. 147-160
- Azmy, K., Veizer, J., Misi, A., de Oliveira, T., F., Sanches, A., Lima, D., M. 2001. Dolomitization and isotope stratigraphy of the Vazante Formation, Sao Francisco Basin, Brazil. *Precambrian Research*, vol. 112. no. 3-4, pp. 303-329
- Azmy, K. 1992. Subsurface diagenetic evolution and porosity evaluation of Middle-Upper Devonian Kee Scarp Reef, Norman wells, N.W.T., Canada. M.Sc. Thesis. pp. 138
- Azmy, K., Kaufman, A., J., Misi, A., de Oliveira, T., F. 2006. Isotope stratigraphy of the Lapa Formation, Sao Francisco Basin, Brazil; implications for late Neoproterozoic glacial events in South America. *Precambrian Research*, vol. 149, no. 3-4, pp. 231-248
- Azmy, K., Veizer, J., Bassett, M.G., Copper, P. 1998. Oxygen and carbon isotopic composition of Silurian Brachiopods: Implications for coeval seawater and glaciations. *GSA Bulletin*. vol. 110. No. 11, pp. 1499-1512

- Balkwill, H. R. 1987. Labrador basin: structural and stratigraphic style. In: Beaumont, C. & Tankard, A. J. (eds) Sedimentary basins and basin-forming mechanisms. Canadian Society of Petroleum Geologists, Memoirs, 12, pp. 17-43
- Balkwill, H.R. and McMillan, N.J. 1990. Mesozoic-Cenozoic geology of the Labrador shelf; geology of the Labrador shelf, Baffin Bay, and Davis Strait. Geology of the continental margin of Eastern Canada. pp. 293-351
- Balkwill, H.R., McMillan, B., Williams, G.L., Srivastava, S.P. 1990. Geology of the Labrador Shelf, Baffin Bay, and Davis Strait, Chapter 7; in: Geology of the Continental Margin of Eastern Canada. Geological Survey of Canada, Geology of Canada, no. 2, pp. 293-348
- Bally, A.W., Watts, A.B., Grow, J.A., Manspeizer, W., Bernoulli, D., Schreiber, C., and Hunt, J.M. 1981. Atlantic-type margins; geology of passive continental margins; history, structure and sedimentologic record (with special emphasis on the Atlantic margin), AAPG Continuing Education Course Note Series, 19: 48
- Barss, M.S., Bujak, J.P., Williams, G.L. 1979. Palynological zonation and correlation of sixty-seven wells, eastern Canada; Geological Survey of Canada, Paper 78-24, pp. 118
- Bell, J.S. 1989. Frontier Geoscience Program. East Coast Basin Atlas Series: Labrador Sea. Geological Survey of Canada. Energy, Mines, and Resources Canada. pp. 109
- Bell, J.S. and Howie, R.D. 1990. Paleozoic Geology. Chapter 3; in: Geology of the Continental Margin of Eastern Canada. Geological Survey of Canada, Geology of Canada, no. 2, pp. 143-165
- Bell, J.S., Howie, R.D., McMillan, N.J., Hawkins, C.M., and Bates, J.L. 1989. Labrador Sea, East Coast Basin Atlas series. Geological Survey of Canada, Canada.
- Bjørlykke, K. 1998. Clay mineral diagenesis in sedimentary basins – a key to the prediction of rock properties. Examples from the North Sea Basin. Clay Minerals. vol 33. pp. 15-34

- Boggs, S. and Krinsley, D. 2006. Application of cathodoluminescence imaging to the study of sedimentary rocks. *Sedimentary petrology*, American Geological Institute. pp. 165
- Brand, U. & Veizer, J. 1980. Chemical diagenesis of a multicomponent carbonate system -1: trace elements. *Journal of Sedimentary Petrology*. vol. 50, no. 4, pp. 1219-1236
- Brand, U. & Veizer, J. 1981. Chemical diagenesis of a multicomponent carbonate system -2: stable isotopes. *Journal of Sedimentary Petrology*. vol. 51, no. 3, pp. 987-997
- Brown, K.M. and Ransom, B. 1996. Porosity corrections for smectite-rich sediments; impact on studies of compaction, fluid generation, and tectonic history. *Geology (Boulder)*. vol. 24, no. 9. pp. 843-846
- Budd, D.A. 1997. Cenozoic dolomites of carbonate islands; their attributes and origin *Earth-Science Reviews*, vol.42, no.1-2, pp.1-47
- Chalmers, J.A. and Pulvertaft, T.C.R. 2001. Development of the continental margins of the Labrador Sea; a review; non-volcanic rifting of continental margins; a comparison of evidence from land and sea, *Geological Society Special Publications*. vol. 187. pp. 77-105
- Choquette, P.W. and James, N.P. 1990. Limestones – the burial diagenetic environment. *Diagenesis*. Geological Association of Canada. IV Series. pp. 75-112
- Choquette, P.W. and Pray, L.C. 1970. Geologic nomenclature and classification of porosity in sedimentary carbonates. *AAPG Bulletin*. vol. 25. pp. 35-51
- Clark, I.D., Fritz, P., 1997. *Environmental Isotopes in Hydrogeology*. Lewis publisher, Boca Raton, p. 328
- Coalson, E.B., Hartmann, D.J., and Thomas, J.B. 1985. Rock types, pore types, and hydrocarbon exploration. *AAPG Bulletin*. vol. 69, no. 5. pp. 845

- Coleman, M.L., Walsh, J.N., Benmore, R.A. 1989. Determination of both chemical and stable isotope composition in milligramme-size carbonate samples. *Sedimentary Geology*. vol. 65, no. 3-4, pp. 233-238
- Davies, G.R. 2006. Structurally-controlled carbonate diagenesis; hydrothermal dolomite and leached limestone reservoirs. *Canadian Society of Petroleum Geologists (CSPG): Reservoir*, vol. 33, no. 11, pp. 10
- Diener, A., Ebner, S., Veizer, J., Buhl, D. 1996. Strontium isotope stratigraphy of the Middle Devonian; brachiopods and conodonts. *Geochimica et Cosmochimica Acta*. vol. 60, no. 4, pp. 639-652
- Dickinson, W.R., 1970. Interpreting detrital modes of greywacke and arkose. *Journal of Sedimentary Petrology*. v. 40, (2), p. 695-707.
- Dickinson, W.R., Beard, L.S., Brakenridge, G.R., Erjavec, J.L, Ferguson, R.C., Inman, K.F., Knepp, R.A., Lindberg, F.A., Ryberg, P.T. 1983. Provenance of North American Phanerozoic sandstones in relation to tectonic setting. *Geological Society of American Bulletin*. vol. 94. no. 2. pp. 222-235
- Dickson, J.A.D. 1966. Carbonate identification and genesis as revealed by staining. *Journal of Sedimentary Petrology*. vol. 36, no. 2, pp. 491-505
- Douma, M. 1987. Clay mineral distribution in Mesozoic and Cenozoic strata of the Labrador Shelf. MSc, Thesis. Dalhousie University. Halifax, Nova Scotia. pp. 119
- Drever, J.I., 1988. *The Geochemistry of Natural Waters*. Prentice Hall, Englewood Cliffs, NJ, pp. 437
- Enachescu, M. E., Martin, M., Stead, J., Hall, J., Carroll, A. and P. Einarsson, 2008. Abstract: Hopedale Basin Exploration Potential, East Coast Atlantic Canada, 2008 AAPG Annual Convention and Exhibition, San Antonio, TX.

- Enachescu, M.E. 2006. Hopedale Basin; 1, Favorable geology, advanced technology may unlock Labrador's substantial resource. *Oil and Gas Journal*. vol. 104, no. 23, pp. 29-34
- Enachescu, M.E. 2006. Hopedale Basin; 2, Atlantic off Labrador poised for modern exploration round. *Oil and Gas Journal*, vol. 104, no. 24, pp. 36-42
- Enachescu, M.E., Kearsley, S., Hogg, J., Fagan, A.J., Einarsson, D., Atkinson, I., and Hardy, V. 2006. Hopedale Basin, offshore Labrador, Canada: Structural and tectonic framework and exploration potential. SEG 2006 Annual Meeting, New Orleans, LA.
- Enachescu, M.E. and Hogg, J. 2005. Exploring for Atlantic Canada's next giant petroleum discovery, *Canadian Society of Exploration Geophysicists Recorder*, 30. pp. 19-30
- Enachescu, M.E., Einarsson, P. and A. Feir, 2007, Extent of sedimentary basins and oceanic crust domain in the northern Labrador Sea. CSPG Gussow Geoscience Conference.
- Enachescu, M.E., 1992. Enigmatic basins offshore Newfoundland. *Canadian Journal of Exploration Geophysics*. v. 28(1) p.44-61.
- Enachescu, M.E. 1992. Enigmatic basins offshore Newfoundland. *Proceedings of the International Conference on Basement Tectonics*. vol.7, vol. 1, pp. 227-256
- Ehrlich, R., Kennedy, S.K., Crabtree, S.J, and Cannon, R.L. 1984. Petrographic image analysis, I. analysis of reservoir pore complexes. *Journal of Sedimentary Petrology*. vol. 54. no. 4. pp. 1365-1378
- Folk, R.L. 1968. *Petrology of sedimentary rocks*; University of Texas Geology 370K, 383L, 383M. pp. 170
- Fowler, M.G., Stasiuk, L.D., and Avery, M. 2005. Potential petroleum systems in the Labrador and Baffin shelf areas, offshore eastern Canada. Abstract: GAC/MAC/CSPG/CSSS

- Galehouse, J.S. 1969. Counting grain mounts; number percentage vs. number frequency. *Journal of Sedimentary Petrology*, vol. 39, no.2, pp. 812-815
- Galehouse, J.S. 1971. Point counting. in: Carver, R.E., ed., *Procedures in sedimentary petrology*. pp. 385-407
- Gazzi, P., 1966. Le arenarie del flysch sopracretaceo dell' appennino modenese; correlazioni con il flysch di monghidoro. *Minerlogica e Petrografica Acta*, v. 12, p. 69-97.
- Goldstein, R.H., Reynolds, T.J. 1994. Systematics of fluid inclusions in diagenetic minerals, Short course 31, SEPM (Society for sedimentary Geology), pp. 199
- Gradstein, F.M. and Williams, G.L. 1976. Biostratigraphy of the Labrador shelf; part 1. 349, Geological Survey of Canada. pp. 39
- Hall, A.J., Boyce, A.J., Fallick, A.E. 1988. A sulphur isotope study of iron sulphides in the late Precambrian Dalradian Easdale slate formation, Argyll, Scotland. *Mineralogical Magazine*, vol. 52, Part 4, no. 367, pp. 483-490
- Heinrich, C.A. 2007. Fluid-fluid interactions in magmatic-hydrothermal ore formation. *Reviews in Mineralogy and Geochemistry*, vol. 65, no. 1., pp. 363-387
- Higgs, K.E., Zwingmann, H., Reyes, A.G., and Funnell, R.H. 2007. Diagenesis, porosity evolution, and petroleum emplacement in tight gas reservoirs, Taranaki Basin, New Zealand. *Journal of Sedimentary Research*. vol. 77, pp. 1003-1025
- Hiscott, R.N. 1983. Clay mineralogy and clay-mineral provenance of Cretaceous and Paleogene strata, Labrador and Baffin Shelves. *Bulletin of Canadian Petroleum Geology*. vo. 32. no. 3. pp. 272-280

- Howarth, R.J. 1998. Improved estimators of uncertainty in proportions, point-counting and pass-fail test results. *American Journal of Science*. vol. 298. pp. 594-607
- Hurst, A.R. 1981. A scale of dissolution of quartz and its implications of diagenetic processes in sandstones. *Sedimentology*. vol 28. no. 4. pp. 451-459
- Hutcheon, I. 1990. Aspects of the diagenesis of coarse-grained siliciclastic rocks. *Diagenesis*. Geological Association of Canada. IV Series. pp. 165-176
- Ingersoll, R.V., Bullard, T.F., Ford, R.L., Grim, J.B., Pickle, J.D., and Sares, S.W., 1984. The effect of grain size on detrital modes: A test of the Gazzi Dickinson point-counting method. *Journal of Sedimentary Petrology*, v. 54, pp. 103-116
- Issler, D.R. 1984. Calculation of organic maturation levels for offshore Eastern Canada; implications for general application of Lopatin's Method. *Canadian Journal of Earth Sciences*. vol. 21. no. 4. pp. 477-488
- Issler, D.R. and Beaumont, C. 1987. Thermal and subsidence history of the Labrador and west Greenland continental margins; sedimentary basins and basin-forming mechanisms, *Atlantic Geoscience Society Special Publication 5*. pp. 45-69
- Jenkins, W.A.M. 1984. The Ordovician rocks in Eastcan et al. Fierjois B-87 and other wells in offshore Atlantic Canada; *Canadian Journal of Earth Sciences*. v. 21, pp. 864-868
- Jiang, W. and Peacor, D.R. 1994. Formation of corrensite, chlorite, and chlorite-mica stacks by replacement of detritals biotite in low-grade pelitic rocks. *Journal of Metamorphic Geology*. vol. 12. pp. 867-884
- Keen, M.J. and Piper, D.J.W. 1990. Geological and historical perspective. Chapter 1. in: *Geology of the continental margin of eastern Canada*. Geological Survey of Canada, no. 2. pp. 5-30
- Keen, M.J. & Williams, G.L. 1990. *Geology of the continental margin of eastern Canada*. Geological Survey of Canada, no. 2, pp. 1-855

- Ketchum, J.W.F., Culshaw, N.G., Barr, S.M. 2002. Anatomy and orogenic history of a Paleoproterozoic accretionary belt: the Makkovik Province, Labrador, Canada. *Canadian Journal of Earth Sciences*. vol. 39. pp. 711-730
- Kierkegaard, T. 1998. Diagenesis and reservoir properties of Campanian-Paleocene sandstones in the GANT#1 well, western Nuussuaq, central West Greenland. *Geology of Greenland Survey Bulletin*. vol. 180. pp. 31-34
- Khidir, A. and Catuneau, O. 2003. Sedimentology and diagenesis of the Scollard sandstones in the Red Deer Valley area, central Alberta. *Bulletin of Canadian Petroleum Geology*. vol. 51. pp. 45-69
- Koponen, A., Kataja, M., and Timonen, J. 1997. Permeability and effective porosity of porous media. *The American Physical Society*. vol. 56, no. 3. 3319-3325
- Land, L.S. 1983. The application of stable isotopes to studies of the origin of dolomite and to problems of diagenesis of clastic sediments. *SEPM Short Course*. vol. 10, pp. 3. 1-3
- Land, L.S. 1992. The dolomite problem: stable and radiogenic isotope clues. In: Clauer, N., Chaudhuri, S. (Eds.), *Isotopic Signature of Sedimentary Records*. Lecture Notes in Earth Science 43, pp. 49-68
- Lanson, B., Beaufort, D., Berger, G., Bauer, A., Cassagnabère, A., and Meunier, A. 2002. Authigenic kaolin and illitic minerals during burial diagenesis of sandstones: a review. *Clay Minerals*. vol. 37. pp. 1-22
- Larson, G. and Chilingar, G.V. 1979. Diagenesis in sediments and sedimentary rocks. *Developments in Sedimentology*. vol. 25A. pp. 579
- Lavoie, D. 2005. Hydrothermal dolomitization in the Lower Silurian La Vielle Formation in northeastern New Brunswick: field evidence and implication for hydrocarbon exploration. *Geological Survey of Canada, Current Research (D1)*. pp. 10

- Lavoie, D., Chi, G., Brennan-Alpert, P., Desrochers, A. and Bertrand, R., 2005. Hydrothermal dolomitization in the Lower Ordovician Romaine Formation of the Anticosti Basin: significance for hydrocarbon exploration. *Bulletin of Canadian Petroleum Geology*, 53, pp. 256-269
- Lavoie, D., and Chi, G., 2006. Hydrothermal dolomitization in the Lower Silurian La Vielle Formation in northern New Brunswick: geological context and significance for hydrocarbon exploration. *Bulletin of Canadian Petroleum Geology*, 54, pp. 380-395
- Layman, J.M. Porosity characterization utilizing petrographic image analysis: implications for identifying and ranking reservoir flow units, Happy Spraberry Field, Garza County, Texas. 2002. MSc. Thesis. Texas A&M University. pp. 114
- Lee, M.R., Thompson, P., Poeml, P., Parsons, I. 2003. Peristeritic plagioclase in North Sea hydrocarbon reservoir rocks; implications for diagenesis, provenance, and stratigraphic correlation. *American Mineralogist*. vol. 88. no. 5-6. pp. 866-875
- Lima, R.D., and De Ros, L.F. 2002. The role of depositional setting and diagenesis on the reservoir quality of Devonian sandstones from the Solimões Basin, Brazilian Amazonia. *Marine and Petroleum Geology*. vol. 19. no. 9. pp. 1047-1071
- Louden, K. 2002. Tectonic evolution of the east coast of Canada. *CSEG Recorder*. pp. 37-48
- Machel, H.G., Mason, R.A., Mariano, A.N., and Mucci, A. 1991. Causes and emission of luminescence in calcite and dolomite. In: *Luminescence microscopy and spectroscopy, quantitative and qualitative applications*, SEPM Short Course 25. pp. 9-25
- Martin, M.R. 2007. Seismic stratigraphy and tectono-structural framework of the Bjarni area, Hopedale Basin, Labrador Sea. M.Sc. Thesis. pp. 186
- Martin, M. and Enachescu, M. E. 2007. New Geoscience Data and Interpretation of the Region Around Bjarni/North Bjarni Field, Hopedale Basin. Poster presentation 2007 CSPG CSEG Convention, May 14-17, Calgary, AB.

- McWhae, J.R.H., Elie, R., Laughton, D.C., Gunther, P.R. 1980. Stratigraphy and petroleum prospects of the Labrador Shelf. *Bulletin of Canadian Petroleum Geology*. vol. 28, no. 4, pp. 460-488
- McWhae, J.R.H. and Michel, W.F.E. 1975. Stratigraphy of Bjarni H-81 and Leif M-48, Labrador shelf, *Bulletin of Canadian Petroleum Geology*, 23. pp. 361-382
- Morrow, D.W. and McIlreath, I.A. 1990. Diagenesis general introduction. *Diagenesis*. Geological Association of Canada. IV Series. pp. 1-8
- Morrow, D.W. 1978. The influence of Mg/Ca ratio and salinity on dolomitization in evaporite basins. *Canadian Petroleum Geology Bulletin*. vol. 26, pp. 389-392
- Midtbø, R.E.A., Rykkje, J.M., Ramm, M. 2000. Deep burial diagenesis and reservoir quality along the eastern flank of the Viking Graben. Evidence for illitization and quartz cementation after hydrocarbon emplacement. *Clay Minerals*. vol. 35. pp. 227-237
- Nesbitt, H.W., Young, G.M., McLennan, S.M., and Keayes, R.R., 1996. Effects of chemical weathering and sorting on the petrogenesis of siliciclastic sediments with implications for provenance studies. *Journal of Geology*, v. 104, p. 525-542
- Normore, L.S. 2006. Origin, distribution, and paragenetic sequence of carbonate cements in the Ben Nevis Formation, White Rose Field, Jeanne d'Arc Basin, offshore Newfoundland, Canada. M.Sc. Thesis. pp. 216
- Pemberton, S.G., and Gingras, M.K. 2005. Classification and characterizations of biogenically enhanced permeability. *AAPG Bulletin*, v. 89; no. 11, pp. 1493-1517
- Pettijohn, F.J. 1975. *Sedimentary rocks*. Harper and Row, New York, pp. 628
- Platt, J.D. 1993. Controls on clay mineral distribution and chemistry in the Early Permian Rotliegendes of Germany. *Clay Minerals*. vol. 28. no. 3. pp. 393-416

- Ramm, M. and Bjørlykke, K. 1994. Porosity/depth trends in reservoir sandstones: assessing the quantitative effects of varying pore-pressure, temperature history and mineralogy, Norwegian Shelf data. *Clay Minerals*. vol. 29. pp. 475-4900
- Rashid, M.A., Purcell, L.P., and Hardy, I.A. 1980. Source rock potential for oil and gas for the east Newfoundland and Labrador shelf areas; facts and principles of world petroleum occurrence, *Memoir - Canadian Society of Petroleum Geologists*. pp. 589-607
- Saigal, G.C., Morad, S., Bjørlykke, K., Egeberg, P.K., Aagaard, P. 1988. Diagenetic albitization of detrital K-feldspar in Jurassic, Lower Cretaceous, and Tertiary clastic reservoir rocks from offshore Norway; I, Textures and origin. *Journal of Sedimentary Petrology*. vol. 58. no. 6. pp. 1003-1013
- Salem, A.M., Ketzer, J.M., Morad, S., Rizk, R.R., and Al-Aasm, I.S. 2005. Diagenesis and reservoir-quality evolution of incised-valley sandstones: evidence from the Abu Madi gas reservoirs (Upper Miocene), the Nile Delta Basin, Egypt. *Journal of Sedimentary Research*. vol. 75, pp. 572-584
- Shields, G.A., Carden, G.A.F., Veizer, J., Meidla, Tonu, Rong, J., Li, RY. 2003. Sr, C, and O isotope geochemistry of Ordovician brachiopods: A major isotopic event around the Middle-Late Ordovician transition. *Geochimica et Cosmochimica Acta*, vol. 67, No. 11, pp. 2005–2025
- Stonecipher, S.A. and May, J.A. 1990. Facies controls on early diagenesis; Wilcox Group, Texas Gulf Coast. *AAPG Memoir*. vol. 49. pp. 25-44
- Stead. 2008. Geological comparison of the South Hopedale and West Orphan Basins, Northwest Atlantic Margin M.Sc. Thesis. pp. 209
- Sørensen, A.B. 2006. Stratigraphy, structure and petroleum potential of the Lady Franklin and Maniitsoq Basins, offshore southern West Greenland. *Petroleum Geoscience*. vol. 12. no. 3. pp. 221-234

- Thyne, G., Boudreau, B.P., Ramm, M., and Midtbø, R.E. 2001. Simulation of potassium feldspar dissolution and illitization in the Statfjord Formation, North Sea. AAPG Bulletin. vol. 85, no. 4. pp. 621-635
- Tucker, M.E. & Wright, V.P., 1990. Carbonate Sedimentology. Backwell Scientific. pp. 482
- Tucker, M.E. 2001. Chapter 2. Siliciclastic sediments I: sandstones, conglomerates and breccias. in: Sedimentary petrology: an introduction to the origin of sedimentary rocks. pp. 58
- Umpleby, D.C. 1979. Geology of the Labrador shelf. Geological Survey of Canada. no. 79-13. pp. 34
- Veizer, J. 1983. Chemical diagenesis of carbonates; theory and application of trace element technique. SEPM Short Course. vol. 10. pp.4. 1-4. 22
- Veizer, J., Ala, D., Azmy, K., Bruckschen, P., Buhl, Di., Bruhn, F., Carden, G.A.F., Diener, A., Ebner, S., Godderis, Y., Jasper, T., Korte, C., Pawellek, F., Podlaha, O.G., and Strauss, H. 1999.  $^{87}\text{Sr}/^{86}\text{Sr}$ ,  $\delta^{13}\text{C}$  and  $\delta^{18}\text{O}$  evolution of Phanerozoic seawater. Chemical Geology, vol. 161, pp. 59-88
- Wardle, R.J. and Van Kranendonk, M.J. 1996. The Palaeoproterozoic Southeastern Churchill Province of Labrador-Quebec, Canada: orogenic development as a consequence of oblique collision and indentation. Geological Society, London, Special Publications. vol. 112. pp. 137-153
- Warren, J. 2000. Dolomite; occurrence, evolution and economically important associations. Earth-Science Reviews, vol.52, pp. 1-81
- Worden, R.H. and Morad, S. 2000. Quartz cementation in oil field sandstones: a review of the key controversies. Special Publication of the International Association of Sedimentologists. vol. 29. pp. 103-117

## Appendix A: Geochemical Data

Well	Phase	Depth (m)	CaCO <sub>3</sub> (%)	MgCO <sub>3</sub> (%)	Fe (ppm)	Mn (ppm)	δ <sup>18</sup> O (‰)	δ <sup>13</sup> C (‰)	Sr (ppm)	<sup>87</sup> Sr/ <sup>86</sup> Sr	norm. fx
<i><u>Roberval K-92</u></i>	D1	1.2	40.7%	59.3%	1348	75	-3.4	-1.9	60	0.708923	0.86
	D1	1.2	41.7%	58.3%	5510	186	-4.9	-1.9	63		0.87
	D1	2.7	39.2%	60.8%	4309	80	-3.9	-2.0	89	0.708883	1.56
	D2	4.4	40.4%	59.6%	2346	98	-6.5	-0.5	59	0.709065	0.65
	D2	4.7	40.7%	59.3%	2602	139	-6.6	-0.6	64	0.709052	0.87
	D2	5.6	40.8%	59.2%	2398	117	-5.3	-0.6	51		1.15
	D2	8.0	39.7%	60.3%	1201	67	-5.7	-0.8	65	0.709264	0.91
	D2	6.8	39.8%	60.2%	2102	98	-6.0	-0.5	37		0.80
	D3	4.4	40.5%	59.5%	7070	375	-7.6	-1.2	58		0.90
	D3	6.8	44.1%	55.9%	16607	809	-9.0	-2.0	88		0.89
	D3	4.7	41.1%	58.9%	7107	360	-6.9	-1.1	55		1.02
	D3	8.0	41.2%	58.8%	9724	490	-7.8	-1.7	90		1.08
	<i><u>Gudrid H-55</u></i>	D1	1.5	40.1%	59.9%	1512	586	-6.0	-1.2	59	
D1		2.0	40.2%	59.8%	1909	713	-6.2	-1.3	53		0.82
D1		1.0	39.5%	60.5%	499	251	-4.7	-0.9	84		0.99
D1		3.4	40.7%	59.3%	633	427	-4.8	-0.9	83		1.16
D1		3.8	40.0%	60.0%	1127	572	-5.2	-1.0	63	0.708864	0.85
D1		2.8	40.2%	59.8%	1727	1262	-5.1	-0.8	56	0.708889	1.76
D1		1.0	39.5%	60.5%	532	299	-4.9	-1.0	82	0.708937	0.87
D2		3.4	40.6%	59.4%	1924	903	-5.5	-1.3	69		0.86
D2		3.8	40.2%	59.8%	1781	866	-5.5	-1.3	65		0.87
D2		3.8	39.7%	60.3%	1395	446	-5.1	-0.8	83	0.708922	0.86
C3		2.0	92.5%	7.5%	1125	2954	-9.0	-7.3	218		1.32
C3		1.5	87.0%	13.0%	1210	2125	-5.7	-1.3	233		0.87
C3		1.0	93.2%	6.8%	1755	4012	-8.3	-10.5	149		1.30
C3		3.4	82.7%	17.3%	1054	2769	-8.6	-5.1	266		2.72
<i><u>Indian Harbour M-52</u></i>		D1	0.4	43.2%	56.8%	2775	79	-8.6	0.4	59	
	D1	4.2	44.3%	55.7%	4336	114	-8.2	0.7	75		0.91
	D1	2.5	44.7%	55.3%	2372	77	-7.9	0.3	70	0.709083	0.72
	D1	5.8	43.7%	56.3%	2798	99	-8.1	0.5	61	0.709366	0.82
	C1	0.4	98.8%	1.2%	506	42	-9.8	-0.2	418		1.17
	C1	4.2	97.2%	2.8%	1379	104	-9.2	-0.3	407		1.25
	C1	2.5	98.6%	1.4%	259	37	-9.1	-0.6	311	0.708897	0.96
	C1	5.8	97.3%	2.7%	519	37	-8.8	-0.3	317	0.708941	1.36

**Appendix B: Siliciclastic Point Count Data**

Point Counted Parameters		North Leif I-05			
Sample		05-1-1	05-1-3	05-1-4	05-1-5
Depth (m)		3113.1	3112.1	3111.3	3110.5
Sorting (µm)		20-100	25-100	50-150	25-150
<b>Detrital</b>	Q (m+p)	181	180	179	130
	K-Feldspar	2	3	12	4
	Plag-Feldspar	2	2		
	F (K+Plag)	4	5	12	4
	Chert	-	-	-	8
	L	15	15	9	58
<b>Authigenic</b>	Chlorite	-	-	-	-
	Oxide	70	38	17	5
	Calcite Cement	-	22	23	-
	IGP	-	5	-	-
	Qtz Overgrowths	-	10	12	-
<b>Porosity</b>	IP + IGP	38	40	7	-
	<b>Total Count</b>	<b>308</b>	<b>315</b>	<b>259</b>	<b>205</b>
<b>Well Total Count</b>		<b>1087</b>			
Calculated QFL (Pettijohn, 1975)					
	Q	181	180	179	130
	F	4	5	12	4
	L	15	15	9	66
	<b>QFL Total</b>	<b>200</b>	<b>200</b>	<b>200</b>	<b>200</b>
	<b>Well Total Count</b>	<b>800</b>			
	<b>Normalized QFL</b>				
	Q%	90.50	90.00	89.50	65.00
	F%	2.00	2.50	6.00	2.00
	L%	7.50	7.50	4.50	33.0

**Appendix B: Siliciclastic Point Count Data**

<b>Point Counted Parameters</b>		<b>North Bjarni F-06</b>		
<b>Sample</b>		<b>06-1-1</b>	<b>06-1-3</b>	<b>06-1-2</b>
<b>Depth (m)</b>		2457.3	2451.9	2451.5
<b>Sorting (µm)</b>		50-125	50-100	50-1050
<b>Detrital</b>	<b>Q (m+p)</b>	137	126	77
	K-Feldspar	7	2	69
	Plag-Feldspar			9
	F (K+Plag)	7	2	78
	Chert	-	-	-
	L	56	72	45
<b>Authigenic</b>	Chlorite	-	-	-
	Oxide-Opaque	50	47	8
	Calcite Cement	8	11	89
	Kaolinite	-	3	-
	IGP	2	-	8
<b>Porosity</b>	IP + IGP	2	6	2
	<b>Total Count</b>	<b>262</b>	<b>267</b>	<b>307</b>
	<b>Well Total Count</b>		<b>836</b>	
<b>Calculated QFL (Pettijohn, 1975)</b>				
	Q	137	126	77
	F	7	2	78
	L	56	72	45
	<b>QFL Total</b>	<b>200</b>	<b>200</b>	<b>200</b>
	<b>Well Total Count</b>		<b>600</b>	
<b>Normalized QFL</b>				
	Q%	68.50	63.00	38.50
	F%	3.50	1.00	39.00
	L%	28.00	36.00	22.50

Appendix B: Siliciclastic Point Count Data

Point Counted Parameters		<b>Bjarni H-81</b>	
<u>Sample</u>		<b>81-1-3</b>	<b>81-1-1</b>
<u>Depth (m)</u>		2156.5	2161
<u>Sorting (<math>\mu</math>)</u>		100-1050	25-300
<b>Detrital</b>	Q (m+p)	91	137
	K-Feldspar	54	37
	Plag-Feldspar	19	25
	F (K+Plag)	100	62
	Chert	16	-
	L	53	1
<b>Auth.</b>	Chlorite	-	-
	Oxide-Opaque	11	38
	Calcite Cement	-	-
	Kaolinite	-	-
	IGP	21	14
<b>Porosity</b>	IP + IGP	38	56
	<b>Total Count</b>	<b>403</b>	<b>370</b>
	<b>Well Total Count</b>		<b>638</b>
<u>Calculated QFL (Pettijohn, 1975)</u>			
	Q	91	137
	F	73	62
	L	69	1
	<b>QFL Total</b>	<b>233</b>	<b>200</b>
	<b>Well Total Count</b>		<b>433</b>
<u>Normalized QFL</u>			
	Q%	39.60	68.50
	F%	31.33	31.00
	L%	29.61	0.50

**Appendix B: Siliciclastic Point Count Data**

Point Counted Parameters		Herjolf M-92									
Sample		HJ-5-1	HJ-4-1	HJ-5-2	HJ-5-3	HJ-1-3	HJ-1-2	HJ-1-1	HJ-2-1	HJ-3-1	HJ-3-2
Depth (m)		2638.2	2637.2	2638.5	2638.2	2633	2633.7	2633.9	2635.4	2636.2	2636
Sorting ( $\mu$ )		50-275	100-175	50-200	100-325	75-150	50-1050	25-	50-200	50-1000	50-1000
<b>Detrital</b>	Q (m+p)	134	121	140	93	96	93	120	120	117	82
	K-Feldspar	12	13	13	51	52	63	49	57	42	38
	Plag-Feldspar	5	1	2	21	22	24	11	13	31	12
	F (K+Plag)	17	14	15	72	74	87	60	70	73	50
	Chert	10	5	10	20	-	-	-	-	-	-
	L	49	65	45	35	30	20	20	10	10	68
<b>Authigenic</b>	Chlorite	10	18	15	7	10	-	5	-	-	-
	Oxide-Opaque	21	20	25	41	20	17	20	10	20	23
	Calcite Cement	-	-	-	-	-	-	-	70	-	-
	Pyrite	-	-	-	-	20	30	-	-	-	-
	IGP	4	17	3	11	12	4	8	3	11	1
	<b>Porosity</b>	IP + IGP	47	17	45	29	20	23	25	10	17
<b>Total Count</b>		<b>292</b>	<b>277</b>	<b>298</b>	<b>308</b>	<b>282</b>	<b>274</b>	<b>258</b>	<b>293</b>	<b>248</b>	<b>242</b>
<b>Well Total Count</b>		<b>2772</b>									
Calculated QFL (Pettijohn, 1975)											
Q (m+p)		134	121	140	93	96	93	120	120	117	82
F		17	14	15	72	74	87	60	70	73	50
L		59	70	55	55	30	20	20	10	10	68
<b>QFL Total</b>		<b>210</b>	<b>205</b>	<b>210</b>	<b>220</b>	<b>200</b>	<b>200</b>	<b>200</b>	<b>200</b>	<b>200</b>	<b>200</b>
<b>Well Total Count</b>		<b>2045</b>									
Normalized QFL											
Q%		63.81	60.98	66.67	42.27	48.00	46.50	60.00	60.00	58.50	41.00
F%		8.10	4.88	7.14	32.73	37.00	43.50	30.00	35.00	36.50	25.00
L%		28.10	34.15	26.19	25.00	15.00	10.00	10.00	5.00	5.00	34.00

**Appendix B: Siliciclastic Point Count Data**

Point Counted Parameters		Roberval K-92			
Sample		92-C2-1a	92-C1-1b	92-C2-3	92-C2-4
<b>Depth (m)</b>		3107.0	3107.7	3110.2	3112.0
<b>Sorting (<math>\mu</math>)</b>		100-1000	100-1100	50-200	75-300
<b>Detrital</b>	Q (m+p)	127	111	102	100
	K-Feldspar	53	39	37	37
	Plag-Feldspar	9	29	4	4
	F (K+Plag)	62	68	41	38
	Chert	-	-	-	-
	L	11	21	57	62
<b>Authigenic</b>	Chlorite	9	7	10	2
	Oxide-Opaque	22	10	11	20
	Kaolinite	15	12	10	2
	IGP	21	10	4	6
<b>Porosity</b>	IP + IGP	44	41	12	16
	<b>Total Count</b>	<b>311</b>	<b>280</b>	<b>247</b>	<b>246</b>
	<b>Well Total Count</b>	<b>1084</b>			
<b>Calculated QFL (Pettijohn, 1975)</b>					
	Q (m+p)	127	111	102	100
	F	62	68	41	38
	L	11	21	57	62
	<b>QFL Total</b>	<b>200</b>	<b>200</b>	<b>200</b>	<b>200</b>
	<b>Well Total Count</b>	<b>800</b>			
<b>Normalized QFL</b>					
	Q%	63.50	55.50	51.00	50.00
	F%	31.00	34.00	20.50	19.00
	L%	5.50	10.50	28.50	31.00

**Appendix B: Siliciclastic Point Count Data**

Point Counted Parameters		Ogmund E-72		
Sample		72-2-2	72-2-1	72-2-3
<b>Depth (m)</b>		2237.2	2239	2233.8
<b>Sorting (<math>\mu</math>)</b>		50-500	25-1000	25-300
<b>Detrital</b>	Q (m+p)	154	93	138
	K-Feldspar	35	70	16
	Plag-Feldspar	11	10	12
	F (K+Pl)	46	80	28
	Chert	-	-	-
	L	2	27	34
<b>Authigenic</b>	Chlorite	77	-	54
	Ox.	8	18	38
	Calcite cement	3	-	-
	IGP	2	16	-
<b>Porosity</b>	IP + IGP	20	60	8
<b>Total Count</b>		<b>312</b>	<b>294</b>	<b>300</b>
<b>Well Total Count</b>			<b>906</b>	
<b>Calculated QFL (Pettijohn, 1975)</b>				
	Q (m+p)			
	F	154	93	138
	L	46	80	28
	<b>QFL Total</b>	2	27	34
	<b>Well Total Count</b>	202	200	200
	<b>Normalized QFL</b>		<b>602</b>	
	Q%	77.00	46.50	69.00
	F%	22.00	40.00	14.00
	L%	1.00	13.50	17.00

**Appendix B**  
**Siliciclastic Point Counted Data**

SAMPLE	Raw data			X-Plot	Y-Plot	Normalised data		
	Q	F	L	value	value	%A	%B	%C
Max-A	20.00	60.00	20.00	22.50	20.00	20.00	60.00	20.00
Max-B	40.00	40.00	20.00	30.00	40.00	40.00	40.00	20.00
Max-C	20.00	40.00	40.00	37.50	20.00	20.00	40.00	40.00
05-1-1	181.00	4.00	15.00	39.56	90.50	90.50	2.00	7.50
05-1-3	180.00	5.00	15.00	39.38	90.00	90.00	2.50	7.50
05-1-4	179.00	12.00	9.00	36.94	89.50	89.50	6.00	4.50
05-1-5	130.00	4.00	66.00	49.13	65.00	65.00	2.00	33.00
05 Avg.	167.50	6.25	26.25	41.25	83.75	83.75	3.13	13.13
06-1-1	137.00	7.00	56.00	46.69	68.50	68.50	3.50	28.00
06-1-3	126.00	2.00	72.00	50.63	63.00	63.00	1.00	36.00
06-1-2	77.00	78.00	45.00	31.31	38.50	38.50	39.00	22.50
06 Avg.	113.33	29.00	57.67	42.88	56.67	56.67	14.50	28.83
81-1-3	91.00	100.00	69.00	33.03	35.00	35.00	38.46	26.54
81-1-1	137.00	62.00	1.00	26.06	68.50	68.50	31.00	0.50
81 Avg.	114.00	81.00	35.00	30.00	49.57	49.57	35.22	15.22
72-2-2	154.00	44.00	2.00	29.63	77.00	77.00	22.00	1.00
72-2-1	93.00	80.00	27.00	27.56	46.50	46.50	40.00	13.50
72-2-3	138.00	28.00	34.00	38.63	69.00	69.00	14.00	17.00
72 Avg.	128.33	50.67	21.00	31.94	64.17	64.17	25.33	10.50
HJ-5-1	134.00	17.00	59.00	45.00	63.81	63.81	8.10	28.10
HJ-4-1	125.00	10.00	70.00	48.48	60.98	60.98	4.88	34.15
HJ-5-2	140.00	15.00	55.00	44.64	66.67	66.67	7.14	26.19
HJ-5-3	93.00	72.00	55.00	34.60	42.27	42.27	32.73	25.00
HJ-1-3	96.00	74.00	30.00	29.25	48.00	48.00	37.00	15.00
HJ-1-2	93.00	87.00	20.00	24.94	46.50	46.50	43.50	10.00

**Appendix B**  
**Siliciclastic Point Counted Data**

HJ-1-1	120.00	60.00	20.00	30.00	60.00	60.00	30.00	10.00
HJ-2-1	120.00	70.00	10.00	26.25	60.00	60.00	35.00	5.00
HJ-3-1	117.00	73.00	10.00	25.69	58.50	58.50	36.50	5.00
HJ-3-2	82.00	50.00	68.00	40.88	41.00	41.00	25.00	34.00
<b>HJ Avg.</b>	<b>112.00</b>	<b>52.80</b>	<b>39.70</b>	<b>35.10</b>	<b>54.77</b>	<b>54.77</b>	<b>25.82</b>	<b>19.41</b>
92-C2-1a	127.00	62.00	11.00	27.94	63.50	63.50	31.00	5.50
92-C1-1b	111.00	68.00	21.00	28.69	55.50	55.50	34.00	10.50
92-C2-3	102.00	41.00	57.00	40.50	51.00	51.00	20.50	28.50
92-C2-4	100.00	38.00	62.00	42.00	50.00	50.00	19.00	31.00
<b>92 Avg.</b>	<b>110.00</b>	<b>52.25</b>	<b>37.75</b>	<b>34.78</b>	<b>55.00</b>	<b>55.00</b>	<b>26.13</b>	<b>18.88</b>
<b>Avg. All</b>	<b>122.42</b>	<b>44.73</b>	<b>36.88</b>	<b>36.06</b>	<b>60.00</b>	<b>60.00</b>	<b>21.92</b>	<b>18.08</b>
	Q	P	K	X-Plot	Y-Plot	%A	%B	%C
05-1-1	181.00	2.00	2.00	37.50	97.84	97.84	1.08	1.08
05-1-3	180.00	0.00	3.00	38.11	98.36	98.36	0.00	1.64
05-1-4	179.00	0.00	12.00	39.86	93.72	93.72	0.00	6.28
05-1-5	130.00	0.00	4.00	38.62	97.01	97.01	0.00	2.99
<b>05 Avg.</b>	<b>167.50</b>							
06-1-1	137.00	0.00	7.00	39.32	95.14	95.14	0.00	4.86
06-1-3	126.00	0.00	2.00	38.09	98.44	98.44	0.00	1.56
06-1-2	77.00	9.00	69.00	52.02	49.68	49.68	5.81	44.52
<b>06 Avg.</b>	<b>113.33</b>							
81-1-3	91.00	19.00	54.00	45.50	55.49	55.49	11.59	32.93
81-1-1	137.00	25.00	37.00	39.76	68.84	68.84	12.56	18.59
<b>81 Avg.</b>	<b>114.00</b>							
72-2-2	154.00	11.00	35.00	42.00	77.00	77.00	5.50	17.50
72-2-1	93.00	10.00	70.00	50.51	53.76	53.76	5.78	40.46
72-2-3	138.00	11.00	35.00	42.39	75.00	75.00	5.98	19.02

**Appendix B**  
**Siliciclastic Point Counted Data**

72 Avg.	128.33							
HJ-5-1	134.00	5.00	12.00	39.24	88.74	88.74	3.31	7.95
HJ-4-1	125.00	1.00	13.00	40.74	89.93	89.93	0.72	9.35
HJ-5-2	140.00	2.00	13.00	40.16	90.32	90.32	1.29	8.39
HJ-5-3	93.00	21.00	51.00	44.32	56.36	56.36	12.73	30.91
HJ-1-3	96.00	22.00	52.00	44.12	56.47	56.47	12.94	30.59
HJ-1-2	93.00	24.00	63.00	45.63	51.67	51.67	13.33	35.00
HJ-1-1	120.00	11.00	49.00	45.42	66.67	66.67	6.11	27.22
HJ-2-1	120.00	13.00	57.00	46.18	63.16	63.16	6.84	30.00
HJ-3-1	117.00	31.00	42.00	39.67	61.58	61.58	16.32	22.11
HJ-3-2	82.00	12.00	32.00	43.45	65.08	65.08	9.52	25.40
HJ Avg.	112.00							
92-C2-1a	127.00	9.00	53.00	46.23	67.20	67.20	4.76	28.04
92-C1-1b	111.00	29.00	39.00	39.60	62.01	62.01	16.20	21.79
92-C2-3	102.00	4.00	37.00	46.15	71.33	71.33	2.80	25.87
92-C2-4	100.00	4.00	37.00	46.28	70.92	70.92	2.84	26.24
92 Avg.	110.00			37.50	100.00	100.00	0.00	0.00
Avg. All	122.42			37.50	100.00	100.00	0.00	0.00
	Q (+chert)	F	L					
05-1-1	181.00	4.00	15.00	39.56	90.50	90.50	2.00	7.50
05-1-3	180.00	5.00	15.00	39.38	90.00	90.00	2.50	7.50
05-1-4	179.00	12.00	9.00	36.94	89.50	89.50	6.00	4.50
05-1-5	138.00	4.00	66.00	48.68	66.35	66.35	1.92	31.73
05 Avg.	169.50	6.25	26.25	41.21	83.91	83.91	3.09	13.00
06-1-1	137.00	7.00	56.00	46.69	68.50	68.50	3.50	28.00

**Appendix B**  
**Siliciclastic Point Counted Data**

06-1-3	126.00	2.00	72.00	50.63	63.00	63.00	1.00	36.00
06-1-2	77.00	78.00	45.00	31.31	38.50	38.50	39.00	22.50
<b>06 Avg.</b>	<b>113.33</b>	<b>29.00</b>	<b>57.67</b>	<b>42.88</b>	<b>56.67</b>	<b>56.67</b>	<b>14.50</b>	<b>28.83</b>
81-1-3	107.00	100.00	69.00	33.29	38.77	38.77	36.23	25.00
81-1-1	137.00	62.00	1.00	26.06	68.50	68.50	31.00	0.50
<b>81 Avg.</b>	<b>122.00</b>	<b>81.00</b>	<b>35.00</b>	<b>30.25</b>	<b>51.26</b>	<b>51.26</b>	<b>34.03</b>	<b>14.71</b>
72-2-2	154.00	44.00	2.00	29.63	77.00	77.00	22.00	1.00
72-2-1	93.00	80.00	27.00	27.56	46.50	46.50	40.00	13.50
72-2-3	138.00	28.00	34.00	38.63	69.00	69.00	14.00	17.00
<b>72 Avg.</b>	<b>128.33</b>	<b>50.67</b>	<b>21.00</b>	<b>31.94</b>	<b>64.17</b>	<b>64.17</b>	<b>25.33</b>	<b>10.50</b>
HJ-5-1	144.00	17.00	59.00	44.66	65.45	65.45	7.73	26.82
HJ-4-1	130.00	10.00	70.00	48.22	61.90	61.90	4.76	33.33
HJ-5-2	150.00	15.00	55.00	44.32	68.18	68.18	6.82	25.00
HJ-5-3	113.00	72.00	55.00	34.84	47.08	47.08	30.00	22.92
HJ-1-3	96.00	74.00	30.00	29.25	48.00	48.00	37.00	15.00
HJ-1-2	93.00	87.00	20.00	24.94	46.50	46.50	43.50	10.00
HJ-1-1	120.00	60.00	20.00	30.00	60.00	60.00	30.00	10.00
HJ-2-1	120.00	70.00	10.00	26.25	60.00	60.00	35.00	5.00
HJ-3-1	117.00	73.00	10.00	25.69	58.50	58.50	36.50	5.00
HJ-3-2	82.00	50.00	68.00	40.88	41.00	41.00	25.00	34.00
<b>HJ Avg.</b>	<b>116.50</b>	<b>52.80</b>	<b>39.70</b>	<b>35.15</b>	<b>55.74</b>	<b>55.74</b>	<b>25.26</b>	<b>19.00</b>
92-C2-1a	127.00	62.00	11.00	27.94	63.50	63.50	31.00	5.50
92-C1-1b	111.00	68.00	21.00	28.69	55.50	55.50	34.00	10.50
92-C2-3	102.00	41.00	57.00	40.50	51.00	51.00	20.50	28.50
92-C2-4	100.00	38.00	62.00	42.00	50.00	50.00	19.00	31.00
<b>92 Avg.</b>	<b>110.00</b>	<b>52.25</b>	<b>37.75</b>	<b>34.78</b>	<b>55.00</b>	<b>55.00</b>	<b>26.13</b>	<b>18.88</b>

05-C5-1	100.00	34.00	65.00	45.00	30.00	20.00	15.00	31.00
05-C5-2	105.00	41.00	64.00	40.20	31.00	21.00	20.20	38.20
05-C1-1P	111.00	68.00	43.00	24.00	48.20	24.20	24.00	10.20
05-C5-1P	153.00	95.00	58.00	31.80	63.20	42.20	31.00	3.20
00-1-1	83.00	20.00	63.00	40.80	41.00	41.00	32.00	34.00
00-1-1	113.00	32.00	81.00	32.80	28.20	28.20	10.20	2.00
00-1-1	130.00	30.00	100.00	39.32	50.00	50.00	24.00	2.00
00-1-1	136.00	60.00	76.00	30.00	60.00	60.00	10.00	10.00
00-1-1	82.00	83.00	30.00	34.84	48.20	48.20	47.00	10.00
00-1-1	80.00	34.00	46.00	36.32	48.00	48.00	33.00	12.00
00-1-1	112.00	35.00	77.00	34.94	43.08	43.08	20.00	27.85
00-1-1	120.00	12.00	108.00	44.32	68.18	68.18	1.25	32.00
00-1-1	130.00	10.00	120.00	40.33	0.00	0.00	8.18	33.33
00-1-1	144.00	33.00	111.00	44.88	62.42	62.42	1.00	30.85
00-1-1	138.00	38.00	100.00	30.82	60.00	60.00	14.00	13.00
00-1-1	93.00	40.00	53.00	33.28	48.20	48.20	40.00	13.20
00-1-1	124.00	44.00	80.00	30.93	33.00	33.00	57.00	1.00
00-1-1	133.00	62.00	71.00	30.68	48.20	48.20	21.00	0.40
00-1-1	103.00	100.00	3.00	32.50	38.33	38.33	30.33	32.00
00-1-1	150.00	5.00	145.00	20.00	43.00	43.00	1.00	20.00
00-1-1	130.00	37.00	93.00	21.11	28.20	28.20	16.00	35.20
00-1-1	150.00	5.00	145.00	20.00	43.00	43.00	1.00	20.00



